MECHANISTIC NUMERICAL STUDY OF THROMBUS GROWTH

A Thesis
Presented to
The Academic Faculty

by

David Lawrence Bark, Jr.

In Partial Fulfillment
of the Requirements for the Degree
Master of Science in the
School of Mechanical Engineering

Georgia Institute of Technology
May 2007

MECHANISTIC NUMERICAL STUDY OF THROMBUS GROWTH

Approved by:

Dr. David N. Ku, Advisor
School of Mechanical Engineering
Georgia Institute of Technology

Dr. Cyrus Aidun
School of Mechanical Engineering
Georgia Institute of Technology

Dr. Don P. Giddens
Department of Biomedical Engineering
Georgia Institute of Technology

Date Approved: April 09, 2007

DEDICATION

This thesis is dedicated in the loving memory of my uncle who passed away because of thrombosis, while he was still young. The family misses him greatly. This thesis is also dedicated to my father who recently had a heart attack because of thrombosis. He has also always been a strong influence toward my career as an engineer. I also, of course, dedicate this to the rest of my family, whom have always been supportive of my endeavors.

ACKNOWLEDGEMENTS

I would like to thank my advisor, Dr. Ku, for his guidance throughout the thesis process. He has led me in a new direction of tackling problems. In addition, he has given me great opportunities and I would like to thank him for this.

I also would like to thank my family and Rachel for their support.

TABLE OF CONTENTS

LIST OF TABLES

Page

LIST OF FIGURES

Page

SUMMARY

Thrombosis can result in acute arterial occlusion thereby causing cerebrovascular accidents and myocardial infarction. However, diagnosing the risk of developing thrombosis is difficult due to the limited understanding of how platelets are transported, adhere, and accumulate in flowing blood. A clinician might be better able to predict a patient's risk for thrombosis with an understanding of how a thrombus forms and why it occludes an artery. Arterial thrombus usually forms on a ruptured atherosclerotic plaque. Most previous studies have focused on initial platelet adhesion to the ruptured region. This study is focused on a growing thrombus past initial platelet attachment to the point of full occlusion, which is the dominant problem in a thrombotic event.

A computational model was proposed to simulate experimental results with minimal assumptions and to separate out the dominate mechanisms involved in the formation and growth of thrombus. The model and experiment were based on an axisymmetric coronary artery with an atherosclerotic lesion. The dominate mechanisms involved in thrombus deposition were evaluated by considering platelet transport and reaction kinetics on the vessel wall. Transport mechanisms that were considered include shear enhanced diffusivity and platelet margination. Adhesion kinetics were considered by specifying a probability for platelet attachment once a platelet reaches the reactive thrombus surface. The results of the study indicate that platelet transport to the thrombotic site is the rate limiting step in thrombus growth. Platelet adhesion becomes the rate limiting mechanism as the flow rate increases. The results also indicate that clinicians should consider shear rate as a criterion for prophylactic treatment, therefore, requiring a different degree stenosis criteria for each atherosclerosis-prone artery.

CHAPTER

1. INTRODUCTION

This thesis explores the development of thrombus near an atheroma lesion in a coronary artery. Only white thrombus or arterial thrombus is considered in this thesis, due to its relation with cardiovascular ischemia and cerebrovascular accidents. Computational fluid mechanics are applied to model the thrombus formation at a Reynolds number for the bulk flow of 40 and 200. This section presents the significance of such a study and explores the background of factors that may affect the development of thrombosis and the growth of a thrombus.

Blood Flow (Application to Coronary Atherosclerosis)

The cardiovascular system is a dynamic complex system of biological reactions, mass transport, fluid flow, and structural mechanics. There a wide variety of theoretical models that can be used to simulate vascular flow. The model choice is dependent on what is of particular interest to the researcher. Mass transport and flow characteristics are most relevant to thrombus formation. Computational fluid mechanics (CFD) are used in this study because of its capabilities in modeling mass transport. This method solves the governing fluid flow equations, the Navier-Stokes equations. The continuity and momentum equations that make up Navier-Stokes equations can be found in Equation 1. Results from the energy equation are considered negligible here because the fluid is modeled as incompressible and isothermal.

Equation 1: Continuity of mass and momentum equations.

$$\left[\frac{\partial \rho}{\partial t} + \vec{v} \bullet \vec{\nabla} \rho\right] = -\rho \vec{\nabla} \bullet \vec{v}$$

$$\rho\left[\frac{\partial \vec{v}}{\partial t} + \vec{v} \bullet \vec{\nabla} \vec{v}\right] = -\vec{\nabla} p + \rho g - \frac{2}{3}\vec{\nabla}\left(\mu \vec{\nabla} \bullet \vec{v}\right) + 2\vec{\nabla} \bullet \left(\mu \tilde{S}\right)$$

Here, ρ is the density of the fluid, $\vec{v}$ is the velocity vector for the fluid, p is the pressure, μ is the dynamic viscosity, g is a gravitational constant, t is the time, and $\tilde{S}$ is the rate of deformation tensor. The time dependent terms drop out for steady flow and the density does not vary for incompressible flow. Gravity and additional body forces to the fluid are neglected in this study because of the minimal effects.

Non-dimensional parameters can be extracted from the Navier-Stokes equations. Such parameters can easily characterize a flow and elucidate characteristics that dominate the equation. The most famous parameter is the Reynolds number, Re. This compares the inertial forces against the viscous forces. Blood flow typically varies in Reynolds numbers from 1 to 4000. Arterial flow is also commonly unsteady, therefore having varying Reynolds numbers at different points in time. The equation for the Reynolds number can be found in Equation 2.

Equation 2: Reynolds number

$$\mathrm{Re} = \frac{\rho u D}{\mu}$$

Here, u is the velocity, D is the characteristic length. The cardiovascular system contains many bifurcations and curves, increasing the complexity of the flow. These are not considered here because this study is focused on characterizing thrombus formation and developing a model to simulate thrombus aggrandizement. A significant nondimensional parameter in blood flow is the Womersley parameter, α. This parameter is a comparison of the pulsatile nature of the flow with the viscous nature of the flow. Values that are much greater than 1 are considered pulsatile, while values much less than 1 are quasi-steady. The coronary arteries are the focus of this study, resulting in a Womersley parameter of 3. The equation for the Womersley parameter can be found in Equation 3.

Equation 3: Womersley parameter

$$\alpha = R\sqrt{\frac{\omega}{\upsilon}}$$

Here, R is the radius of the vessel, ν is the kinematic viscosity, and ω is the frequency of the waves involved in the unsteady term. The pulsation of the flow is not considered in this study because the Womersley parameter will reduce at high degree stenosis. Also, such considerations would complicate the characterization of thrombus formation, as well as having minimal effect on particle transport (Goldsmith 1972). Therefore, steady flow is only considered in this study. In addition entrance effects and curvature are neglected to avoid complications and to focus on a developed flow section of the artery.

Shear stress and shear rate are important when considering the effects of mass transport in blood flow. The reasoning is further explained in the biorheology portion of this thesis. Shear rate is the velocity gradient of the fluid flow. In tubular flow, this number increases significantly near the vessel wall. Shear stress, τ, is the shear rate, $\dot{\gamma}$, multiplied with the dynamic viscosity. It can be approximated by the gradient in one direction for Poiseuille, or tube flow Equation 4. This is no longer true near the thrombus because of the sudden change in the radial velocity gradient.

Equation 4: Shear stress and shear rate

$$\tau_{rz} = \mu\left[\frac{\partial v_z}{\partial r} + \frac{\partial v_r}{\partial z}\right] = \mu\dot{\gamma} \approx \mu\left[\frac{\partial v_z}{\partial r}\right]$$

Fluid viscosity in a Newtonian fluid is independent of shear rate. However, as explained in the biorheology section, it can change with shear rate for Non-Newtonian fluids. Increased viscosity, requires greater forces in the fluid to transport a liquid in a given volume at a given flow rate. This is known as viscous work, whereas work required to accelerate flow is inertial work. The Poiseuille flow velocity profile can be simplified to Equation 5.

Equation 5: Velocity profile of Poiseuille flow

$$v_z = \frac{k}{2}\left(R_0^2 - r^2\right)$$

$$k = \frac{4Q}{\pi R_0^2}$$

$$k = \frac{\Delta P}{\Delta x} \bullet \frac{1}{2\mu_0}$$

The velocity profile, as seen from the equation is parabolic. These approximations can be used for the wall shear stress at a particular point in Poiseuille flow, Equation 6.

Equation 6: Approximation of wall shear stress

$$\tau_{wall} = \frac{32\mu Q}{\pi D^3}$$

Biorheology and Blood Constituents

It is necessary to understand particle transport in blood flow when studying thrombogenesis and thrombus aggrandizement. There are many constituents that are found in blood. However, the bulk volume fraction of constituents is dominated by erythrocytes or red blood cells (RBCs). Typical values for percent volume of blood associated with thrombus formation can be found in Figure 1. The plasma proteins that are the most pertinent to thrombus formation are Fibrinogen and von Willebrand Factor (VWF), however they only take up a small volume of the blood.

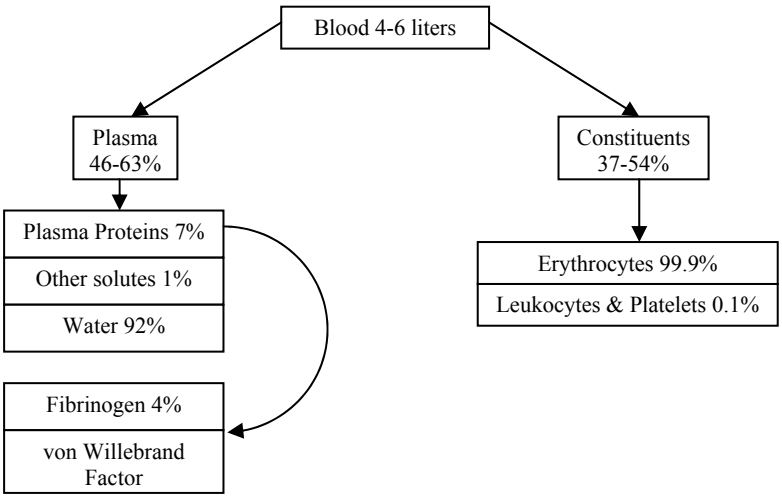

Figure 1: % volume of blood that is pertinent to thrombus formation.

Platelets make up the majority of a thrombus, therefore their transport must be considered when studying arterial thrombus formation. The motion of platelets and plasma proteins are generally governed by the motion of erythrocytes since erythrocytes, by large, make up the majority of the particulate or constituent volume. Erythrocytes are deformable biconcave disks. Average parameters describing a RBC can be given in Figure 2.

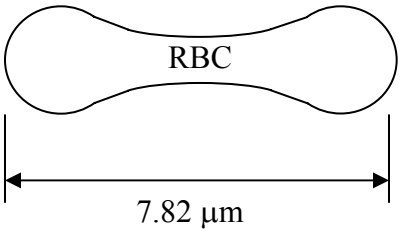

$SA = 135\ \mu m^2$
$V = 85\text{-}100\ \mu m^3$
$D_{eff} = 5.64\ \mu m$
$\rho = 1125\ kg/m^3$
$\phi = 0.40$

Figure 2: Diagram of erythrocyte with list of parameters

In the Figure 2, ϕ represents the volume fraction, V is the volume, SA is the surface area, and D_{eff} is the effective diameter.

Liquid drops and solid spheres in a flow field have been extensively studied. However, the complexity of the motion is still not well understood, as there are many factors that are involved in controlling the motion of the particulates in a fluid. A RBC has characteristics that are between that of a solid and liquid particulate. Liquid drops undergo deformation into a discoid, Figure 3, where an equilibrium occurs between forces in the drop (Taylor 1934). In contrast a solid particle will not generally deform. The outer membrane of a drop will spin due to the imbalance between velocities across the diameter of the drop. A solid particle will instead rotate around its center of mass. A RBC at high Reynolds numbers will tend to lie with their major axis at a 20 degree angle or less from the axial axis (Goldsmith 1972) and may spin as a liquid droplet, or may spin as a solid particle. If the RBC is spinning as a solid particle, then the rotational velocity will decrease as the particle orients along the streamlines due to its shape. Therefore, statistically the average orientation should be 20 degrees or less. According to

Goldsmith, erythrocytes lose their rigid motion characteristics at shear rates exceeding 20 s^{-1} and begin to spin as a fluid. When this occurs, the RBC membrane may rotate around its axis, without changing the RBC major axis orientation, as seen in Figure 3 b). These differences have been noted at low Reynolds numbers, but may not spin in such a way at high Reynolds numbers because inertial forces of the fluid may begin to dominate.

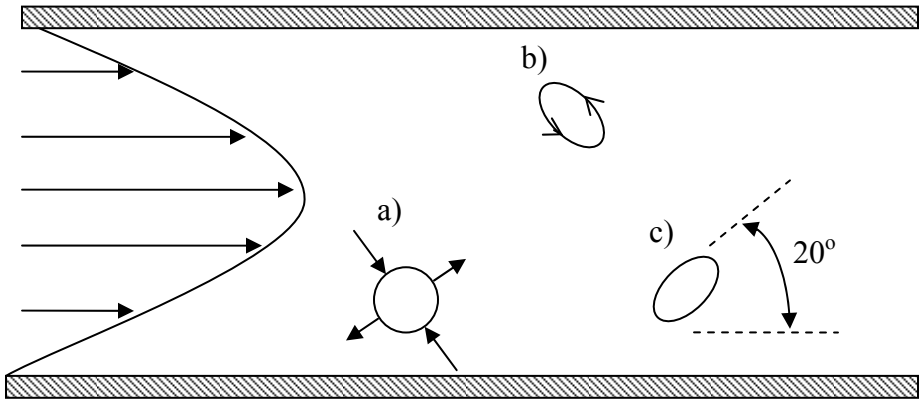

Figure 3: Recreated from (Goldsmith 1972). Poiseuille flow with a parabolic velocity profile. a) Fluid stresses on a liquid drop, which deform the drop into an ellipsoid. b) Rotation as a fluidic particle, instead of a rigid particle. c) Orientation of a liquid drop in the Poiseuille flow after stress induced deformation.

In the sense of molecular dynamics, particles should arrange in a manner so that the concentration is evenly distributed across a fully developed flow. The constituents in blood flow do not exhibit this behavior (Goldsmith 1972; Goldsmith and Marlow 1979; Aarts, Bolhuis et al. 1983; Eckstein, Bilsker et al. 1987). Erythrocytes, instead, migrate to the center axis of a tubular vessel. One hypothesis for this migration is that the deformability of the particle causes the migration toward the central axis (Goldsmith 1972); non-deformable particles exhibit different migration, described later. However, in healthy subjects, the erythrocyte concentration is high enough to cause axial migration, even if the particles were not deformable (Minsoo, Chongyoup et al. 1999). The reason for the axial migration at moderate to high concentrations could result from the increased particle motion near the vessel wall and decreased motion near the central axis. In

addition, (Goldsmith 1972) noted that the axial migration increased markedly when viscosity of the surrounding fluid was increased. Increasing the hematocrit, or erythrocyte concentration, increases viscosity. Increasing viscosity would increase the viscous boundary layer, decreasing the inertial forces in blood. Therefore, using the three arguments above, the axial migration may result from a balance of viscous and inertial forces, which changes as hematocrit changes. The flow field of whole blood is highly dependent on the locomotion of RBCs. Whole blood properties may change, depending on the RBC concentration, deformability, aggregation tendency, mechanical interactions, and vessel confinement dimensions (Thurston and Henderson 2006). Aggregation of RBCs usually refers to the formation of rouleaux, a stack of RBCs. Disaggregation of rouleaux is found to occur at shear rates greater than 10 s^{-1} and complete disaggregation occurs at a shear rate of about 200 s^{-1} (Chien 1970; Snabre, Bitbol et al. 1987). At larger shear rates, the rouleaux begin to bend as they rotate in the fluid, increasing the stresses on the bonds between RBCs. In addition, the liquid-like spin of RBCs at higher shear rates could also increase the stresses on the bonds.

The RBC locomotion is considered here because of its significant importance to platelet and thrombus constituent locomotion. Particles in blood other than RBCs are lower in volume fraction and therefore passively orient in accordance with the fluid forces. Platelet motion in the absence of RBCs is now described; similarly plasma proteins could exhibit motion like platelets, or may exhibit a uniform concentration like molecular dynamics. Rigid spheres and discs have been found to migrate away from the wall of a cylindrical vessel, similar to RBCs, which is possibly due to wall collisions. In contrast with RBCs, rigid spheres and discs tend to also migrate away from the central axis, which has been attributed to inertial forces in the fluid, specifically, lift forces (Saffman 1965) for neutrally buoyant particles. The migration away from the central axis and away from the wall is known as tubular pinch. Tubular pinch only occurs for dilute solutions, where particle collisions have secondary effects. This particle migration has a

tendency to occur for Reynolds numbers larger than 1. Tubular pinch migration has been seen with platelet concentrations in platelet rich plasma (Aarts, van den Broek et al. 1988).

The maximum concentration of particles has a tendency to be found near 60% of the cylindrical radius away from the center axis at low Re. Platelets shift toward the central axis when they lag the flow, and shift toward the wall when they lead it. (Matas, Morris et al. 2004) study tubular pinch for Poiseuille flow at physiologically relevant Reynolds numbers (67-2400) for arterial flow. They found that peak particle concentration moves toward the wall as Re increases. Reynolds numbers around 200 have a location of 70-80% the radius away from the central axis. In addition, another peak in concentration can occur more toward the central axis as the Re increases. Rigid particles have been found to shift toward the central axis as the concentration increases. It is likely that plasma proteins either exhibit motion similar to platelets, or exhibit motion that results in a uniform concentration.

The rigidity of platelets results from a circumferential band of microtubules that maintain the platelet shape. Platelets are formed in cytoplasm of megakaryocytes in bone marrow and actually make up approximately 0.25% of the blood by volume. The average platelet concentration per microliter of blood is in a range of 150,000 to 300,000. Inactivated platelets usually have a discoid shape, as seen in Figure 4 and are smaller than erythrocytes. Activated platelets have more of an amorphous shape with prongs that sting out. Activation of platelets will be described in the section devoted to the process of arterial thrombogenesis.

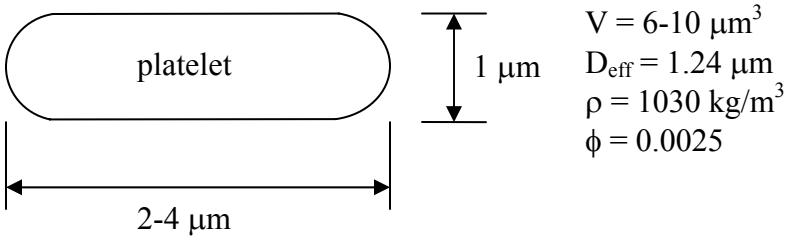

Figure 4: Diagram of platelets with list of parameters

In whole blood, platelets migrate differently, likely due to the presence of RBCs. RBCs dominate collisions with platelets, due to their, generally, higher momentum. In addition, the presence of RBCs changes the overall flow field, as was noted by the effect on viscosity. Platelet and plasma concentrations are askew in whole blood, with a high concentration near the vascular wall and a low concentration near the central region, dominated by the presence of RBCs. This effect is known as margination; similarly it is known as plasma skimming, where the small size of the platelets could cause them to be squeezed out of the central flow, like plasma. The localization is prevalent in arteries (Tangelder, Slaaf et al. 1982; Tilles and Eckstein 1987; Aarts, van den Broek et al. 1988). The RBCs are speculated to cause the platelets to expel toward the wall region, since platelets have been found to concentrate in an inverse fashion from RBCs. There is also speculation that platelet transport toward the vessel wall is increased from a shear rate-dependent rotary motion (Keller 1971), increasing platelet transport by several orders of magnitude from Brownian motion diffusion of platelets. The tubular pinch effect may act synergistically with collisions among erythrocytes and platelets, and therefore may contribute to the localization of platelets near the vessel wall. The margination effect described here is less prominent in pulsatile flow (Chun and Wootton 2002). The pulsatile nature can change equilibrium positions to move closer to the wall (Goldsmith 1972).

Both increasing hematocrit and increasing the shear rate increases the near wall platelet concentration in whole blood; (Aarts, van den Broek et al. 1988) found this using *in vitro* experiments. (Tangelder, Slaaf et al. 1982) used rabbit arterioles to evaluate *in vivo* small vessel platelet concentrations. They labeled platelets with Acridine Red and leukocytes with Acridine Orange and studied the blood flow using fluorescence microscopy. (Aarts, van den Broek et al. 1988) used a laser-Doppler technique, which has high resolution, with RBC ghosts in place of RBCs. They focused on larger blood vessels under high shear conditions. The ghosts provide a good physical model for red blood cells assuming a large enough concentration of ghost cells. For 40% hematocrit, Aarts found 72%, 79%, and 85% of platelets in the wall region for 240, 760, and 1260 s^{-1} respectively. His shear rate to RBC volume fraction results can be seen in Table 1.

Shear rate s^{-1}	% Hematocrit			
	0	20	40	60
240	33%	59%	72%	71%
760	34%	66%	79%	79%
1260	38%	73%	85%	90%

Table 1: % of average platelet concentration that is found in the outer 3/2 of a 1.5 cm diameter tube (Aarts, van den Broek et al. 1988). These results show how the platelet concentration near the wall changes based on platelet margination. One should reference the Aarts paper to obtain plots of the actual concentration variation along the blood vessel diameter.

(Aarts, van den Broek et al. 1988) noted that the effect of increased concentrations shown in, Table 1, decrease when the average number of platelets in the flow increases. The quadratic relationship is presented in Figure 5, where the actual physiologic concentration generally ranges from 150,000 to 300,000 platelets/μl.

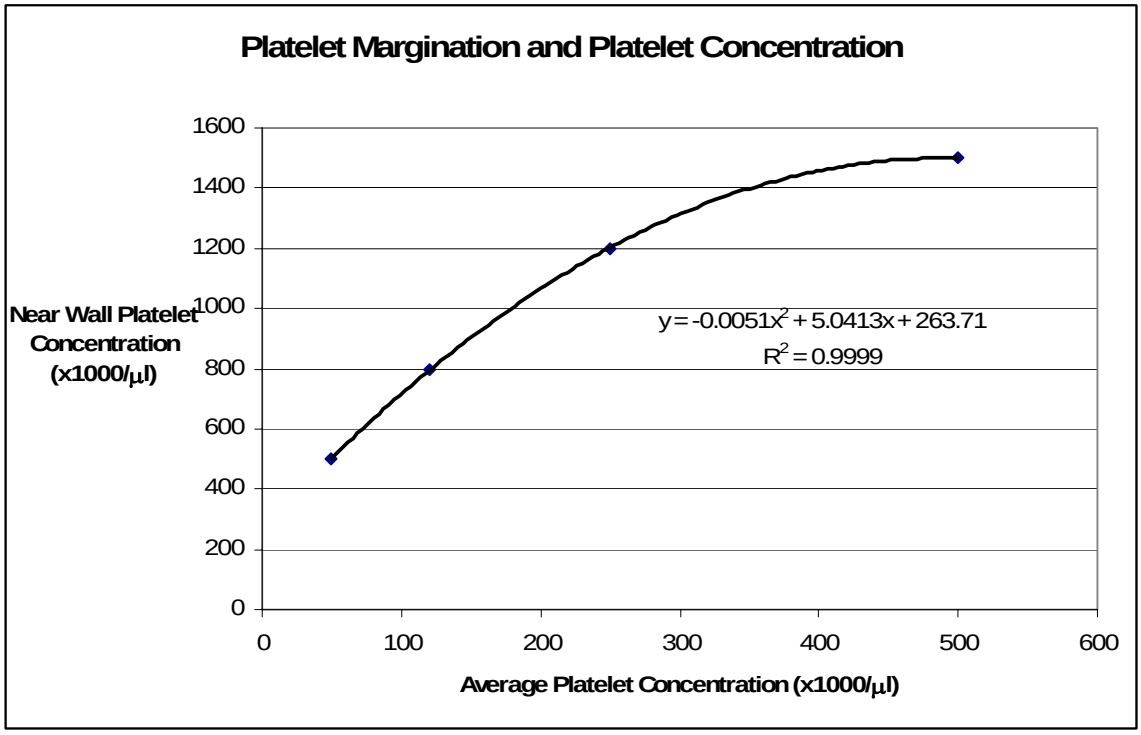

Figure 5: Near wall platelet concentration change with respect to average platelet concentration for hematocrit of 0.4 and shear rate of 1200 s^{-1}. The plot is generated from data given in (Aarts, van den Broek et al. 1988).

A wall shear rate of 1260 s^{-1} only results in approximately a 5 fold increase in platelet concentration at the wall. This result is not precise, since the resolution by Aart's experiments is limited, but the order of magnitude for increased platelets at the wall should be the same. Adhesion of platelets in relation to thrombus generation is dependent on the presence of platelets at the thrombus site, as well as the kinetic rate of bonding. Margination effects, in exclusion of any other effects could only marginally increase the presence of platelets at the wall. However, the increased concentration of platelets near the wall would increase the number of mechanical induced forces caused by other platelets. The concentration in relation to motion of particles due to mechanically induced forces can be found in data collected by (Zydney and Colton 1988). The increased motion of particles in the plasma skimming layer would result in an increased rate of platelets to wall, as well as increased rate of platelet motion from the

wall, essentially generating a mixing effect. If platelets at the wall adhere to the thrombus site, then additional platelets could normally only reach the site through diffusion. However, the increased mixing of platelets enhances diffusion and allows for the replacement of platelets near the wall that had adhered to the thrombus site.

Margination increases mechanical interactions between particles near a vessel wall, which was found to have shear rate dependency. In addition, shear rate also magnifies mechanical interactions between particles. Mechanical interactions described here, are denoted as collisions, although the particles might not actually touch each other. Platelets have actually been found to form doublets, in which case they do not touch (Goldsmith 1972). In addition, the disturbance to the flow field near a moving platelet will likely repel an incoming platelet before they actually touch. Shear rate can affect collisions through an increase in the velocity gradient. An increased velocity gradient increases the velocity differential between two neighboring streamlines, allowing one particle to overtake another. Therefore, a particle on one streamline will collide with a particle on a lower streamline at a faster rate, increasing the collision magnitude. This would also increase the number of collisions at a given time, as the velocity differential between two neighboring particles increase. Shear rate magnification of collisions could occur through fluid motion from rotating particles, causing a mixing effect near a given particle. The rotational motion generates eddies, which disturb the flow, causing increased particle motion, by exerting drag forces on neighboring particles. The rotational velocity of a particle increases as the shear rate increases, since velocity at one end of a particle will increase at a greater rate then the velocity at the other end as the shear rate increases.

To summarize, shear rate likely dominates the number and magnitude of particle collisions. Multiple interactions occur at one time and the motion of an individual particle should exhibit statistical behavior similar to the random walk process, Brownian motion. These ideas of increased motion are supported in a paper by (Zydney and Colton

1988). Therefore, shear rate is likely the dominating factor involved in generating platelet motion to the wall of a vessel. This idea is a major focus of this thesis. Shear rate in blood flow can change through a number of factors. For example, RBCs cause blunting of a velocity profile, so that the profile is between Poiseuille and plug flow. The blunting will vary depending on the RBC localization and hematocrit count. In straight tube flow, RBCs increase the shear rate near the wall, making a larger increase in platelet motion. (Goldsmith 1972) studies the velocity profiles and how they change to either plug or Poiseuille flow under certain conditions. In this study the hematocrit is generally held constant. The shear rate should only change with the changing of the vessel diameter and fluid speed, resulting from the stenosis geometry.

Atherosclerosis

Atherosclerotic plaques or lesions generally develop in specific arteries and can result in the initiation of a thrombotic event. Atherogenesis has been found in areas of altered fluid mechanical characteristics, specifically low and oscillating shear stress (Caro, Fitz-Gerald et al. 1971; Ku 1997; Tarbell 2003). These characteristics exist in the carotid artery sinus, abdominal aorta, coronary arteries, and the superficial femoral arteries, all of which are prone to atherosclerosis. The characteristics of these arteries can be found in Table 2. Such areas have flow separation and high particle residence times. One plausible theory is that the intimal layer of the arterial wall thickens to maintain a normal wall shear stress of approximately 15 dynes cm^{-2} (Ku, Giddens et al. 1985; Glagov, Zarins et al. 1988; He and Ku 1996; Ku 1997). The value is consistent throughout the vasculature of a particular animal and across different animal species. This growth is believed to be caused by an increase in membrane transport for macromolecules such as low density lipoproteins that results from low shear regions (Ma, Li et al. 1994; Tarbell 2003). Data was put together (Thubrikar, Labrosse et al. 2001)

comparing intimal thickening to the mean shear stress and determined that most thickening occurs when the shear stress is less than 10 dyn/cm^2.

Vessel	Diameter (mm)	Average flow rate (ml/s)	Mean Reynolds number	Mean wall shear rate (s^{-1})	Mean wall shear stress (dyne/cm^2)
Femoral artery†	5.0	3.7	280	300	11.00
Common carotid†	5.9	5.1	330	250	8.90
Ascending aorta†	23-43	36.0	3200-6100	45-310	1.6-11
Carotid sinus†	5.2	3.3	244	240	0.84
Left main coronary*	4.0	2.9	240	460	16.00
Right coronary*	3.4	1.7	150	440	15.00

Table 2: Atherosclerotic prone arterial flow parameters. † (Goldsmith and Turitto 1986) *(He 1993)

The lesion or fibrofatty plaque consists of a core of lipid, cells, connective-tissue elements, debris, and a covering fibrous cap (Stary, Chandler et al. 1995). A fibroatheroma refers to the formation of fibrous tissue in an atheroma, which mainly consists of collagen between endothelial cells and the lipid core (Richardson 2002). A rupture of this fibrous cap is believed to be the cause of the acute events resulting in thrombosis (Davies and Thomas 1985). Such an event is difficult to predict since the thrombus forms at an expedited rate (Flannery 2005). Approximately 60% occur in the shoulder, while 40% occur in the center of the plaque (Maehara, Mintz et al. 2002). Fatigue may be the cause of rupture at the shoulder. The shoulder is assumed to be the region of highest stress in an atherosclerotic plaque (Dalin, Chun et al. 2002). However, the stresses should be well below the finite element analysis average rupture circumferential stress of 545 kPa (Cheng, Loree et al. 1993). Therefore, other mechanisms such as material fatigue or material imperfections would be required for structural failure.

The fatigue could result from compression and tension oscillations, associated with cyclic low pressure at the apex of a stenosis. The increased fluid velocity, resulting from the stenotic region, causes a decrease in pressure at the apex of the stenosis from Bernoulli's law. Bernoulli's law is only an approximation for the pressure. However,

this pressure reduction has been shown experimentally and computationally to decrease below the vessel external pressure causing the lumen to compress (Downing and Ku 1997; Dalin, Chun et al. 2002). This results in the choking of flow and possible cyclic fatigue of the cap resulting from the cyclic motion. Fatigue may act synergistically with another mechanism, the presence of an impurity in the cap (Vengrenyuk, Carlier et al. 2006). Vengrenyuk et al. suggest that an impurity in the cap, such as a calcified dead macrophage may result in a 2 fold increase in the stresses seen in that region. Material imperfections like this cause a stress concentration near the imperfection.

The ruptured region exposes the blood flow to the underlying subendothelial and medial layers of an atheroma, instead of the usual endothelial layer. The underlying layers induce platelet adhesion, which has been most closely associated with collagen in the extracellular matrix (Baumgartner 1977; Sakariassen, Joss et al. 1990; Sixma, van Zanten et al. 1997; Richardson 2002; Vanhoorelbeke, Ulrichts et al. 2003). In addition the fissure may result in exposure to lipids, macrophages, smooth muscle, and addition to other constituents of a blood vessel (Richardson 2002). Platelets would likely adhere to most materials, most notably collagen, excluding endothelial cells and normal blood constituents. Atherosclerotic lesions result in what is known as a stenotic shape. This blood vessel constriction is assumed to directly affect thrombus formation. Therefore the geometry has been studied extensively (Young and Tsai 1973; Young 1979; Berger and Jou 2000). The stenotic geometry results in unusual particulate dynamics. However, to understand mass transport near an atheromatic lesion, it is necessary to understand the flow characteristics based on the geometry.

Stenosis Characteristics

As previously stated, a stenosis is a constriction in the blood vessel. An atheroma can be shaped in many ways. Most commonly they can be characterized as a concentric or an eccentric lesion. However, an atheroma may also have multiple irregularities. The

simplest shape for characterizing a stenosis is a concentric shape. This allows computational models to use axisymmetric geometry, which reduces computational expense. Studies have been performed to analyze a stenosis since plaque cap rupture occurs in this region. In addition, thrombus formation commonly develops in areas of low flow, high shear rates, and turbulence (Folie and McIntire 1989) in *in vitro* experiments of collagen coating. The stenotic geometry has the potential to embody all of these characteristics and has been studied by (Young and Tsai 1973; Young 1979; Berger and Jou 2000). The percent stenosis is often denoted by a reduction in area, or diameter to describe the degree of constriction. A stenosis is commonly described by clinicians as the percent diameter reduction in a vessel, since this is easiest to evaluate based on imaging techniques. Stenosis by area, Equation 7, is usually described by engineers, since it is directly related to the flow rate.

Equation 7: % Stenosis by area

$$\%Stenosis = \frac{A_1 - A_2}{A_1} * 100\%$$

There are three regimes that can be associated with flow through a stenosis (Young and Tsai 1973). For non-pulsatile low Reynolds numbers, flow is laminar, unidirectional, and there is no separation. For higher Reynolds numbers, flow remains laminar, but there is some back-flow and separation. The third regime is associated with significant turbulence. The post-stenotic recirculation region is associated with separated flow that that reattaches further downstream. It is similar in concept to a cylinder in cross flow. The critical Reynolds number for flow separation is dependent on geometry (Young and Tsai 1973). The reattachment moved further downstream, as Reynolds number increased. Young and Tsai extensively evaluated flow differences between an axisymmetric and an eccentric stenosis. Additionally, they evaluated the critical Reynolds number for turbulence upstream of a stenosis. Periodic vortex shedding results downstream of stenoses having a Reynolds number greater than or equal to 375

(Bluestein, Gutierrez et al. 1999). They also found that the vortices initiate closer to the stenosis, have shorter lifespans, and move from the central axis of the vessel toward to the vessel wall, as the Reynolds number increases.

The pressure distribution for a stenosis begins to decrease in the converging region, reaching a minimum around the apex. The wall shear stress increases in this region, reaching a maximum at the apex. The pressure slowly rises again in the diverging region, but returns to a value lower than the pressure upstream of the stenosis, causing an overall pressure drop across the stenosis. The vessel wall has been found to dilate in the post-stenotic region, which could result from the sudden rise in pressure (Young 1979) coupled with the decrease in velocity due to area expansion. The wall shear stress decreases in this region, and can become negative for high Reynolds numbers, as the flow separates (Young and Tsai 1973). There have been extensive studies concerning how the maximum wall shear moves with respect to the degree of stenosis and Reynolds number, but there has been no consensus on the subject (Berger and Jou 2000); blood vessels have cyclical and nonuniform wall stresses.

Thrombosis Overview

Thrombosis is the pathological formation of a blood clot, which can cause blockage of blood vessels as a result of hemostasis dysfunction. Hemostasis is a necessary body reaction for the prevention of blood loss, but can be life threatening in the event of thrombus formation. Two main categories have been created to describe two distinct types of thrombi. One category is red thrombosis, which usually occurs in the veins. This thrombus is usually found in areas of low shear rates and flow stasis. A coagulation cascade develops in these regions resulting in a thrombus mostly composed of platelets and a fibrin reticulum trapping many RBCs. Most red thrombus forms in the recirculation region of vein valves. The name red thrombus results from the significant RBC composition in the thrombus. The other type of thrombus is a white thrombus,

which generally forms in arteries. White, or arterial thrombosis has been found to occur under high shear rates, and its contents are densely packed, unlike a red thrombus. White thrombus mostly consists of platelets and fibrin and plasma proteins. It also has relatively few RBCs, thus explaining the origin of the name, white thrombus. Acute coronary syndrome (ACS) is the focus of this study because of its relevance to myocardial infarction. The coronary flow with a stenosis is associated with high shear rates, and thus white thrombus. Red thrombus is generally referred to as coagulation, while white thrombus is the usual type referred to when the type is not specified. White thrombus formation will be just denoted as thrombus for the remaining portion of this thesis.

Platelets typically circulate as inert particles. However, they are prone to adhesion when they come in contact with a substance other than normal blood constituents or endothelial cells. Platelets are particularly adherent to collagen, which is readily exposed after a plaque cap rupture. Thrombosis and coagulation can develop when platelets contact a reactive medical device or implantation, depending on the fluid conditions. The initial tethering of platelets to a surface can function irrespective of activation. If platelets become activated, they transform to an amorphous shape and release agonists. In addition, more permanent binding is allowed. Various agonists can synergistically activate additional platelets. Activation can also occur when a platelet reacts synergistically to large shear stresses and residence times. Platelet to platelet binding can begin to occur, causing thrombus aggrandizement, once platelets are activated. As additional platelets transport to this active region, they can deposit and continue the thrombus growth. Growth of the thrombus has been found to surcease in some circumstances. Other times it will grow to full occlusion. The cessation of thrombus growth has been hypothesized to result form embolization. In addition particles will experience higher drag forces as the thrombus nears occlusion. Therefore,

some platelets may skim off the surface, or resist attachment because of these large forces.

Process of Arterial Thrombogenesis and Aggrandizement

Thrombogenesis has been studied for many years, dating back to at least the 1840s during the studies of Rudolf Virchow. Arterial thrombi have been found to overlay ruptured atherosclerotic plaques. A study done by (Friedman and Van den Bovenkamp 1966) showed thrombus overlays on ruptured plaque in 39 of 40 coronary artery segments. (Horie, Sekiguchi et al. 1978) reported that 91 % of occlusive thrombi in coronary arteries form over ruptured plaques. It is possible that the minority of these cases don't show formation on ruptured plaques because of possible thrombus embolization. In normal blood flow, or flow without pathological injuries, platelets act as inert particulates. The mechanisms of thrombus formation are complex and have been assumed to emanate from the marriage of fluid dynamic behavior and mass transport behavior.

Platelet functions associated with thrombus formation can be generalized into three functional categories: adhesion, activation, and aggregation. In addition (Wootton and Ku 1999; Wootton, Markou et al. 2001) suggest that platelet deposition can be divided into three phases, seen in Figure 6, based on experimental results (Markou, Hanson et al. 1993). (Flannery 2005) found very similar results. The three phases are distinct from the three platelet functions.

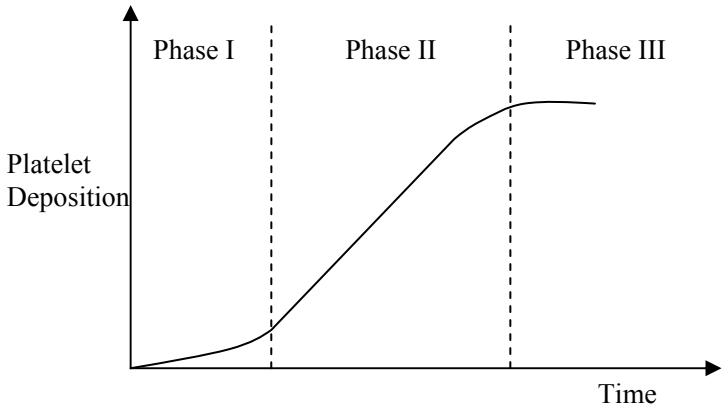

Figure 6: Rate of platelet deposition characteristic divisions

An experimental example of phase I and phase II is represented in Figure 7. The plot was developed by (Flannery 2005) who extracted the platelet deposition values through an image analysis of the stenotic tube at various time points.

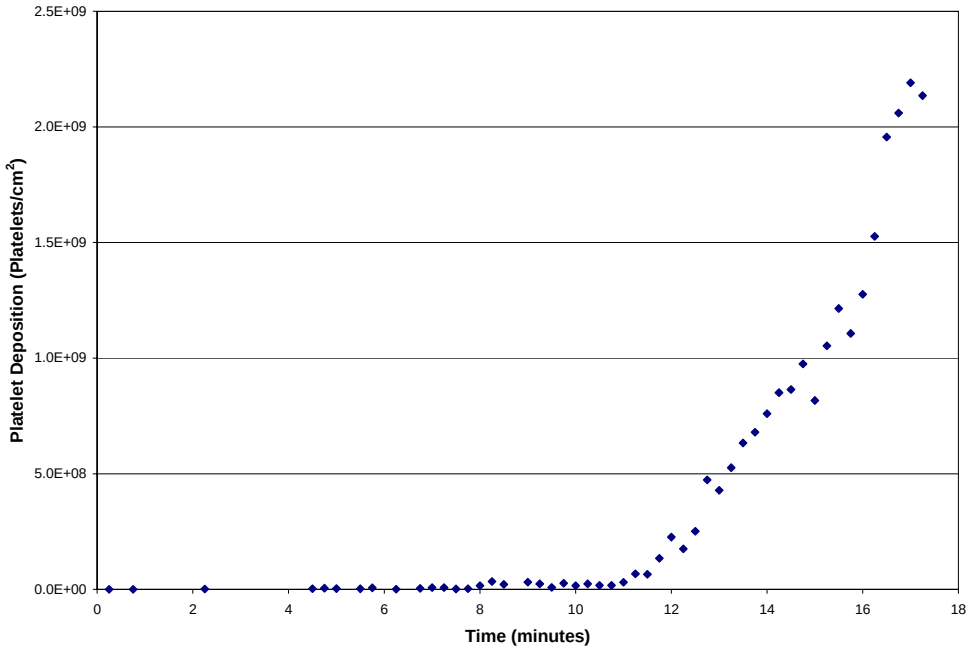

Figure 7: Plot of thrombus growth on a collagen coated glass tube. The data is from a 85% stenosis of the experimental model used for validation in the current study. Flow cessation was at 16.5 minutes. The diameter of non-stenotic portion of the tube is 1.5 mm. The figure is taken from (Flannery 2005).

The first phase consists of accelerated deposition which could be attributed to initial platelet adhesion. More activation agonists are released as more platelets attach to the thrombus site. In addition there are different mechanisms that can limit the rate of platelet adhesion depending on if it attaches to the ruptured plaque or if it attaches to other platelets. It is assumed that the second phase could begin once a layer of platelets attach to the reactive surface and a steady state of agonist release is reached. The second phase consists of a linear approximation relating platelet deposition and time, known as the acute phase. The final phase is a deceleration phase, which will tend to only occur when there is no occlusion. This is an observation of experiments in our laboratory. The source of deposition rate deceleration has not been determined up to this point. One postulate is that this phase occurs because of the large drag forces on individual platelets or platelet aggregates, which increases the stress on formed bonds. In addition, adhered platelets may be skimmed off because of the significant amount of particulates moving past the apex region at a very high rate. This could create a sand blasting effect. A final explanation is that the deposition rate may slow down, because platelets pass by at a quicker rate and may not leave enough time for an adhesive reaction.

The intermittent deceleration phase increases the difficulty in predicting full thrombus occlusion. In addition, there have been few studies on this phenomenon. Large fragments of thrombus may also embolize off of the forming thrombus. This is known as thromboembolization and is also a clinical problem. Large masses rake off, flowing distal to the thrombus, causing blockage downstream. Studies have been done to model embolization in both steady and pulsatile flows (Hanson, Kotze et al. 1985; Basmadjian 1986; Basmadjian 1989). Badimon found that embolizing shear stresses are approximately five times the maximum wall shear stress, 15 dynes/cm^2, in the absence of a thrombus. Forces that act to disengage the thrombus have been found to be a function of protrusion height, wall shear rate, and exposure time. This is similar to the function associated with platelet activation. The nature of the underlying surface has also been

found to play a role in the embolizing forces. Thromboemolization traits may be cognate with particle embolization.

The location for thrombus formation near a stenosis is dependent on whether whole blood or platelet rich plasma (PRP) is used. PRP results in the largest aggregation of platelets in the recirculation region of a stenosis (Schoephoerster, Oynes et al. 1993; Bluestein, Niu et al. 1997; Raz, Einav et al. 2002). They attributed the aggregation location to the entrapment of agonists and platelets in one location, after they experience elevated shear stresses. The number of platelets deposited was directly correlated with the length of the recirculation zone (Schoephoerster, Oynes et al. 1993). The lowered shear stress also reduces the chance of embolization, thus increasing the rate of accumulation in that region. These researchers also found increased platelet deposition in the converging region of the stenosis and attribute it to contraction of streamlines relating to convective acceleration. Other studies have found the highest number of platelets deposited to be in the apex region (Folts, Crowell et al. 1976; Badimon and Badimon 1989; Lassila, Badimon et al. 1990; Markou, Hanson et al. 1993; Wootton, Markou et al. 2001; Flannery 2005), with secondary deposition in the converging region. Plaque cap rupture, *in vivo* is assumed to be highly localized (Richardson 2002). This would be the point of thrombus initiation, where there is more significant exposure of platelets to agents such as collagen. However, *in vitro* studies have shown that if a stenosis is completely covered in collagen, signifying no endothelial cells in a vessel, then the thrombus forms in the region of highest shear stress, even without the localized injury (Flannery 2005).

Adhesion

The adhesion of platelets occurs on the subendothelium and atheroma contents through platelet membrane receptors, glycoproteins (Gps), which are on the peripheral of each platelet. Collagen, Proteoglycans, nidogen, laminin, and fibulin are the main

basement membrane components exposed to the blood in the occurrence of endothelial disruption, often resulting from atheroma plaque rupture (Ruggeri 2002). Collagen is likely the main instigator in the adhesion of platelets (Baumgartner 1977; Saelman, Nieuwenhuis et al. 1994; Sixma, van Zanten et al. 1997; Ruggeri 2002). However, platelets are reactive with most surfaces other than endothelial cells. The medial layer of a blood vessel may be exposed in addition to the subendothelial layer. Glycoproteins are involved in the initial tethering of platelets to the wounded vessel, as well as in platelet to platelet bonding. Glycoproteins, GPIV (Tandon, Ockenhouse et al. 1991), GPVI (Moroi, Jung et al. 1989), and GPIaIIa (integrin-$\alpha_2\beta_1$) (Kunicki, Orchekowski et al. 1993; Saelman, Nieuwenhuis et al. 1994) bind to collagen in the exposed subendothelial layer. (Ruggeri 2002) suggests that GPIaIIa is the dominant non-activated adherent glycoprotein, while GPVI is involved with signaling the activation of the platelet once it is attached with collagen. He also suggests higher affinity for GPIaIIa attachment to collagen once a platelet is active.

von Willebrand Factor (VWF) may also act as a bridge between platelets and subendothelial collagens (Savage, Saldívar et al. 1996; Novák, Deckmyn et al. 2002; Ruggeri 2002). VWF is vital in platelet adhesion at high shear rates (Savage, Saldívar et al. 1996; Novák, Deckmyn et al. 2002; Vanhoorelbeke, Ulrichts et al. 2003; Ruggeri, Orje et al. 2006). Its function is considered to be dynamically regulated by shear stress (Savage, Saldívar et al. 1996; Ruggeri, Orje et al. 2006). GPIbα, a component of GPIb-IX-V complex, initially transiently adheres (800-20000 s^{-1}) to surface VWF to slow the platelet, or stop the platelet (>20000 s^{-1}) (Ruggeri, Orje et al. 2006). Once the platelet activates, GPIIb-IIIa (integrin $\alpha_{IIb}\beta_{3)}$ allows a more permanent binding (Savage, Saldívar et al. 1996) to VWF. The binding of GPIbα to VWF becomes essential for normal platelet adhesion above a threshold shear on the order of 1000 s^{-1} (Savage, Saldívar et al. 1996; Ruggeri 2002; Ruggeri, Orje et al. 2006). Savage et al found that platelets bound to VWF can withstand at least 1 μN of drag force. Such strengths are necessary as the

shear rate increases as a thrombus grows. (Li, Li et al. 2004) separated GPIbα from platelets, and showed a GPIbα-VWF shear induced binding, giving additional evidence that platelet adhesion is shear induced. It was found that minimal binding with VWF occurs under low shear conditions, but that binding increases as the shear rate increased (Kroll, Hellums et al. 1996; Savage, Saldívar et al. 1996). Platelets may continue to roll along the surface, at approximately 10 μm/s (Savage, Saldívar et al. 1996), before they become more permanently bound to a location.

VWF is thought to play a vital role in adhesion, explained above, and also in aggregation. It is a multimeric glycoprotein, synthesized and stored in α-granules of megakaryocytes/platelets (Sporn, Chavin et al. 1985), as well as the Weibel-Palade bodies of endothelial cells (Ruggeri, Lombardi et al. 1982) and is released after induction by agonists. VWF protomers are multimers of variable polymerization (Novák, Deckmyn et al. 2002; Dong 2005). The multimeric VWF is usually found as a coiled structure that is about the size of 100 to 300 nm (Novák, Deckmyn et al. 2002). VWF may uncoil at shear stresses greater than 35 dyn/cm^2 or 3.5 N/m^2 (Siedlecki, Lestini et al. 1996). This would be associated with a shear rate of approximately 1000 s^{-1}, which commonly exists at a stenotic throat. 1000 s^{-1} is approximately double the wall shear rate of healthy coronary arteries. (Novák, Deckmyn et al. 2002) suggests that the morphological change may not be likely on physiologically relevant surfaces. When VWF is released from endothelial cells, it is rich in the ultra-large form (ULVWF), but is usually quickly cleaved by ADAMTS13 (Dong 2005; Donadelli, Orje et al. 2006). ULVWF can be at least 3mm long (Dong 2005). Such a length could have significant effect on thrombus formation, since platelets do not have to be activated to bind through GPIbα, and then more permanently through GPIIbIIIa, once the platelet is activated. This could theoretically develop into the fibrin tail that is described later on.

Platelet adhesion to the vessel wall increases with shear rate up to at least the value of 40000 s^{-1} (Flannery 2005). Fibrin-1, found in smooth muscle can bind to fibrinogen and may contribute to thrombogenesis and aggrandizement, since GPIIb-IIIa readily binds to fibrinogen at low shear rates (Godyna, Diaz-Ricart et al. 1996; Savage, Saldívar et al. 1996). The post-stenotic recirculation region behind the stenosis would have low enough shear stress for this phenomenon to occur. Therefore, a rupture at the shoulder may result in a red thrombus formation, mostly consisting of a fibrin mesh. However, as the structure grows higher shear stress would exist and therefore, fibrinogen would have little effect there. The number of the dominant glycoproteins can be found in Table 3.

Table 3: Glycoprotein count on individual platelets

Glycoprotein	Number on a platelet	Reference
GPIaIIa	1000-2000	(Pischel, Bluestein et al. 1988; Kunicki, Orchekowski et al. 1993; Saelman, Nieuwenhuis et al. 1994)
GPIbα	25,000	(Berndt, Gregory et al. 1983; Li, Li et al. 2004)
GPIIb-IIIa	50,000	(Bennett and Vilaire 1979; Johnston, Heptinstall et al. 1984)

A diagram of platelet adhesion, activation, and aggregation is shown in Figure 8 to clarify the discussion of the dominating factors involved in thrombus formation. First platelets transiently attach to the site of injury through GPIbα–VWF and GPIa-collagen. The platelets activate under synergistic activity of agonists, shear stress, and binding of GPVI. The GPIIb-IIIa receptors become active allowing VWF and fibrinogen binding, in addition to more permanent binding to surface VWF.

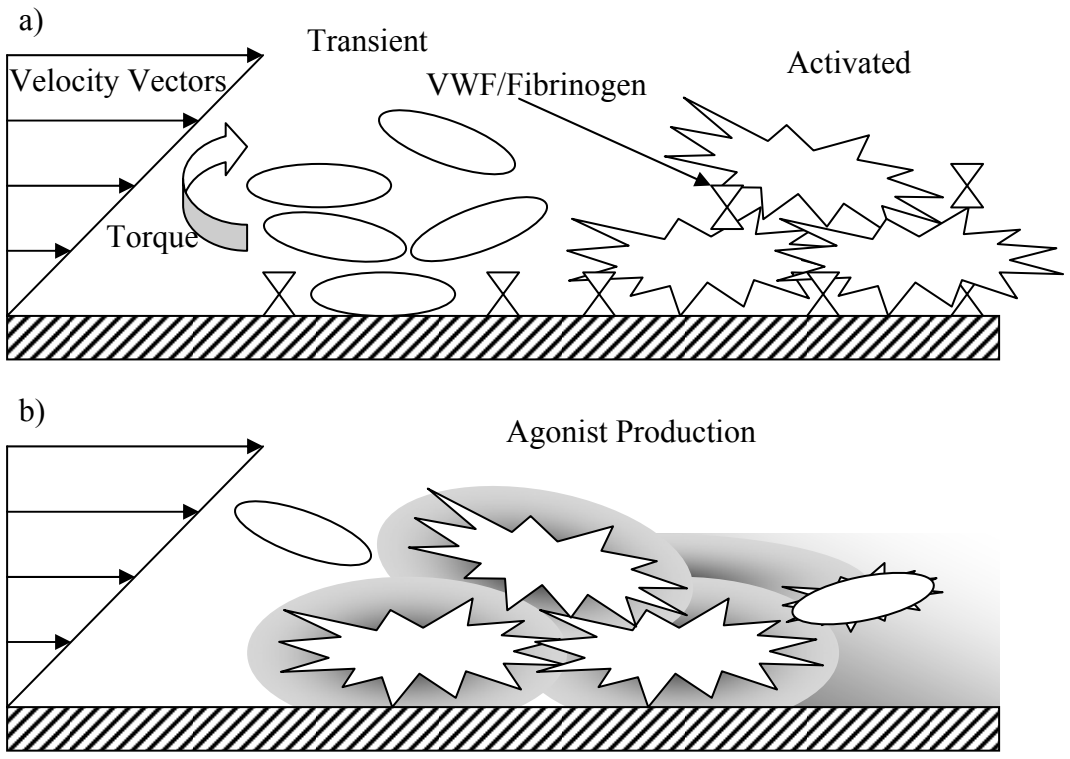

Figure 8: Diagram of platelet adhesion and aggregation. A) Platelet adhesion and aggregation under high shear stress. VWF and fibrinogen attach to the collagen and activated platelets. Inactivated platelets transiently roll and rotate near the thrombus, while the activated platelets are relatively motionless. B) Agonist production near activated platelets. Platelets entering the region may become activated if a sufficient amount of agonists synergistically activate platelets.

Figure 8 b) shows a diagram which shows agonist production from activated platelets. (Folie and McIntire 1989) showed that it is unlikely that the agonists exist far from the active thrombus region. The agonists concentrate around the thrombus and convect downstream as they become more diluted. A magnified schematic of the platelet reactions is included in Figure 9 to provide further clarification of the platelet interactions.

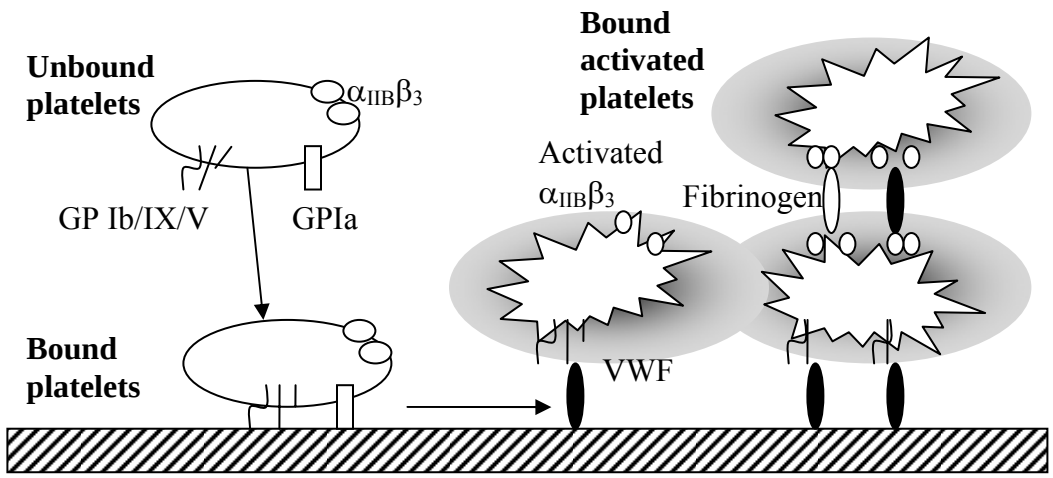

Figure 9: Main mechanisms involved in initial platelet tethering. Platelets transport from the free stream to the exposed reactive surface. GPIbα transiently binds to the surface. The platelet becomes activated through agonists, GPIb-IX-V attachment signaling, and shear. This activates the $\alpha_{IIB}\beta_3$ receptors in addition to the platelet undergoing a shape change. Activated $\alpha_{IIB}\beta_3$ allows for VWF and fibrinogen binding. VWF is the dominant bridge at high shear stress, while fibrinogen plays a dominant role at low shear stresses. This schematic is loosely recreated from.

The adhesion can occur without platelet activation, but activation must occur for additional aggregation of platelets.

Activation

Activation has been known to occur through chemical stimulation, contact with reactive surfaces, or through mechanical stimulation through shear stress (Bluestein, Gutierrez et al. 1999). Activation causes more permanent adhesion and allows platelet to platelet adhesion, therefore is a necessity for platelet aggregation. Activated platelets change from a disc shape to an amorphous shape with extended pseudopods. They also secrete agonists into the blood stream and activate GPIIb-IIIa. The activation agonists cause a feed-forward loop resulting in activation of other platelets. Platelets without activation agonists are found to have reduced thrombus formation on the subendothelium (Baumgartner, Muggli et al. 1976), which would indicate the importance of platelet activation. Activation initiates with adhesive ligands and excitatory agonists binding to receptors on the platelet membrane. Propagation occurs through intracellular signaling.

One activation pathway is through GPIbα activation of GPIIb-IIIa (integrin-$\alpha_{IIb}\beta_3$) (Li, Li et al. 2004).

High concentrations of agonists exist near the thrombus, but there is a sharp decline in gradient when moving away from the thrombus (Hubbell and McIntire 1986; Folie and McIntire 1989). Convection sweeps away agonists that extend from the thrombus region, which is a function of shear rate. (Hubbell and McIntire 1986) found that the agonists convect away at locations further than 5 μm away from the wall, even at lower shear rates (100 s^{-1}), relative to those that exist at a stenosis. This would lead to the conclusion that platelets do not likely activate through agonists at a distance greater than 5 μm, which is approximately 2 platelet diameters from the wall. This localizes the aggregation to the newly forming thrombus and the atheroma. Local concentration maxima exists for the agonists in the recirculation regions of a stenosis (Folie and McIntire 1989). This results in increased residence time for agonists in that region. Agonists' concentrations are dependent on wall shear rate, thrombus size, and thrombus shape (Folie and McIntire 1989), but display different responses depending on the specific agonist. The agonists' concentrations act synergistically to reach an activation threshold causing more platelets to activate.

Some chemical agonists include Thrombin, which is enzymatically generated on the membrane of stimulated platelets, ADP, from vascular cells and stimulated platelets, Thromboxane A_2 (TxA_2), enzymatically synthesized by stimulated platelets, and epinephrine (Ruggeri 2002). (Hubbell and McIntire 1986) suggest that Thrombin may be the most important agonist, because it is one that maintains concentration well above threshold levels, and is known to structurally stabilize a growing thrombus by catalyzing fibrin formation. They concluded this from evaluation of computations that were based on experimental data. ADP amplifies the responses induced by other agonists and is released from the dense granules of a platelet. (Joist, Bauman et al. 1998) consider ADP release from erythrocytes and suggest that this may contribute to thrombus growth, based

on release at increasing shear rates. Activation can be approximated at 1-3 s based on agonist activation by ADP (Frojmovic and Wong 1991; Frojmovic, Wong et al. 1991).

Aggregation

Platelet aggregation, in the context used here, describes the localized accumulation of platelets on other platelets through bonding at the thrombotic site. Aggregation occurs through different mechanisms, depending on the shear stress. GPIIb-IIIa promotes immediate arrest onto fibrinogen but is fully efficient only at wall shear rates below 600–900 s^{-1}, perhaps because of a relatively slow rate of bond formation or low resistance to tensile stress (Savage, Saldívar et al. 1996). At shear rates between 50 and 900 s^{-1} VWF competes with fibrinogen in GPIIb-IIIa binding, but has a higher likelihood as the shear rate increases. At higher shear rates (>1000 s^{-1}), the binding will be mostly through VWF and GPIIb-IIIa (Alevriadou, Moake et al. 1993; Savage, Saldívar et al. 1996). In 1978 Weiss demonstrated platelet adhesion to a vascular surface is both shear rate and VWF-dependent (Weiss, Turitto et al. 1978), possibly the first experiment to do so. However, binding of GPIIb-IIIa to VWF must occur after activation, while binding of GPIIB-IIIa to fibrinogen can occur without activation.

The shear rates become exceedingly high as a thrombus nears occlusion. Therefore, fibrinogen would have minimal contributions to arterial thrombosis (Savage, Saldívar et al. 1996), but may be involved in stabilizing the thrombus. GPIIb-IIIa contributes to stable adhesion and mediates the immobilization of soluble adhesive proteins. It is a receptor for fibronectin, VWF, vitronectin, and thrombospondin (Kieffer and Phillips 1990). Also, an integrin recognition sequence for VWF has been found in fibrinogen, laminin, and collagen (Pierschbacher and Ruoslahti 1984; Pierschbacher and Ruoslahti 1987). GPIIb-IIIa changes its ligand-binding function after activation and contributes to stable adhesion, which is important in determining whether an artery will occlude (Woodside, Liu et al. 2001; Li, Li et al. 2004). Stability of the thrombus is

essential when considering complete occlusion. Otherwise, particulates embolize off of the thrombus and occlusion would not occur.

Mechanisms at high shear rates

Shear rates increase in the converging region of a stenosis, and continue to increase as platelets aggregate and locally narrow the vessel lumen. In addition, velocities in this region become very high, decreasing the residence time for platelets at the vessel wall. A simple calculation, assuming a platelet travels at the fluid speed, suggests that a platelet traveling at a platelet length from the wall travels its own length in 2.5 ms for a wall shear rate of 500 s^{-1}. This calculation is performed by taking the inverse of the shear rate. As the platelet enters the apex of the stenosis (20000-40000 s^{-1}), there is a very short time for it to adhere to the vessel wall, 25-50 μs. However, as stated previously, this is where thrombus prevalently forms, which continues to increase the shear rate at the apex. Adhesion mechanisms therefore must be extremely fast. In addition activation has been found to take time on the order of seconds (Frojmovic and Wong 1991).

A new theory has been developed regarding platelet attachment at high shear rates. The previous theory was that GPIbα transiently binds to VWF and rolls on the surface until there is more permanent binding through GPIIb-IIIa after activation. (Ruggeri, Orje et al. 2006) has suggested that GPIbα will actually develop a relatively static bond with soluble VWF as the shear rate exceeds 20000 s^{-1}. The VWF-GPIbα bond will actually remain static for minutes. This is sufficient time for more permanent binding through activation. At 24000 s^{-1} (Ruggeri, Orje et al. 2006) observed platelet aggregation at 100-200 μm away from the reactive wall. They also found that aggregates that do not develop stationary adhesion at these high shear rates will disaggregate when they enter lower shear regions. Therefore, aggregation through the VWF-GPIbα binding would unbind in the recirculation region of a stenosis. They also state that the platelet-

VWF aggregate elongates, stretching out the bond, when the aggregate adheres to the surface. They found promotion of additional platelet binding when this occurred. Binding of platelets to VWF probably competes with cleaving of VWF through ADAMTS13 in thrombus formation (Donadelli, Orje et al. 2006). They found that reduction in cluster size could occur up to 70%.

Shear dependent margination and effective diffusivity are both transport related phenomenon and could be similar in nature. These phenomena are described in the biorheology section. Increased margination would locally increase the concentration of platelets at the wall, and thus the number of collisions. The term collision, here, includes the expulsion of platelets due to fluid forces generated by the motion of other platelets. As particle collisions or speeds increase, margination phenomena may be affected. However, at this point margination and effective diffusion are not well understood from a theoretical standpoint. They have both been shown to increase as shear rate increases, as previously described. Therefore, one could deduce that increasing shear rate would increase platelet transport to the blood vessel wall. The maximum transport would exist near the peak of the stenosis. The culmination of all of the shear rate dependent effects on platelet accumulation may result in the actual rate seen experimentally. The culmination of all effects is shown in a plot of past experiments in Figure 10.

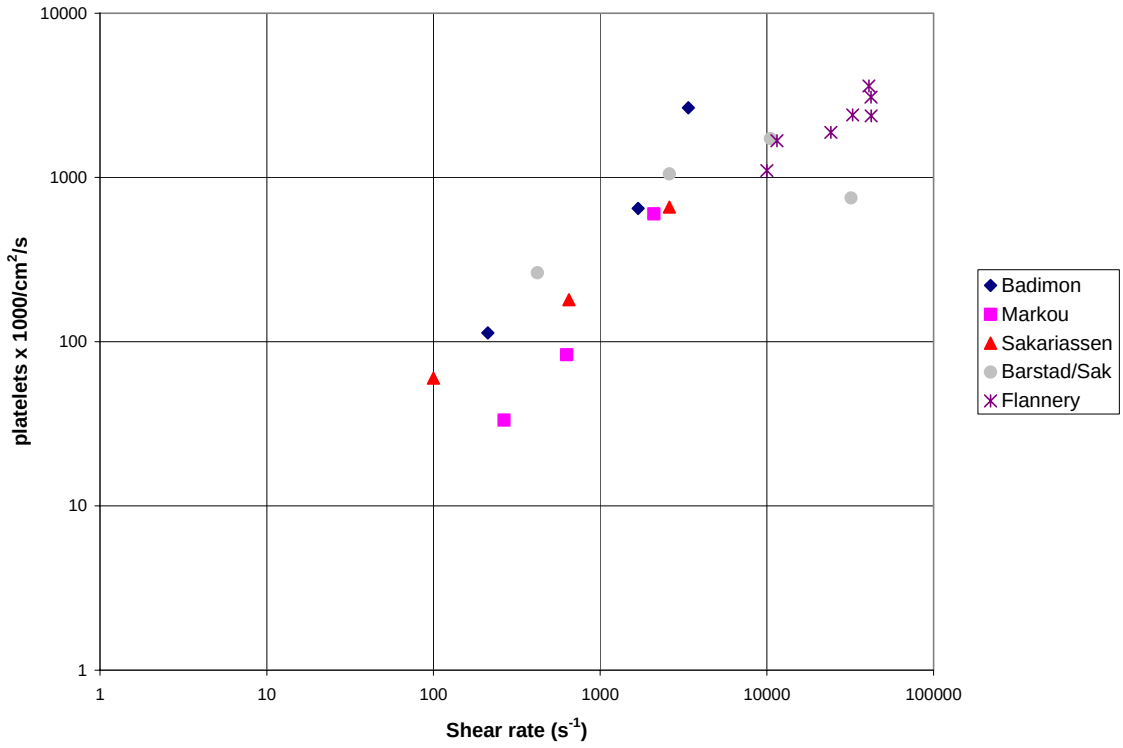

Figure 10: Plot of platelet deposition with shear rate in the first five minutes of thrombus deposition, on a log-log plot. Data was taken from (Badimon, Badimon et al. 1986; Sakariassen, Joss et al. 1990; Markou, Hanson et al. 1993; Barstad, Kierulf et al. 1996; Flannery 2005).

Fibrin tail

Fibrin tails have been found to form on a growing thrombus (Hanson, Griffin et al. 1993; Barstad, Roald et al. 1994; Barstad, Kierulf et al. 1996; Wootton 1998; Flannery 2005). Barstad found that the tail forms particularly at high shear rates and develops relatively quickly in the thrombotic process. However, a collection of data from Wootton showed that the fibrin tail, on average, was more prominent at low shear rates. Tail development was intermittent at higher shear rates. Fibrin polymerization proactive environmental conditions exist in the recirculation region. Therefore, the tail may result from the polymerization. In addition the tail has been found to be rich in fibrin and red blood cells (Davies 1990; Wootton 1998). Another possibility is that the tail develops from VWF and platelets attaching and rolling on the thrombus surface. This is supported

from the results of (Savage, Saldívar et al. 1996; Flannery 2005), where the histological sample consisted mostly of platelets VWF, and fibrin. Further downstream, he found a fibrin rich region with RBCs trapped within the mesh.

The tail can develop to a substantial length of 10 to 20 millimeters. Another possibility is that a tail begins to develop with platelets and VWF on the thrombus, while at the same time a tail develops in the recirculation region. These may attach to each other at a later stage, since the post-stenotic turbulent region would cause the tail to oscillate. In addition the RBC and fibrin mesh may develop underneath the forming tail of platelets and VWF. It would be difficult to capture this tail in a model because the model may need to consist of a rolling condition for platelets and the development of a fibrin mesh. There would be very large drag forces on the tail due to the significant length. However, the tail has not been found to detach. Detachment of the tail could cause ischemic conditions downstream of the occluding thrombus. This would indicate the significant strength of the thrombus particulate bonding. While interesting, the fibrin tail will not be included in the model design, since there is still little that is known about the tail. In addition the main thrombus structure has been found to be the significant factor in ischemic conditions.

Surface Roughness

Surface roughness has a number of definitions when referring to thrombosis. First of all, a rough surface will increase the fluid disturbance in the region near the surface. This reduces the shear drag that can be found on a surface. Therefore, any surface roughness may increase mass transfer near the surface because of increased fluid motion, and thus increased particle motion. In addition to roughness, larger protrusions can also disturb the flow. Fingerlike thrombus protrusions have been experimentally found to project from the base thrombus (Wootton, Markou et al. 2001; Flannery 2005). A thrombus does not grow in a smooth manner and instead grows out of multiple regions

along the thrombotic surface. These projections withstand flow forces to maintain erect structures, while some bend down. This statement is based on experimental observations seen in our laboratory. Such projections increase the roughness of the flow surface, as well as disturbing the flow in a macro manner. Protrusions are difficult to include in either a theoretical model, or a static computational model that predicts thrombus occlusion from the platelet flux into region of a growing thrombus. Instead a real time transient model of forming thrombus, like the ones used in this thesis, could possibly capture the fingerlike protrusions from a thrombotic surface.

Modeling

Molecular Collisions and Mean Free Path

The mean free path for particles in a fluid flow is very important for characterizing the particle motion. The mean free path is the average distance a particle travels before it will collide with another particle. The value can be estimated from kinetic theory. The mean free path's relevance is used in various areas of this thesis, beginning with defining the Knudsen number. The Knudsen number is a dimensionless parameter, used to determine whether statistical mechanics or continuum mechanics should be used for a specific application. Statistical or quantum mechanics are generally used for Knudsen numbers greater than one. Continuum mechanics are usually used for Knudsen numbers less than one. Knudsen numbers on the order of one would likely use a combination of the two methods. The Knudsen number is derived from Equation 8.

Equation 8: Knudsen number

$$Kn = \frac{\lambda}{L}$$

In this equation, λ is the mean free path, while L is a representative physical length scale. The mean free path is derived by considering the collision of two molecules. As molecules are about to collide, the separation distance between their centers is 2*d/2,

where d is their diameter assuming spherical particles. Therefore, the collision cross section of two molecules is πd^2, seen in Figure 11.

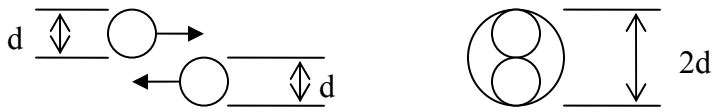

Figure 11: Collision cross section area.

The two particles would have to be somewhere within this collision cross section for a collision to occur, assuming hard sphere collisions. The relative average speed of the particles at <v> sweeps out a fluid volume of <v> πd^2 per second. The number of particles, N, per unit volume, V, are involved in the collision. The relative velocity can be estimated as $2^{1/2}$<v>. The number of collisions for one molecule per second can then be represented by Equation 9.

Equation 9: Number of collisions for one particle per second

$$n = \sqrt{2}\,\frac{N}{V}\langle v\rangle \pi d^2$$

The calculation for the distance the particle travels between these collisions can be calculated based on this equation and knowing the average speed of the collision. This results in Equation 10.

Equation 10: Mean free path approximation

$$\lambda = \frac{\langle v\rangle}{\sqrt{2}\pi d^2 \langle v\rangle (N/V)} = \frac{1}{\sqrt{2}\pi d^2 (N/V)}$$

The mean free path is difficult to calculate for platelets in whole blood because platelets have been shown to have a skewed distribution, known as margination (Eckstein, Bilsker et al. 1987; Aarts, van den Broek et al. 1988). Aarts paper stated that platelets have a higher concentration near a vessel wall, which is approximately nine times the average concentration. His results also showed a negligible amount of red blood cells in this region. Assuming that platelets are 0.25% of the blood volume, then

this would make the near wall concentration approximately 2.25% of the blood volume. Concentrations of 2.25% would result in 0.0028 platelets per μm^3. This is based on the assumption that the platelet's volume is 8 μm^3. An effective diameter for a sphere of volume 8 μm^3 would be 2.5 μm. This results in a mean free path of approximately 13 μm. On the other hand, if the concentration is assumed to be uniform in the blood without collisions with red blood cells, then the mean free path would be 115 μm. The mean free path of 13 μm would result in a Knudsen number of 5.2 based on the length scale of an average platelet diameter. Knudsen numbers near 1, such as this would use a combination of continuum and statistical mechanics.

Numerical Models of Thrombosis

Arterial thrombosis models must include a model of blood flow, based on platelet transport, and a model of platelet adhesion. This discussion will focus specifically on models that have been used to describe cell adhesion; although, there are a wide variety of mathematical blood models in existence. A highly used model (Stubley, Strong et al. 1987) for thrombus formation implements the Eulerian convection-diffusion equation (Strong, Stubley et al. 1987; Eckstein and Belgacem 1991; Sorensen, Burgreen et al. 1999; Wootton, Markou et al. 2001; Goodman, Barlow et al. 2005). Theory from this method is used for the model that is developed in this thesis, and is described further below. In general a diffusion coefficient is assigned to simulate particle motion, while a first order kinetic rate is used to simulate absorption of platelets into the vessel wall, or thin layer thrombus formation. Other mathematical modeling methods are gaining popularity because the convection-diffusion method is intended for particles, of molecular size, that passively move with the flow. Newer methods attempt to model particle motion based on proven first principles. The advantage to the convection-diffusion model is that it is much more computationally efficient than methods that model individual particles.

A method that has been used to evaluate suspension flows is the Lattice Boltzmann method. The method was first used to analyze a solid particle in a fluid (Ladd 1993). Red blood cell motion has been evaluated based on this method, including the formation and degradation of particle clusters (Ding and Aidun 2006). (Artoli, Hoekstra et al. 2006) achieved reasonable accuracy using the Lattice Boltzmann technique in a human abdominal aorta. (Li, Fang et al. 2004) studied flow through a high degree stenosis with an opening of two times the diameter of a RBC. (Boyd, Buick et al. 2005) studied wall shear stress over stenosis at the carotid artery sinus in two-dimensions. The Lattice Boltzmann method has also been extended to model red thrombus formation based on transport phenomenon, and shear stress dependent thrombogenesis probability (Tamagawa and Matsuo 2004; Ouared and Chopard 2005). Tamagawa and Matsuo applied a threshold condition of low shear rate and low wall to particle distance. Their study was performed on a backward facing step and a cylinder in cross flow. Ouared and Chopard also applied a low shear rate condition. They focused on making qualitative comparisons of a stented aneurysm to determine the effects on thrombus formation in the aneurysm. (Sun and Munn 2005) used the Lattice Boltzmann method to include particulate-surface bonding. They implemented their method at very low Reynolds numbers and a small channel of 40 microns and used a mass-spring system to simulate the receptor-ligand bonds.

The general discretized simplified Boltzmann equation can be represented by:

Equation 11: Simplified Boltzmann equation

$$f_i\left(t+\tau, r+c_i\tau\right) = f_i\left(t,r\right)+\Omega\left[\, f_i\left(t,r\right)\right]$$

where f_i, is the component of the velocity distribution function, t is time, r is the particle position, c_i is the component of particle velocity, τ is the time step, and Ω is the collision operator of the Boltzmann equation. Velocity distributions implement the Maxwell-Boltzmann distribution. Equations of mass, momentum, and isotropy are solved along a lattice, through the distribution functions. This results in equations similar to the Navier-

Stokes equations. (Zhaoli, Baochang et al. 2000) were able to exactly recover the incompressible Navier-Stokes equations. The maximum velocities used for this method are topology dependent because motion is along the lattice. The method still requires simplification of RBC motion, for the purpose of computational efficiency, in the pathological arteries associated with thrombosis.

The discrete phase method can also be used to analyze particle motion. This method analyzes particles in a Lagrangian sense, where each particle is individually modeled. This method has been used to study both particle dynamics (Bossis and Brady 1984) and platelet adhesion (Fiechter 1998). Particle to wall adhesion has been evaluated for non-biological flows by (Heinl and Bohnet 2005). This is a powerful method because the modeler can evaluate individual particles. This method is used in this thesis and is described further, below. Another method which is just recently gaining popularity is the immersed boundary method, developed by (Peskin 2002). It can be used to model the mechanics of biological systems at a large range of length scales (Wing Kam, Yaling et al. 2006). This method is particularly useful for modeling fluid structure interactions involving significant motion. The immersed boundary method or immersed finite element method implements an Eulerian-Lagrangian approach, where the fluid is described in an Eulerian reference frame, and the structure is described in a Lagrangian reference frame, usually.

There is mainly one group that has been using the immersed boundary method to model platelet adhesion and thrombus growth, although the method is widely used for other applications. Fogelson has modeled platelets as a discrete phase using immersed boundary techniques (Fogelson 1984), which was further refined (Fogelson and Peskin 1988). They also model a bonding strength between adhered platelets. This allows the platelet or thrombus structure to move freely as fluid forces act on the structure. (Fogelson and Guy 2004) has shown the method to be useful for generating particle to particle interactions. This modeling technique is very useful for modeling initial platelet

adhesion. However, the computational power that would be required to model complete occlusion would be enormous. The advantage to this method is that it is very capable of modeling the physics of particle motion and aggregation. This method is complex, involving over fifteen equations, and therefore will be left out for brevity. This method is used in this study to model platelet motion, but will not include modeling of platelet to platelet bonding.

Convection-Diffusion

A common method that has been used to model molecular motion in a flow is the convection-diffusion equation, given in Equation 12 (Stubley, Strong et al. 1987). This equation describes the change in concentration for a particular region based on convection, diffusion, and species source/sink terms. It is a continuum method for modeling platelet locomotion.

Equation 12: Convection-diffusion equations of continuity of mass and conservation of momentum, shown in respective order

$$\frac{\partial \alpha_c C_j}{\partial t} + \vec{v} \bullet \nabla \alpha_c C_j - D_j \nabla^2 \alpha_c C_j = S_j$$

where C_j is the species concentration, α_c is the mass fraction of the species, D_j is the diffusivity of the species, $\vec{v}$ is the velocity vector, and S_j is a source term The equation describes the motion of molecules as they move from high concentration regions to low concentration regions. The convection-diffusion equations have been used to model platelets, which are not of molecular size. However, the justification is that particle collisions result in random motion and once these motions are averaged over time, the motion is generally similar to Brownian motion. D_j is the diffusivity and is the term in the equations which describes Brownian motion. Particulates that are the size of platelets, however, depend on more than the concentration gradient. The number of particulate collisions has been found to increase as shear rates increase, as described in the biorheology section. In addition, the collision number increases as the concentrations

of particles increase. Therefore, the effect of motion down a concentration gradient will be similar to that of molecules, with the addition of a shear rate expression. (Zydney and Colton 1988) analyzed this concept and evaluated how the diffusion coefficient would change with respect to shear rate and volume fraction (Peclet number). The best fit empirical curve based on past experiments can be found in Equation 13. The thermal diffusivity is added to a term of shear rate proportionality. Results from the evaluation appear to approximately have a direct relationship between particle motion augmentation and Peclet number.

Equation 13: Zydney and Colton diffusion representation of particulate locomotion

$$D_e = \alpha\dot{\gamma} + D_{th}$$
$$\alpha = ka^2\phi(1-\phi)^n$$
$$D_{th} = \frac{k_B T}{6\pi\mu a}$$
$$k_B = 1.38X10^{-23}\, J/K$$
$$T = 310K$$
$$\mu = 1.2X10^{-3}\, Ns/m^2$$
$$a = 4X10^{-6}\, m^3$$

The diffusivity is dependant on the volume fraction ϕ, which changes with hematocrit (Aarts, van den Broek et al. 1988) and shear rate. The value for k was found to be 0.15 ± 0.03 and the value for n was found to be 0.8 ± 0.3. (Turitto and Baumgartner 1975) assumed the coefficient to be related to the shear rate by a power law and did not include an additional thermal diffusivity term, which can be estimated as $1.6X10^{-9}$ cm^2/s, but becomes negligible when the shear rate exceeds 3 s^{-1} (Wootton, Markou et al. 2001). The α term can essentially be approximated as a constant (Wootton and Ku 1999). Diffusion in the axial direction of a blood vessel is negligible relative to the convection. However, there is no convection in the radial direction in fully developed Poiseuille flow. Therefore, the flux in this direction can be represented by Equation 14.

Equation 14: Flux of particulates to the

$$J_r = -D\frac{\partial c}{\partial r}$$

The flux of particles in the radial direction can be stated to be in equilibrium with particulate uptake at the wall. This leads to the boundary condition for the convection-diffusion equation. Adhesion is generally modeled as a first order rate reaction. The flux for this reaction is generally set equal to the flux of platelets to the wall based on the diffusive motion. This can be modeled as Equation 15.

Equation 15: Flux of platelets at the wall

$$J_r = -D\frac{\partial c}{\partial r}\bigg|_{wall} = k_t c_0$$

where k_t is the rate constant and c_0 is the concentration at the wall.

(Turitto and Baumgartner 1975) simplified the convection-diffusion equations and determined an estimate of the mass flux, J, shown in Equation 16. They based their results on a axial velocity field, which assumed Newtonian and annular flow. This can be used to theoretically evaluate the extremes of platelet deposition based on many assumptions.

Equation 16: (Turitto and Baumgartner 1975) flux of platelets at a injured wall in a axisymmetric tube

$$J = \frac{C_0}{1/K + 1.48/\left(v_0 f\left(k\right) D_w^2/d_e x\right)^{1/3}}$$

C_0 is the bulk platelet concentration, K, the platelet-surface reactivity, d_e is the equivalent diameter of the annulus, v_0 is the average velocity of the annulus, f(k) is a constant determined by the dimensions of the annulus, D_w the platelet diffusion coefficient at the wall, and x is the axial distance to the leading edge. The platelet diffusivity at the wall can be represented as a power-law relation:

Equation 17: Platelet diffusivity used by (Turitto, Weiss et al. 1979)

$$D_W = m\left(\gamma_W / \gamma_0\right)^n$$

Turitto used γ_0 as an arbitrary parameter, 1 s^{-1} for nondimensionalizing. (Aarts, Steendijk et al. 1986) did a further study to determine the variation of D_W with the amount of hematocrit. The study showed a qualitative relation suggesting that increasing hematocrit also increases the platelet diffusivity at the wall. They went on to tabulate the change in n and m parameters with the amount of hematocrit. They then followed up with a 2nd order polynomial curve fit for the value of n, assuming m stays relatively constant. For the normal hematocrit concentration of 0.4 an m value of $1.10 \pm 0.08X10^{-9}$ cm^2s^{-1} and an n value of 0.68 ± 0.04 was found. When the reaction rate is much faster than the diffusional transport, the function becomes independent of K, and dependent on mass transport to the vessel wall. On the other hand, when K is small compared to mass transport to the wall, then the rate of adhesion dominates platelet deposition.

Additional reaction rates can be included in the analysis to analyze the limiting case of platelet adhesion. For example, the rate of platelet activation could be included, and platelet to platelet binding. (Wootton, Markou et al. 2001) lumped these into one parameter, since one of the rates will limit the kinetics of the other rates. Their results were similar to experiments, except in the recirculation region of a stenosis. The comparison was based on the rate of thrombus aggrandizement in phase II described in Figure 6. Others have evaluated an all encompassing model of agonist effect and includes many of the rates (Sorensen, Burgreen et al. 1999; Goodman, Barlow et al. 2005). The disadvantage to this technique is that there is little data on these rates and their cross-correlations (Sorensen, Burgreen et al. 1999). Sorenson assumed a threshold level of activation from agonists based on Equation 18

Equation 18: Activation rate based on agonist effects

$$k_{pa} = \begin{cases} 0, & \Omega < 1.0 \\ \dfrac{\Omega}{t_{act}}, & \Omega \geq 1.0 \end{cases}$$

$$\Omega = \sum_{j=1}^{n_a} w_j \frac{\left[a_j \right]}{\left[a_{j,crit} \right]}$$

where $[a_j]$ is the agonist concentration, $[a_{j,crit}]$ is the agonist's threshold concentration , n_a is the number of agonists, w_j is the agonist-specific weight to mimic the differential effects of strong and weak agonists on the activation reaction, and tact is a time constant for platelet activation. Such a calculation may be extraneous because agonists will generally exist in the same region (Hubbell and McIntire 1986) and for this reason could be lumped into one. Including agonists could have the advantage of more accurately predicting thrombus growth in the recirculation region.

Discrete Phase

In the discrete phase model, blood is treated as a two-phase flow. Plasma is considered a continuous phase, modeled in Eulerian coordinates; while platelets are considered a discrete phase, modeled in Lagrangian coordinates. Each particle is individually described in this method, where the motion is governed by a force balance on the particle, Equation 19. The particles are released by defining an injection region and the characteristics of the particles in the region. The time histories of individual particles are recorded and therefore, the particle residence time in specific shear stresses can be recorded. This is a powerful capability, because the particle residence time at particular shear stresses has been found to be important for platelet activation.

Equation 19: Force balance on a particle

$$\frac{\partial u_{i,p}}{\partial t} = F_D\left(u_i - u_{i,p}\right) + F_x$$

The term F_x includes any additional forces applied to a particle, such as the Saffman lift force (Saffman 1965). F_D is the drag force on a given particle. This is represented in Equation 20.

Equation 20: Drag force

$$F_D = \frac{3}{4}\frac{\rho}{d_p \rho_p}\left|u_i - u_{i,p}\right| C_D$$

The advantage to discrete methods is that individual forces can be applied to the particles. (Longest and Kleinstreuer 2003; Longest, Kleinstreuer et al. 2004) uses discrete methods to model near wall forces that influence platelet motion. They modeled platelets as a point mass and determined probability for thrombus formation based on a nondimensional factor developed from particle-wall distance and residence time. If the wall shear stress was below a certain threshold at a particular value of the factor, they considered the platelet to be adherent.

Experimental Model

The parameters for the computational models developed in this thesis are based on the experimental work by (Flannery 2005) in addition to the experimental work that is currently being performed in our lab. The experiment is performed by perfusing lightly heparinized porcine blood through a stenosis in a collagen coated drawn glass tube. The flow is considered fully developed before the region of the stenosis. One should refer to (Flannery 2005) for a full explanation of the methodology used for the experimental setup. All occlusive experiments performed in our lab have resulted in the most significant thrombus formation near the apex of the stenosis. An example is shown in Figure 12. The Reynolds number at the throat for the experiment is near 130 for a stenosis with 85% reduction by area.

The thrombus appears, in the figure, to form from the converging region of the stenosis to the apex of the stenosis. This is the region of highest wall shear rate. There is minimal thrombus formation in the diverging and recirculation region of the stenosis. The thrombus in the converging region appears to retard, while the thrombus at the central apex extends to occlusion. This observation may be a residual of image quality and viewing a three-dimensional thrombus in two-dimensions. *A priori* knowledge of the location of thrombus formation for the stenotic tubes allows one to more appropriately

choose modeling techniques. Unfortunately having this knowledge could skew the model to match the experimental results.

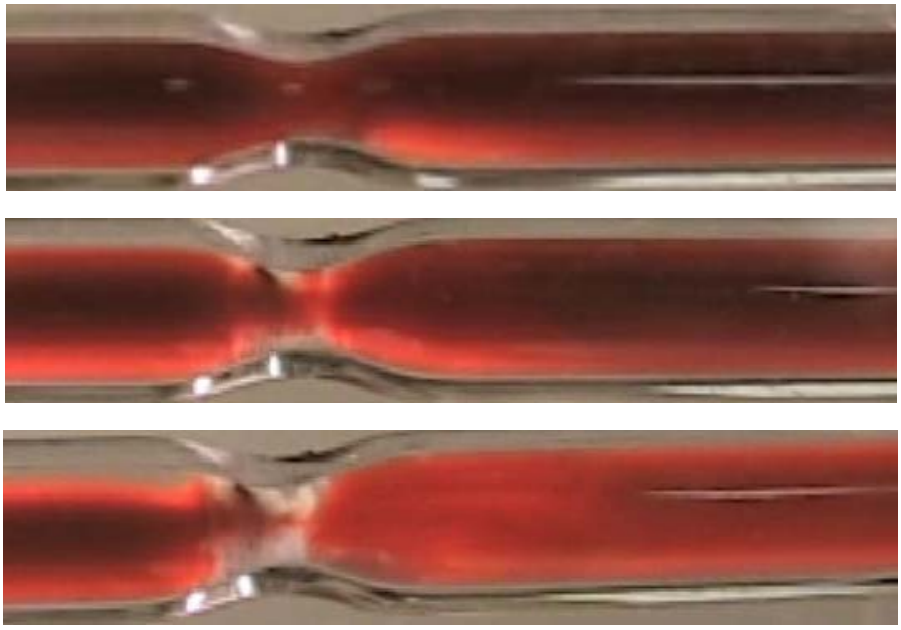

Figure 12: Experimental results of thrombus growth, performed in our lab by Andrea Para. The time sequence is 0:06, 8:06, and 13:21 minutes after initialization of the flow.

Research Goals

The thesis is focused on the generation of a model, which simulates thrombus generation and growth. The specific goals of this model are to:

1) Model an occluding thrombus using computational fluid mechanics to determine the location and time for occlusion. The model is aimed at simulating phase II of the platelet deposition curve. The criteria for the simulation are that the location and time of thrombus occlusion matches to within an order of magnitude of the experimental results. The time to occlusion is compared to phase II of the experimental results. The thrombus location and shape are also compared to the experiments.
2) Separate the mechanisms involved in thrombus aggrandizement to determine which mechanisms are needed to simulate the thrombus occlusion seen in the experimental results. The mechanisms are divided into two transport related

phenomena and one that considers reaction kinetics. The transport related phenomena are enhanced diffusivity and platelet margination. The reaction kinetics considers shear rate dependent platelet adhesion to a reactive surface or VWF based binding.

A model that can accurately predict the time and location of thrombus occlusion could theoretically be used as a technique for diagnosing a patient's risk of thrombus formation based on the characteristics of an atherosclerotic lesion. I hypothesize that:

1) A shear rate dependent function is needed for thrombus to form in the throat of a stenosis, which is often found in myocardial infarctions and cerebral vascular accidents.
2) A quantitative shear dependent adhesion function may be extracted from knowledge of actual platelet deposition and platelet deposition predicted by transport mechanisms.

CHAPTER

2. METHODS

Numerical Methods for Flow Solution

Governing Equations of Flow

The computational models developed in this thesis were implemented in Fluent® 6.2.16 (Fluent Inc, Lebanon, NH), based on a validated finite-volume based scheme. A segregated, implicit, steady, axisymmetric solver was used. The steady assumption abides by the methods used in the experimental laboratory flow setup (Flannery 2005). In addition unsteady flow should only have secondary effects on mass transport (Basmadjian 1990). The implicit solver used a block Gauss-Seidel linear equation solver. An algebraic multigrid (AMG) method was used to solve the discretized partial differential equations. Pressure is solved through the pressure-velocity coupling method known as the SIMPLEC (Semi-Implicit Pressure-Linked Equations Consistent) algorithm. The flow field is determined through the incompressible Navier-Stokes equations, Equation 21.

Equation 21: Incompressible continuity of mass and conservation of momentum

$$\vec{\nabla} \bullet \vec{v} = 0$$

$$\partial_t \vec{v} + \vec{v} \bullet \vec{\nabla} \vec{v} = -\frac{1}{\rho} \vec{\nabla} p + \upsilon \left(\vec{\nabla}^2 \bullet \vec{v} \right)$$

where $\vec{v}$ is the velocity vector, t is time, and ν is the kinematic viscosity.

Turbulence

Reynolds numbers (Re) in this flow are relatively low for turbulence to exist. However, as the thrombus grows, the effective boundary of the stenosis causes further constriction to the flow, increasing the Reynolds number. In addition two sets of flow fields are considered in this study. One is setup to match the experiment in the lab, to

verify the accuracy of the approaches used in this thesis, where the upstream Re is approximately 50. The throat Re is near 130. Another setup considers a higher flow rate in the same vessel, which results in a higher upstream Re of 220. The throat Re for the study is approximated at 570. A study performed by (Young and Tsai 1973) suggests that the lower Re, for the experimental simulation configuration, is in a laminar regime; while the higher Re, associated with the coronary artery, is in the turbulent transition regime in the region of the 85% stenosis by area. The turbulence effect was accounted for, when appropriate, by using the k-ω model for this study. This method is based on modeling transport equations through turbulent kinetic energy, k, and the specific dissipation rate, ω. The shear-stress transport (SST) k-ω model, developed by (Menter 1994), was applied in this study. The choice of turbulence model was based on the capability to accurately model wall-bounded flows. In addition it is more appropriate than other models for low-Reynolds number models. The transitional flow option was chosen when turbulence was modeled, based on the studies by Young and Tsai. It also has the capability of modifying the turbulent viscosity for transport of the principle turbulent stress. The basic equations used for this method are represented in Equation 22.

Equation 22: Transport equations of turbulent kinetic energy and dissipation terms.

$$\frac{\partial}{\partial t}(\rho k)+\frac{\partial}{\partial x_i}(\rho k u_i)=\frac{\partial}{\partial x_j}\left(\Gamma_k \frac{\partial k}{\partial x_j}\right)+\tilde{G}_k-Y_k+S_k$$

$$\frac{\partial}{\partial t}(\rho \omega)+\frac{\partial}{\partial x_i}(\rho \omega u_i)=\frac{\partial}{\partial x_j}\left(\Gamma_\omega \frac{\partial \omega}{\partial x_j}\right)+\tilde{G}_\omega-Y_\omega+D_\omega+S_\omega$$

where $\tilde{G}_k$ is the generation of turbulent kinetic energy due to mean velocity gradients; $\tilde{G}_\omega$ is the generation of ω; Γ_k and Γ_ω are the effective diffusivity terms; Y_k and Y_ω are the dissipation terms; and D_ω is the cross-diffusion term. One should refer to Fluent 6.2.16 documentation or (Menter 1994) for the calculation of these values. The choice of turbulence model should not have a large effect on the solution of interest in this study,

since platelet deposition has been found to mostly occur upstream of the stenosis, as previously described, and shown in the experimental results section of the introduction.

Geometry and Mesh

An axisymmetric stenosis is modeled based on the experimental setup in our lab. Axisymmetry is only an approximation of the experimental blown glass tubes that are used to simulate an arterial stenosis. The two-dimensional axisymmetry assumption simplifies calculations and thus increases the speed of the solver significantly. The tube radius in the non-stenotic region is 0.75 mm to simulate the test specimen. An equation to model an axisymmetric stenosis is given in Equation 23. The equation simulates a streamlined stenotic region. Through trial and error it was determined that L should be taken as 4 mm to simulate the spacing in the test specimen. A qualitative comparison can be made by contrasting Figure 13 with Figure 14. However, the degree of stenosis is different between the two figures. The experimental specimen is a 75% stenosis by area, while the model is an 85% stenosis by area.

Equation 23: Equation for two-dimensional stenosis boundary (Young 1979)

$$S(x) = \begin{cases} \frac{S_0 R_0}{4}\left[1-\cos\left(\frac{2\pi\left(x-x_0\right)}{L}\right)\right]^2 & x_0 \le x \le \left(x_0+L\right) \\ 0 & \text{otherwise} \end{cases}$$

S(x) is the boundary as it varies from a value of 0. x_0 is the initial location where the stenosis begins, R_0 is the initial radius of the non-stenotic region, and S_0 is the fraction of the radius that the stenosis extends to. The tube extends 15 mm in either direction of the stenosis. This value was taken as 10x the diameter of the tube, to assure fully developed flow at the stenosis. In addition, 10x the diameter gives a sufficient distance for the flow to become fully developed again after the stenotic region. These distances are necessary to avoid affecting the thrombus formation in the region of the stenosis, by affecting the flow through poorly prescribed boundary conditions.

Figure 13: Specimen geometry

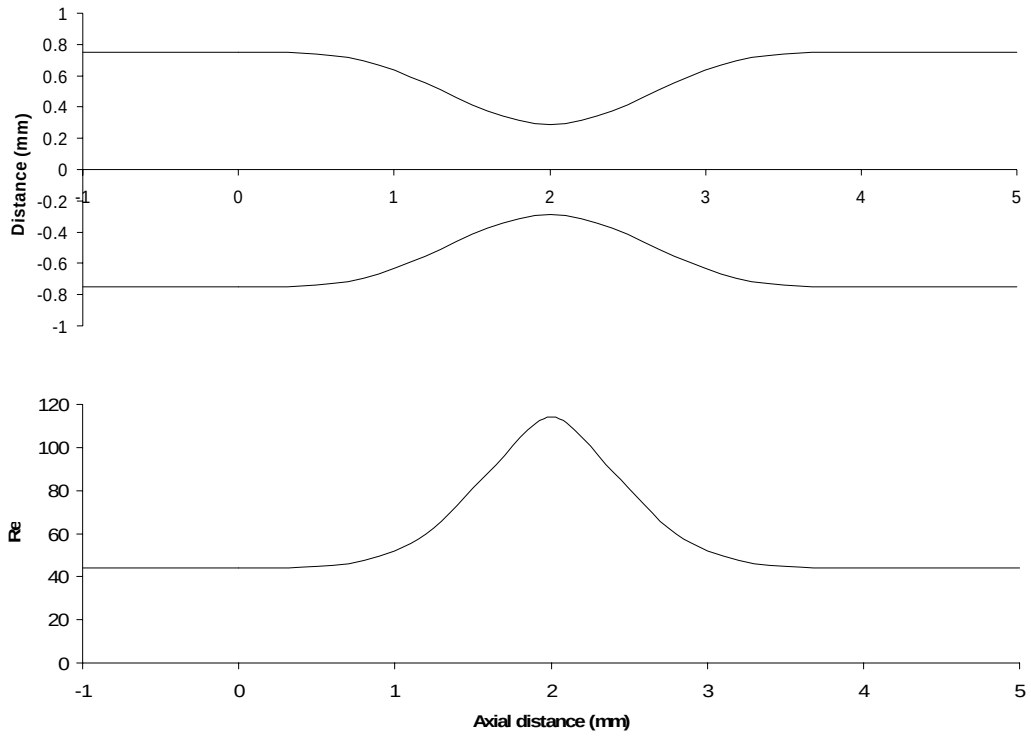

Figure 14: The computational stenotic geometry with the relative variation in Reynolds number across the stenotic region, for an inlet Reynolds number of 44. Re was calculated based on the diameter and estimated flow rate if there were no flow separation.

The grid was generated by defining edge spacing. The spacing was stretched in a manner so that the there was increased grid orthogonality near the stenosis region. In addition, a smoothing algorithm was used in the region of the stenosis. The smoothing defined a necessary condition of orthogonality at the grid boundaries. The smoothing additionally increases orthogonality for the inner grid. The disadvantage to the smoothing technique is that it increases the grid spacing in the boundary layer of the stenosis region. However, the boundary changes in this region as a thrombus grows. Therefore, the grid spacing in the central region of the grid is just as important to the

solution as grid spacing near the initial wall boundary. Therefore no grid stretching was applied at the inlet and outlet boundary edges to increase the ability to capture the boundary layer. It is a tradeoff of error from orthogonal edges to fine grid spacing in the boundary layer. The grid is illustrated in Figure 15.

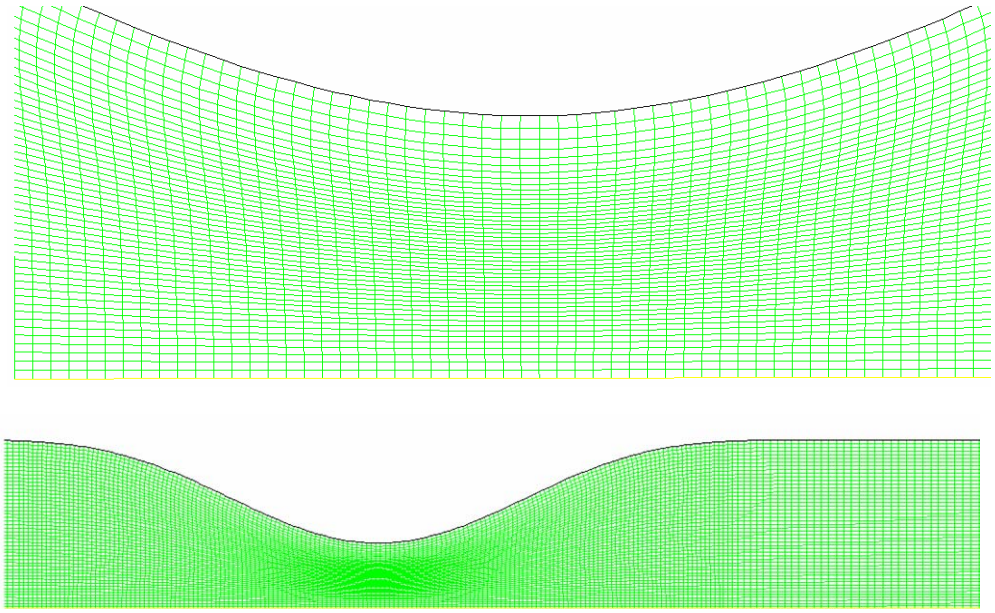

Figure 15: Computational domain for the discrete phase simulation. There are 44933 cells, 90832 faces, and 45900 nodes. The stenotic region is defined across 4 mm with 15 mm of additional length on either side for a 0.75 mm tube radius.

The defined grid spacing is illustrated in Figure 16. A structured grid was used. The inlet and outlet of the computational domain are a length of 0.75 mm and have 50 grid points. The grid is stretched toward the wall, shown by the arrow near the inlet, by using the power law to a power of 1.1. The grid spacing along the non-stenotic section of the wall on the inlet side was 15.4 mm in length, and consisted of 400 points. The grid was stretched using the power law to a power of 1.1 in the direction of the stenosis. The stenosis geometry was defined by Equation 23. An axial distance of 0.4 mm in from the outside of the stenosis was included in the outer non-stenotic grid spacing. Therefore, for the full axial distance of 4 mm of the stenosis, only 3.2 mm was considered in the stenosis when the grid spacing was defined. This section included 160 grid points and

did not include any grid stretching. The non-stenotic wall in the direction of the outlet was 15.4 mm long, with 360 points. The power law was used to a power of 1.1 for grid stretching in the direction of the stenosis. The axisymmetric section of the grid was divided into three sections corresponding with the three sections along the wall. Each section was divided at the same axial location as the wall sections. The same grid stretching was used in the axisymmetric sections as their radial counterparts.

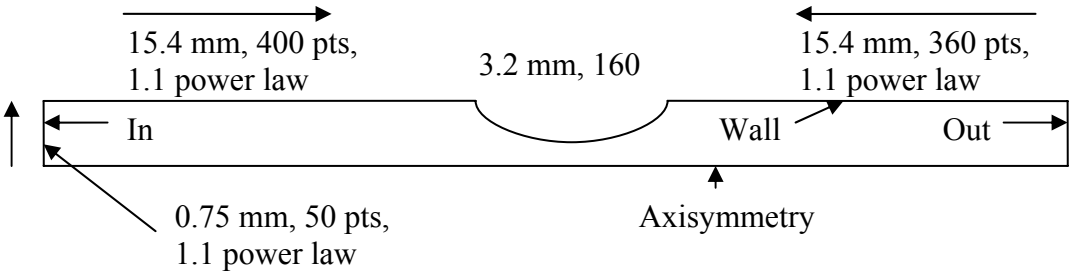

Figure 16: Grid spacing for the computational models

Boundary Conditions and Material Parameters

- Inlet: A uniform velocity profile was applied. The velocity for the experimental simulation was set for a Re of 44, while the coronary artery simulation condition was set for a Re of 220. The temperature was set at 300 ^{o}K. Particles are allowed to escape through the boundary for the mechanistic model of thrombus formation. When turbulence was applied, the inlet turbulent kinetic energy parameter, k, was chosen based the turbulence intensity in core flow. The value was set at 0.002. ω was determined by the relationship between the turbulence length scale, an empirical parameter estimate, and the turbulent kinetic energy. The value was set at 5000.
- Outlet: The condition is defined as a pressure outlet. The static pressure was set at 0. The temperature was set at 300 ^{o}K. Particles are allowed to escape through the boundary for the mechanistic model of thrombus formation. When turbulence was applied, the outlet turbulent kinetic energy parameter, k, was chosen based

the turbulence intensity in core flow. The value was set at 0.002. ω was determined by the relationship between the turbulence length scale, an empirical parameter estimate, and the turbulent kinetic energy. The value was set at 5000.

- Axisymmetry: The variables are set equal to the cell values adjacent to the axis.
- Wall: The no-slip boundary condition is applied at the wall, specifying velocities as u=v=0. Particles are reflected as inelastic collisions for the mechanistic model of thrombus formation.
- Thrombus: A porous media is prescribed to computational cells that contain thrombus. The porosity essentially provides a resistance to the flow proportional to the volume ratio of fluid blockage. The porosity is set to decrease as platelets are considered to adhere to the region within the cell. The porosity effect on the mass conservation and momentum equations can be seen in Equation 24. A porosity of 0.2 was arbitrarily chosen as a threshold for full computational cell occlusion. The value was then set at the smallest possible value 0.08 thereafter, to simulate full blockage. A different threshold value should only change the time scale for occlusion.

Equation 24: Porous media modification to the mass and momentum equations.

$$\partial_t(\gamma\rho) + \vec{\nabla}\bullet(\gamma\rho\vec{v}) = 0$$
$$\partial_t(\gamma\rho\vec{v}) + \vec{\nabla}\bullet(\gamma\rho\vec{v}\vec{v}) = -\gamma\vec{\nabla}p + +\upsilon\left(\vec{\nabla}^2\bullet\gamma\vec{v}\right)$$

where γ is the porosity, p is the pressure, $\vec{v}$ is the velocity vector, t is time, and ν is the kinematic viscosity. The porosity is specified by Equation 25.

Equation 25: Defined porosity

$$\gamma = 1 - \sum\left(\frac{n(t)\pi d^2}{4A_{\text{comp cell}}}\right)$$

where $A_{\text{comp cell}}$ is the computational cell area, n(t) is the time dependent number of platelets that have entered the cell, and d is the platelet diameter.

Phenomenological Model of Thrombus Formation

A phenomenological model of platelet deposition was developed based on data from (Flannery 2005). Flannery recorded platelet deposition over time at varying degrees of stenosis. He determined the deposition rate, based on these recording, for the second phase of thrombus formation, described earlier in the "Introduction," Figure 6. The second phase has been shown to have an approximately linear relationship between deposition and time (Wootton, Markou et al. 2001; Flannery 2005); therefore constant deposition rate can be extracted from data in this region, as assumed by Flannery. The second phase corresponds to the majority of platelet deposition over the time span of thrombus growth to occlusion. Therefore, an approximation of this phase, should lead to the location of occlusion. Flannery's platelet deposition rate, which he predicted in phase II, was plotted against the maximum wall shear rate, shown in Figure 17. A linear regression line was fit to the data from the value of 10000 s^{-1} to 40000 s^{-1}, which is on the high end of shear rates found in the 85% stenosis by area studied for the experimental simulation condition. It is in the median range for a coronary artery stenosis. The maximum wall shear rate corresponds with the point of thrombotic occlusion and the point of most thrombus formation. Therefore, growth rate across the entire stenosis might be predicted from the deposition rate/shear rate data from an extrapolation, assuming the relationship remains linear outside the bounds of the data.

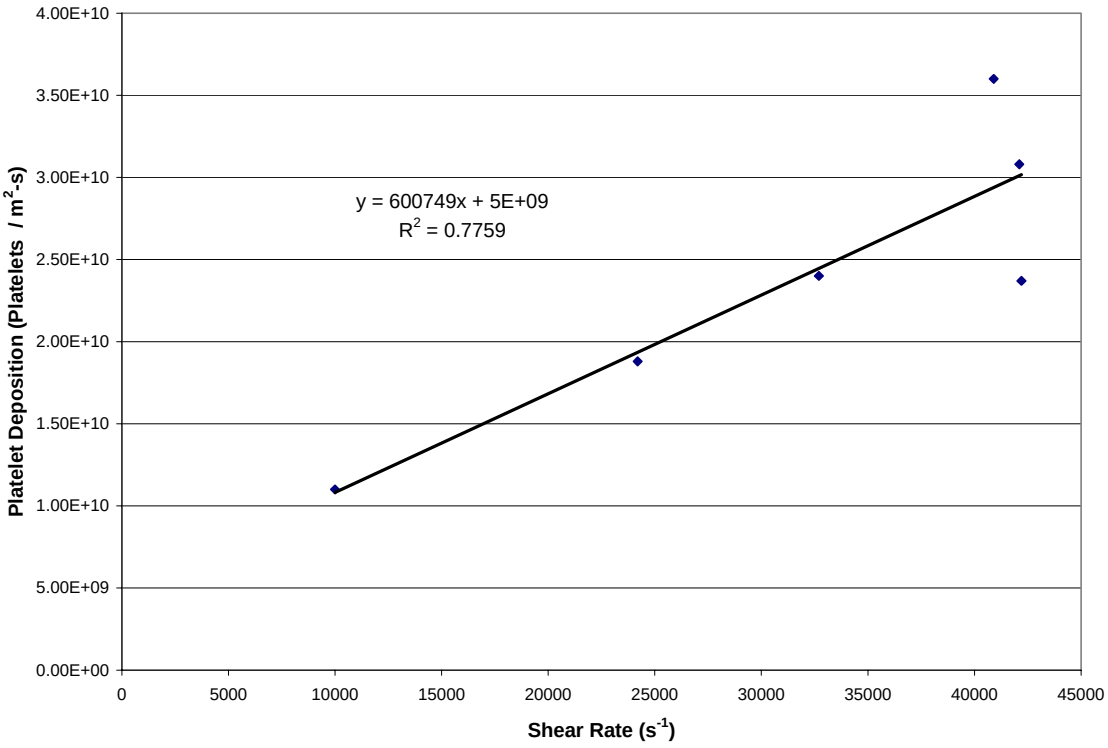

Figure 17: Plot of platelet deposition rate with shear rate during phase II of platelet deposition. A linear regression line was fit to data from (Flannery 2005).

The linear correlation in Figure 17 was used to develop a phenomenological model to estimate how thrombus growth may vary with time and location around a stenosis. Therefore, it was assumed that that the data could be extrapolated to lower shear rates, and that the thrombus deposition rate in a localized region could be predicted by the shear rate in a localized region. Therefore, the shear rate in a particular computational cell was used to estimate the platelet deposition in the computational cell. This was a dynamic process, because the shear rates were updated as the thrombus grows from the wall. Thrombus deposition effects on flow were modeled by varying the porosity in a specific computational cell. The porosity specification for platelet deposition was set as Equation 26.

Equation 26: Equation for porosity based on the linear regression shown in Figure 17.

$$\gamma = 1 - \sum \left[\frac{\left(600749\ \dot{\gamma} + 5\times 10^{9}\ \text{Platelets/m}^2\text{-s}\right) SA_{\text{outer face}} \bullet \Delta t \bullet A_p}{A_{\text{comp cell}}} \right]$$

where γ is the porosity $\dot{\gamma}$ is the shear rate, SA is the surface area calculated from the line "face" closest to the wall extrapolated around the circumference of the vessel, Δt is the time step, A_p is the platelet effective area, and $A_{comp\ cell}$ is the computational cells two-dimensional face area.

The model was setup so that computational cells next the vessel wall were set to an active state, and thus were permissive to thrombus formation. All other cells were set as inactive. The Model was initiated, so that the porosity in these cells is updated based on Equation 24. The porosity of an active cell decreases with each time step based on the equation. In addition, the flow solution is updated between each time step. Once a computational cell reaches the porosity threshold of 0.2, then the neighboring computational cells are activated. This process iterates until full thrombus occlusion occurs. The density for the plasma was set to 1025 kg/m^3, while the dynamic viscosity was set at 0.0035 kg/m-s.

Mechanistic Model of Thrombus Formation

A mechanistic model of thrombus formation was also considered. The purpose of the mechanistic model is to divide thrombus growth into three major mechanisms and to determine how each mechanism affects thrombus propagation. The mechanisms that were considered here are platelet enhanced diffusivity, platelet margination, and platelet adhesion. All three mechanisms are assumed to be shear rate dependent.

Stochastic Discrete Phase Model

Two-Phase Flow

This model uses a two-phase method for modeling blood. Plasma is considered a continuous phase, based on an Eulerian reference frame; while platelets are considered a discrete phase, based on a Lagrangian reference frame. The continuous phase is determined through the incompressible Navier-Stokes equations, Equation 27.

Equation 27: Navier-Stokes equations with source and sink terms to account for platelets in the flow

$$\vec{\nabla}\bullet\vec{v} + M = 0$$

$$\partial_t\vec{v} + \vec{v}\bullet\vec{\nabla}\vec{v} = -\frac{1}{\rho}\vec{\nabla}p + \upsilon\left(\vec{\nabla}^2\bullet\vec{v}\right) + \vec{f}$$

where $\vec{v}$ is the velocity vector, t is time, ν is the kinematic viscosity, M is a source/sink term to account for platelet mass in the computational cell, and $\vec{f}$ is a source/sink term to account for the change in momentum in the cell based on platelet motion.

Each platelet is individually modeled as a point mass and is tracked through the flow in a Lagrangian fashion. Each computational cell contains a number of platelets. Each platelet is described independently in this model, allowing a time history of platelets. Newtonian equations are solved for the particle dynamics Equation 28.

Equation 28: Newtonian equations for particle motion

$$\frac{\partial u_{i,p}}{\partial t} = F_D\left(u_i - u_{i,p}\right) + F_x$$

F_D is the drag force, F_x is additional forces, $u_{i,p}$ is the particle velocity, t is time, and u_i is the velocity of the fluid. Equation 28 is in units of length per square unit of time. Additional forces included in the model are the "Virtual mass" force, associated with displacing fluid, and the pressure gradient force. The force term values are represented in Equation 29.

Equation 29: Drag force term, virtual mass force, and pressure gradient force

$$F_D = \frac{3}{4}\frac{\rho}{d_p\rho_p}\left|u_i - u_{i,p}\right|C_D$$

$$F_x = \underbrace{\frac{1}{2}\frac{\rho}{\rho_p}\frac{\partial}{\partial t}\left(u_i - u_{i,p}\right)}_{\text{Virtual mass force}} + \underbrace{\left(\frac{\rho}{\rho_p}\right)u_{i,p}\frac{\partial u_i}{\partial x_i}}_{\text{Pressure gradient force}}$$

where ρ is the density of the fluid, ρ_p is the density of the particle, C_D is the drag coefficient, d_p is the particle diameter. The drag coefficient, represented in Equation 30, is taken as a nonspherical particle based on work by (Morsi and Alexander 1972). This is automatically calculated by Fluent based on the shape factor ϕ.

Equation 30: Drag coefficient

$$C_D = \frac{24}{\mathrm{Re}_{sph}}\left(1 + b_1 \mathrm{Re}_{sph}^{b_2}\right) + \frac{b_3 \mathrm{Re}_{sph}}{b_4 + \mathrm{Re}_{sph}}$$

where

$$b_1 = \exp\left(2.3288 - 6.4581\phi + 2.4486\phi^2\right)$$

$$b_2 = 0.0964 + 0.5565\phi$$

$$b_3 = \exp\left(4.905 - 13.8944\phi + 18.4222\phi^2 - 10.2599\phi^3\right)$$

$$b_4 = \exp\left(1.4681 + 12.2584\phi - 20.7322\phi^2 + 15.8855\phi^3\right)$$

where

$$\phi = \frac{s}{S}$$

Re_{sph} in the equation is the particle Reynolds number of a sphere. The shape factor, ϕ, is the surface area the particle, s, over the surface area of the equivalent particle as a sphere, S. The value is ~0.75 for a platelet. An additional lift force was excluded, although it was described as affecting the particle motion toward the tube wall in the biorheology section. The lift force would affect the radial motion of platelets in this thesis. However, the radial motion used in this thesis was chosen to be governed by the shear enhanced diffusivity and platelet margination described later in "Methods." The primary force opposing the defined radial motion is the drag force, which is included in the model. The margination condition used in this thesis encompasses inertial and viscous forces that control the concentration of platelets, therefore neglecting forces like the lift force.

The force term, f, in the momentum equation, Equation 27, can be described now that the continuous phase and discrete phase fundamental equations have been presented. This term is used to consider the change in momentum due to the existence of a particle. The momentum exchange term, f is

Equation 31: Discrete phase momentum exchange term

$$\vec{f} = \sum\left(\frac{\partial \vec{u}_p}{\partial t}\right)\dot{m}_p \Delta t$$

The term acts a momentum sink. The term in parenthesis is the term calculated in Equation 28. Additionally the mass term, M, in Equation 27 is represented by Equation 32. This term accounts for the change in mass due to the existence of particles in a computational cell.

Equation 32: Discrete phase mass exchange term

$$M = \frac{\dot{m}_{p,0}}{m_{p,0}}$$

where $\dot{m}_{p,0}$ is the mass flow rate for the particles entering and exiting the computational cell.

Turbulent diffusion

A turbulent diffusion condition is applied in some cases, where the particle trajectory is calculated by the instantaneous velocity, instead of the mean velocity. Fluent uses a discrete random walk method, where random values are taken as a constant during an eddy lifetime. This method generally forces particles into low-turbulence areas. This method implements a time scale based on the time a particle spends in turbulence. This is given by Equation 33.

Equation 33: Characteristic eddy lifetime time.

$$T = \int_0^\infty \frac{u_p'(t) + u_p'(t+s)}{\overline{u_p'^2}} ds$$

Where s is the particle path distance, u_p' is the instantaneous velocity of the particle. If diffusivity based on Equation 33, is set equal to the diffusivity of particles with no drift, then the Lagrangian integral time, T_L can be obtained, Equation 34.

Equation 34: Lagrangian integral time for k-ε model.

$$T_L = 0.15\frac{k}{\varepsilon}$$

The characteristic eddy lifetime is taken as two times this value. Additionally an eddy crossing time can be defined as Equation 35.

Equation 35: Particle eddy crossing time

$$t_{cross} = -\tau \ln\left[1 - \left(\frac{L_e}{\tau\left|u - u_p\right|}\right)\right]$$

Where τ is the particle relaxation time, L_e is the eddy length scale, and abs($u-u_p$) is the slip velocity. Finally, when a particle crosses two times Equation 34, or the time in Equation 35, then the particle is considered to have a new random motion. The random motion is described by a Gaussian random number multiplied with the absolute value of the average instantaneous velocity.

Discrete Phase Injection

The discrete phase methodology of modeling particles requires an injection point, where particles enter the flow. The injection point was set to 1 mm away from the entrance. The location was chosen so there was a sufficient distance for the particles to transport to time averaged steady state positions before the stenosis. The diameter of each platelet was set at 2.5 microns as an effective spherical diametrical representation of a platelet. The mean free path was used to determine how many platelets would be injected at a specific time interval. Assuming platelets take 0.25% of the volume of blood, then the mean free path can be calculated to be 115 microns, based on Equation 10. Therefore, approximately 7 platelets would enter the axisymmetric region every 0.00023 seconds for a velocity of 0.5 m/s. A random radial velocity was applied to the incoming platelets for a length of 1 mm to disperse them across the flow. The density for each platelet was set at 1060 kg/m^3, while the density for the plasma was set to 1025 kg/m^3. The dynamic viscosity of plasma was set at 0.0035 kg/m-s. The accuracy of discrete phase calculations depends on the length scale, Equation 36, for time integration of the particle trajectories, which is specified *a priori*.

Equation 36: Determination of the length scale that is appropriate for discrete phase model

$$L = \Delta t\left(u + u_p\right)$$

L is the length scales equivalent to particle travel distance before equations are solved again. This was taken as the mean free path of 115 microns.

Diffusive Motion

Shear-augmented effective diffusion, or dispersion was defined based on empirical data correlation performed by (Zydney and Colton 1988). The justification for the shear augmentation was described in the biorheology section. Equation 13 is the shear augmented diffusion defined for this study. The volume fraction used in the equation is taken as a constant, which is set to the hematocrit, 0.45. Physically, it would vary across the vessel. It is taken as a constant because larger hematocrit counts exist toward the center axis of a vessel, while they decrease near the vessel wall. However, platelet count is low in the center of the vessel and increases near the wall. For the sake of simplicity, it assumed that the volume fraction is the same in both regions and that the effective diffusivity is solely shear dependent, similar to (Wootton, Markou et al. 2001). Generally, the volume fraction should not vary significantly in the axial direction, even near the stenosis. The effective diffusivity used in this study is represented in Equation 37.

Equation 37: Effective diffusivity

$$D_e = \left(7 \times 10^{-5} m^2\right) \dot{\gamma} + 1.6 \times 10^{-5}\, m^2/s$$

Diffusivity is converted to the discrete phase by considering the basis behind diffusion. Diffusion develops from Brownian motion, and in one-dimension the particle would have equal likelihood in traveling in either direction of its current location. The mean square distance of which the particle will travel is given by Equation 38, in one dimension.

Equation 38: Mean square distance of particle travel based on one-dimension diffusion

$$\left\langle x^2 \right\rangle = 2D\Delta t$$

In this study, a condition was specified in which a particle velocity has a term added to it based on the idea of Brownian motion. The term that is used here is represented in Equation 39.

Equation 39: Adjustment of particle velocity based on effective diffusion.

$$\vec{v}_p = \vec{v}_p + \zeta\sqrt{\alpha\dot{\gamma} + \beta}$$

where ζ is a random variable based on a Gaussian distribution set around 0, α is a constant, and β is a constant. ζ is changed at every time step. The justification for this variation is that on average the platelets would collide with other platelets, changing their velocity in a statistical way, similar to what is given in Equation 39. In addition, the time scale for the random velocity term is synonymous with the time between collisions based on the mean free path. This is similar in theory to the diffusive time scales developed in for the "Turbulent diffusion" condition described earlier in the "Methods" section. The constants are determined by developing a curve fit between the mean square distances a particle travels from Equation 39 with the mean square distance a particle travels based on Equation 38. Equation 39 is set so that the random particle motion will only occur in the radial direction during the correlation. It is later applied in all directions to account for the stenosis region, even though the axial random motion will tend to be negligible compared to convection. The motion of particles were tracked for the correlation based on calculating the mean square distance a particle has traveled Equation 40.

Equation 40: Mean square distance calculation

$$\left\langle x^2 \right\rangle = \left(r_p - r_{p,0}\right)^2$$

where r_p is the current particle position and $r_{p,0}$ is the last particle position in the radial direction. The values of α and β were adjusted to match the calculations of Equation 38 and Equation 40 at various shear rates. The correlation results are presented in Figure 18.

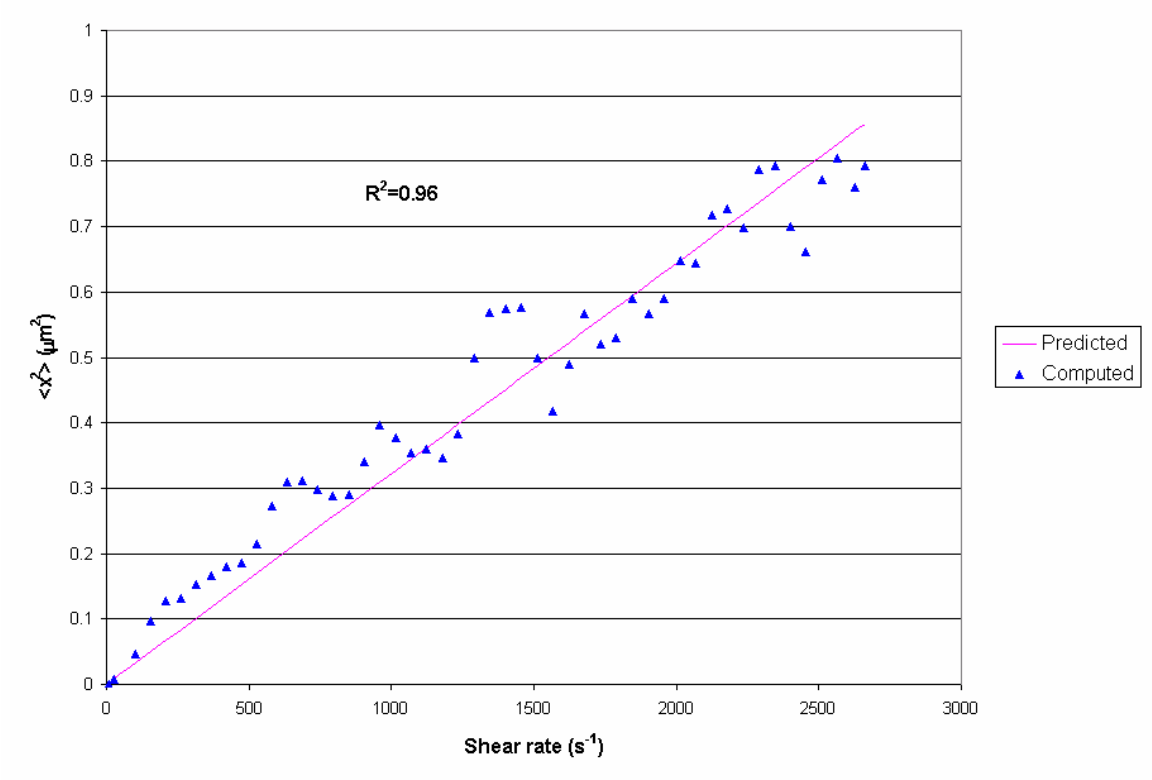

Figure 18: Mean square distance of measured particle travel compared with the predicted value.

The curve in Figure 18 was sufficient, since the original effective diffusivity value was an estimate from a correlation. Therefore, an exact fit would be extraneous. The values of α and β were determined to be 0.10 and 3.71 X 10^{-22} respectively.

Platelet Margination

(Eckstein and Belgacem 1991) used the method of adding a drift term, based on potential theory (Gardiner 1985), to account for margination. This method employs an additional term in the convection-diffusion equation to account for the probability that a particle exists in one region over another. His method was extended by (Buchanan and Kleinstreuer 1998) to include a shear term inherent in the first scalar invariant in the rate of deformation tensor. The method employed here is a variation of Eckstein and Belgacem's method, with the idea behind Buchanan and Kleinstreuer's work. The

methods had to be extended for a discrete phase model in this study, since their methods were used for convection-diffusion. This was done by considering the probability that a particle will travel in one direction over another. The purpose is to develop a concentration profile similar to (Aarts, van den Broek et al. 1988) and to include the shear effects measured by Aarts. This was based on the drift definition given from (Eckstein and Belgacem 1991), shown in Equation 41.

Equation 41: Local drift in the radial direction

$$-\Phi' = D\frac{dc_{fd}/dr}{c_{fd}} = D\frac{C_0K\left((m-1)r^{m-2}(1-r)^{n-1}-(n-1)r^{m-1}(1-r)^{n-2}\right)}{C_0\left(1+Kr^{m-1}(1-r)^{n-1}\right)}$$

-Φ' is the drift term; D is the diffusion constant; c_{fd} is the concentration profile in fully developed flow; C_0 is the average concentration; m, n, and K are constants. A drift term specified in this manner should result in a concentration profile defined by c_{fd}. The value of K defines the relative amplitude of the concentration, a large m and a n value of 2 result in a near wall concentration profile (Eckstein and Belgacem 1991).

In addition, the work by Aarts showed shear rate dependent margination. Near-wall concentrations increased in an approximately linear manner with shear rate, Table 1. Therefore, the strain rate was added to the term in Equation 41 with multiplication by a length factor, a platelet effective diameter. The drift term is translated into the discrete phase model through the use of directional probability. The probability function is given in Equation 42. A random value is chosen from zero to one out of a uniform distribution. If the value is positive and is less than the probability given in Equation 42, then the random velocity term in Equation 39 is set to a positive value. If the negative of the value taken from the uniform distribution is greater than the probability function in Equation 42 and greater than -0.5, then the random velocity in Equation 39 is set to a negative value. Otherwise, the random velocity has equal probability of being negative or positive. This technique is only performed in the radial direction, which is not normal

to the surface near the stenosis. However, it can be used as an approximation to administering a margination effect.

Equation 42: Probability for particle to move in positive direction

$$p = 0.01\frac{K\left((m-1)r^{m-2}(1-r)^{n-1} - (n-1)r^{m-1}(1-r)^{n-2}\right)}{\left(1+Kr^{m-1}(1-r)^{n-1}\right)} + a_p\dot{\gamma}$$

The choice of controlling the velocity fluctuation direction is based on conserving the specified shear rate dependent effective diffusivity. Other techniques for developing margination could affect the effective diffusivity definition. Figure 19 is a plot of the predicted normalized concentration against the probability of forcing the random velocity in Equation 39 to a positive or a negative value. The limit of the negative probability is set at -0.5 as shown in the figure. This is more representative of a physical system because a particle in blood flow is not likely to have a 100% probability of going in one direction. The values in the figure are set such that K is taken as 300, n as 2, and m as 15.

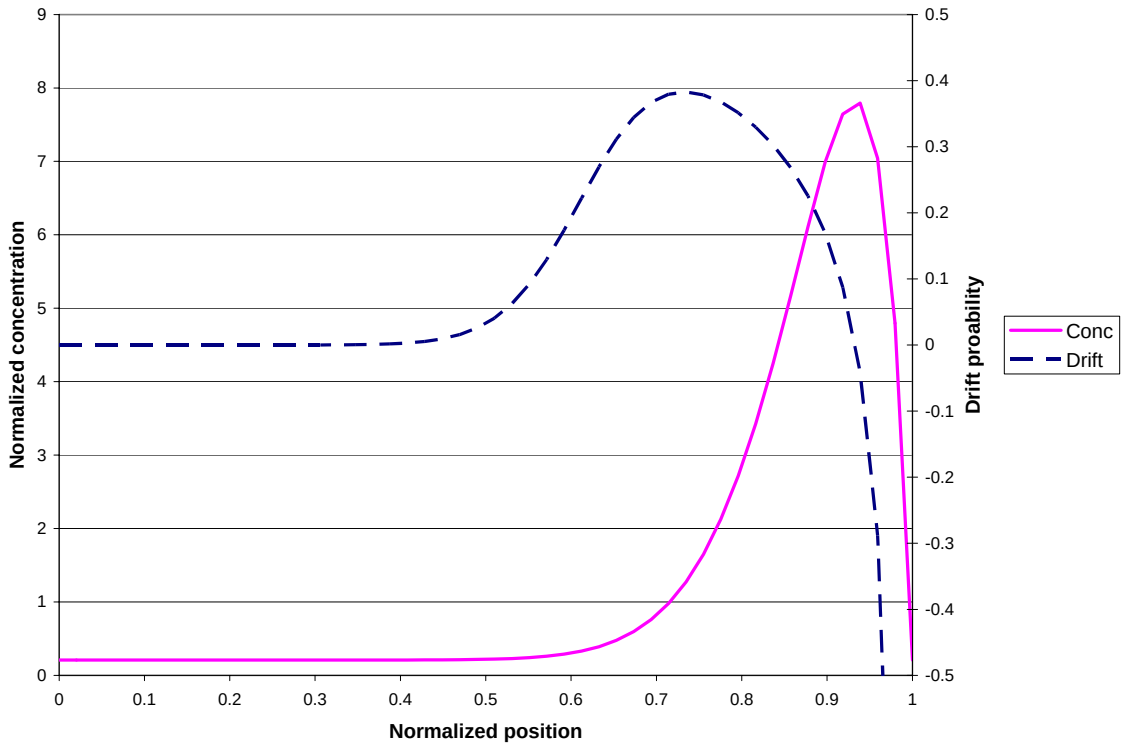

Figure 19: Drift and concentration profiles determined from Equation 41 with a value of K=300, n=2, m=15, D=0.01. The concentration profile is normalized by the average concentration.

This technique is tested in a pipe flow to determine the accuracy of using the probability method to generate a desired concentration profile. The results of the test are shown in Figure 20. The concentration is normalized by the average concentration, such that if there was no margination, then there would be a straight line at a value of 1. The radius was normalized with the maximum radius, such that the value of 1 is at the wall, and the value of 0 as is at the center axis of the pipe.

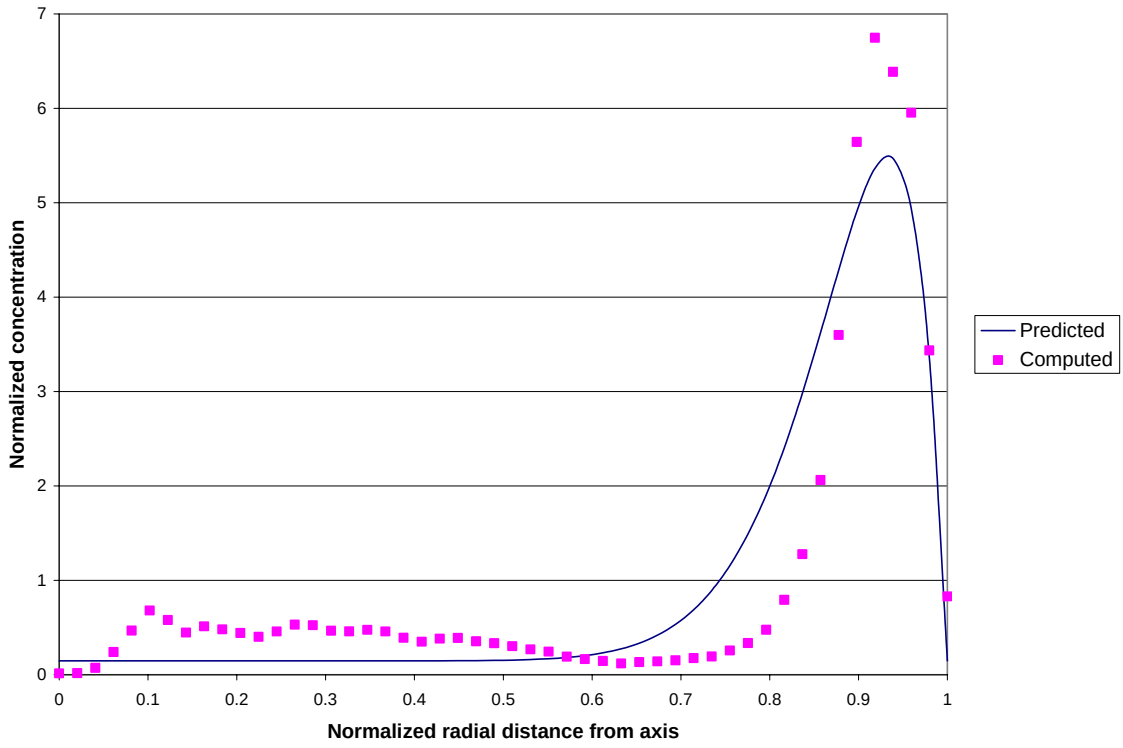

Figure 20: Normalized computed concentration profile plotted with the predicted profile. The concentration was normalized by the average concentration.

The margination method was tested with a stenotic specimen to determine the concentration profile. The profile can be seen in Figure 21. The dark blue region has the smallest concentration, while the red region has the largest concentration. It can be seen from the figure that there is a higher concentration near the wall.

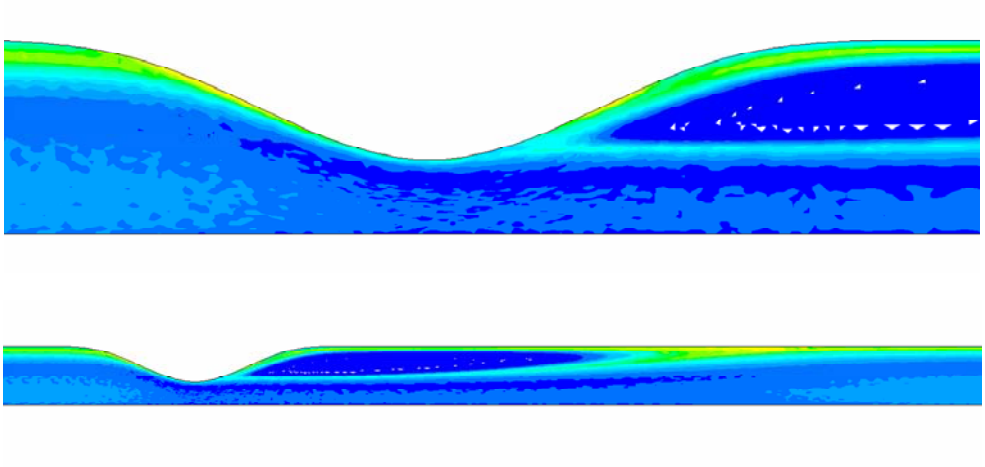

Figure 21: Platelet concentration profile along stenotic vessel.

The vessel radius effectively decreases as the thrombus grows. This is taken to account when the radius is determined for the margination calculation. Therefore, the calculation assumes a dynamic wall, which grows with time.

Adhesion

Three conditions were considered for the adhesion mechanism. The first considered 100% efficiency in platelet binding once a platelet reaches the wall. Therefore, adhesion was assumed to be infinitely fast. This is used for any case that does not specify a different adhesion mechanism. The second considers a shear rate threshold. The third considers a linear relationship between adhesion probability and shear rate. Platelets, in the threshold method, were placed in a condition that if the nearby shear rate is less than 1000 s^{-1} or greater than 20000 s^{-1}, then adherence was admissible at an infinite rate. Otherwise, a platelet was not allowed to adhere. These limits are based on results from (Savage, Saldívar et al. 1996) to determine the lower threshold and (Ruggeri, Orje et al. 2006) to determine the larger threshold. The assumption is that platelets at shear rates less than 1000 s^{-1} can adhere through Fibrinogen, while platelets at shear rates grater than 20000 s^{-1} can readily adhere through VWF. Otherwise, Savage suggests that platelets will transiently adhere and roll along the surface.

Transient adherence was considered by adding a condition for activated adherence shown in Equation 43. This equation is based off of a method used by (Goodman, Barlow et al. 2005), who fit a curve to data collected by (Hellums 1994). However, the condition used here includes a summation over the time history of a particle. If the summation exceeds a threshold, then the particle is considered activated.

Equation 43: Activation condition. The summation is over the time history of a individual particle.

$$\sum t\tau^{2.3} < 4.0\times10^{6} \ \frac{\text{dynes-s}}{\text{cm}^2}$$

Platelets that are considered for adherence through activation must be activated and then transport to a surface at a shear rate greater than 1000 s^{-1}, but less than 20000 s^{-1}. The platelets exited the computational domain before ever reaching the threshold. It should also be mentioned that there is no limit on the condition in Equation 43, meaning that a platelet would activate if it traveled an infinite amount of time. If platelets did activate within the computational domain, then the logistic equation, a common equation to represent a population, should be applied to Equation 43. Therefore, if the shear stress is below a level, there would be no additional term to the summation. Degradation of activation threshold would also need to be considered.

Another method was also considered for shear rate dependent adhesion, based on a linear relationship between adhesion probability and shear rate. This relationship was chosen based on the correlation between platelet deposition rate and shear rate (Flannery 2005), Figure 17, during phase II of platelet deposition. The linear relationship was further supported after reviewing the phenomenological model results. The phenomenological results approximately matched thrombus occlusion time and location. Therefore, the same linear relationship used to develop the phenomenological model is used here to consider the probability of platelet adhesion, given in Equation 47.

Equation 44: Probability for platelet adherence.

$$p = \frac{600749\ \dot{\gamma} + 5\times10^{9}}{600749\ \left(\dot{\gamma}_a\right) + 5\times10^{9}}$$

where p is the probability and $\dot{\gamma}_a$ is a constant based on maximum shear rate. A value is randomly chosen from a uniform distribution ranging from zero to one, and if the value is less than p in Equation 47, then adherence is permitted. $\dot{\gamma}_a$ was chosen to be a value of 50000 s^{-1}, for experimental simulation condition, to simulate slightly over twice maximum wall shear rate. This would almost always result in a calculation between 0 and 1. Values at 1 are always permitted to adhere.

The shear threshold condition for adhesion and the linear shear dependent adhesion condition are illustrated in Figure 22 for clarification. A random number is taken from a uniform distribution from zero to one and when the number falls below the shaded in part of the illustration, then the platelet adherence is considered admissible. The linear shear rate dependent adhesion is different from the phenomenological model. For the linear adhesion case, transport is also considered, and a platelet must be located in an active computational cell before it is considered admissible for adherence. A low probability for adherence with a high concentration of platelet could result in the same deposition as a high probability for adherence and a low concentration of platelets. This is different from the phenomenological model, which did not depend on platelet transport.

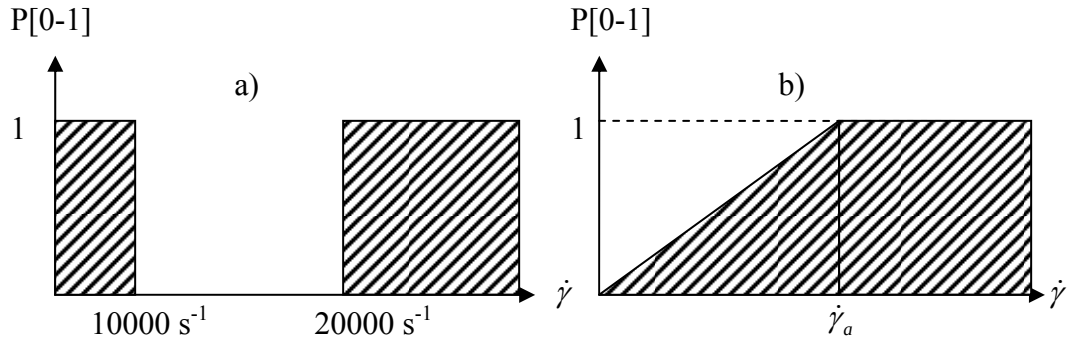

Figure 22: a) Threshold condition for adhesion. b) Linear shear rate dependent adhesion. $\dot{\gamma}_a$ is the shear threshold for the linear condition. All platelets bind with 100% efficiency above this number, which is set at 50000 s^{-1}.

CHAPTER

3. RESULTS

The results section is divided into four subsections. The first subsection, "Validation of Shear Rate and Continuous Phase Solution," was used to evaluate the flow regime and to validate flow characteristics near the stenosis. The second subsection, "Phenomenological Model of Platelet Deposition," considers thrombus growth based on thrombus deposition rate to peak wall shear rate data from (Flannery 2005). The third subsection, "Mechanistic Models of Platelet Deposition," evaluates three major mechanisms that are assumed to affect thrombus growth: shear enhanced diffusivity, margination, and shear dependent adhesion. The final subsection, "Mechanistic Models of Platelet Deposition Extrapolation," considers the extension of the experimental simulation model for flow at a Reynolds number found in coronary arteries. This subsection contains a select portion of the model extension. The study is continued in Appendix A. All models considered in the results are intended to simulate phase II of the platelet deposition curve, which is the phase consisting of the majority of thrombus growth. In addition all flow is from left to right in the figures.

Validation of Shear Rate and Continuous Phase Solution

Data from (Flannery 2005) exists for an 85% stenosis by reduction in area. Therefore, an 85% stenosis reduction by area is chosen to computationally evaluate thrombus formation. It is instructive to consider the flow patterns near the stenosis before thrombus is evaluated. Pathlines, colored by velocity magnitude contours, are illustrated in Figure 23. Flow is from left to right, as it is for all following figures in the results section. A recirculation region extends from the post-stenotic region by approximately 7mm from the stenotic peak. 7mm corresponds to a data extrapolation for

an 89% stenosis by area (Young and Tsai 1973) and an interpolation based on work by (Siegel Jr. 1992).

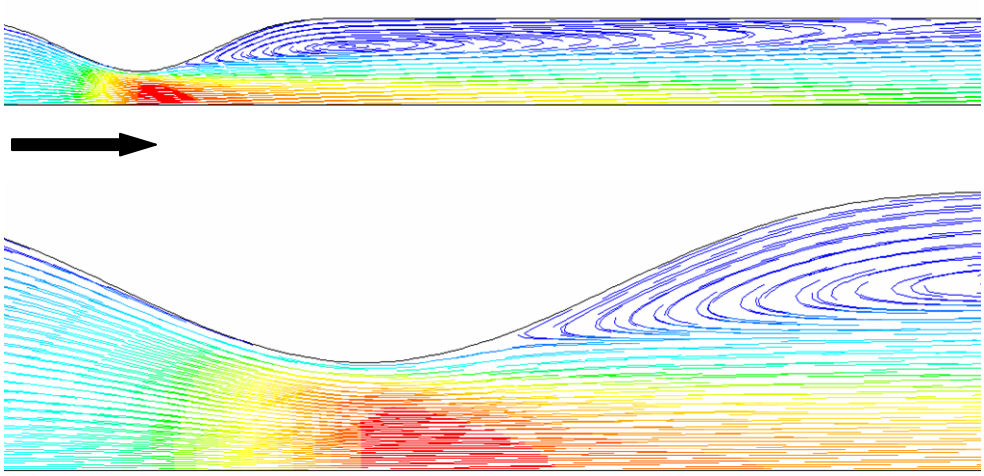

Figure 23: Pathlines colored by the velocity magnitude. The peak velocity is at the apex with low velocity in the recirculation region and near the wall due to the no-slip boundary condition.

A contour plot of the shear rate, also known as the strain rate, is presented in Figure 24. The methods used in the model are highly dependent on shear rate, and therefore it is important to understand how it varies in the flow field. The shear rate increases near the converging region of the stenosis and is highest at the wall. The high shear rate begins to extend from the wall once the flow undergoes separation. The post-stenotic region in the inner flow domain has an increased level of shear rate that dissipates away from the stenotic apex.

Figure 24: Strain rate contour plots across the stenotic region. The red region corresponds with the highest shear rate, occurring along the wall near the apex of the stenosis. The values along the wall can be taken from Figure 25.

A plot of the wall shear rate is shown in Figure 25 to supplement the flow field contour plot of shear rate, given in Figure 24. Figure 25 displays a higher shear rate near the entrance of the flow, as the velocity profile changes from a uniform profile to a parabolic

profile. The flow enters the stenotic region at a position of 15 mm, displaying increasing shear rate. The shear rate peaks slightly before the center of the stenosis, 17 mm, and begins to decrease thereafter. It reaches a value of 0 s^{-1} slightly before 24 mm, which is indicative of the flow reattachment point. Other regions correspond with the wall shear rate of Poiseuille flow of 533 s^{-1}, which can be predicted from Equation 6.

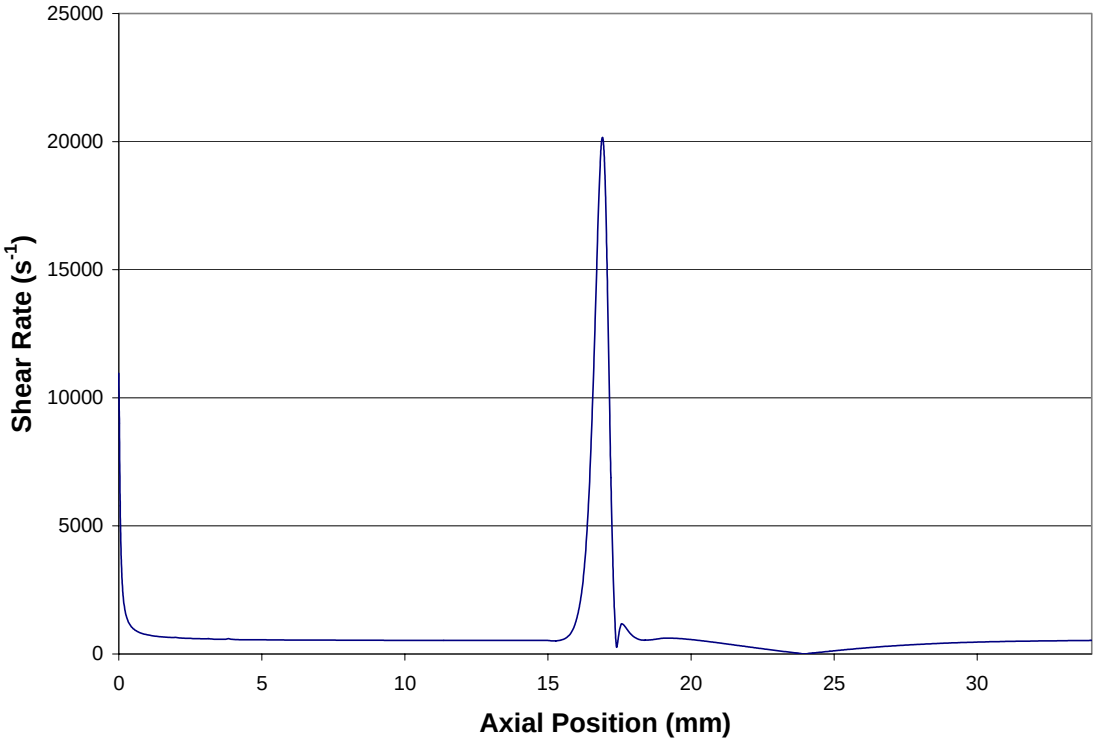

Figure 25: Wall shear rate across the entire flow field.

A magnified view of the wall shear rate plot at the stenosis is presented in Figure 26. The peak shear rate occurs slightly before the apex of the stenosis, 17 mm, and then dips down in the recirculation region. The peak shear rate is at a value of approximately 20000 s^{-1}, which corresponds with that predicted in (Siegel Jr. 1992).

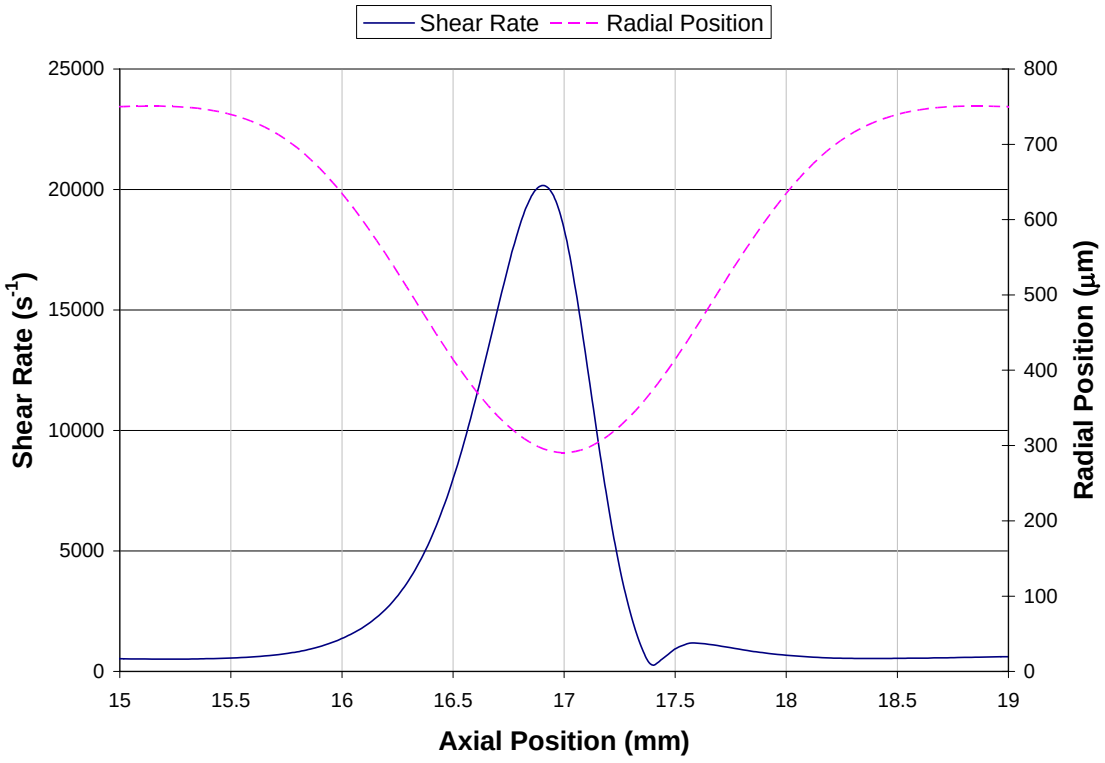

Figure 26: Magnified region around the stenosis. The wall shear rate is plotted relative to axial distance. The radial coordinate of the wall is also plotted across the axial position.

The pressure drop is also evaluated across the stenosis, Figure 27 matches closely with the data taken by (Young and Tsai 1973). The pressure slowly decreases along the axis of the vessel. There is a sudden pressure drop near the apex of the stenosis, with the lowest pressure slightly after the apex. The pressure rises again to its second peak at the flow reattachment point of ~25mm. The pressure does not represent the actual pressure in the vessel. The pressure is plotted as a pressure differential referenced from the pressure at the inlet.

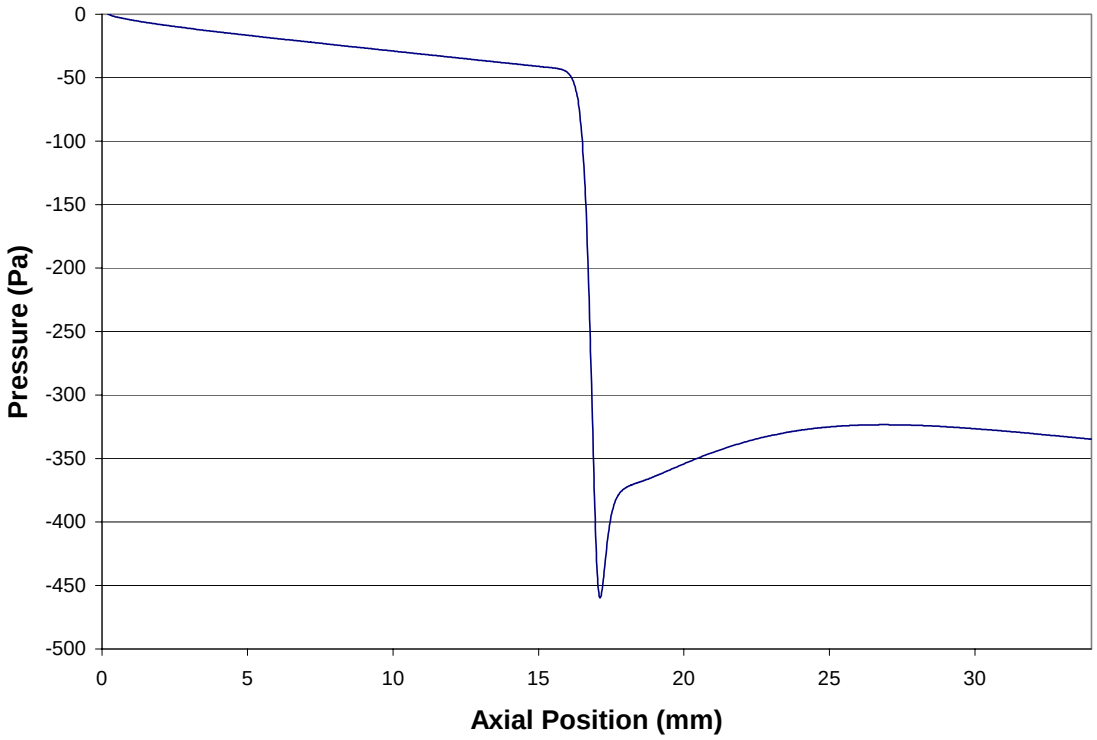

Figure 27: Static pressure differential versus axial position

Phenomenological Model of Platelet Deposition

The phenomenological model was performed for steady, laminar flow. The model considers platelet deposition based only on a data correlation between platelet deposition rate and peak wall shear rate ranging from 10000-40000 s^{-1} as described in the ”Methods” section. Platelet deposition is updated at every time step for all active cells. Active cells begin at the wall and when they reach a platelet volume fraction threshold, they activate neighboring cells. The time step exists in the user-defined function that contains the condition for platelet deposition. The flow solution is updated after each of these time steps to account for the changing porosity in active cells. Convergence of the flow field was reached before the phenomenological model began running.

Assumptions and Limitations

- Newtonian fluid: Approximation at the high flow rate and large vessel diameter used here.
- Flow is steady: Pulsatile flow has been shown to have secondary effects on convective transport (Basmadjian 1990) and diffusive transport (Fiechter 1998).
- Flow is laminar: Turbulence is only possible as the thrombus nears occlusion (Young and Tsai 1973). The addition of a turbulent model was found to have negligible effects on the platelet deposition for the studies used to simulate the experimental conditions.
- Flow is fully developed near the stenosis: A length of ten times the diameter was included between the inlet and the stenosis.
- Two-dimensional axisymmetric flow in the axial and radial direction: Approximation to the experimental flow.
- Adhered platelet volume fraction in a computational cell is 0.2 before thrombus grows to next cell: A change in the volume fraction threshold would affect the time scale of the computational results, but would not affect the relative time scales between the computational results. 0.2 was approximated as an "atomic packing factor" for platelets in a thrombus.
- The vessel wall is inelastic: The test specimen's wall was made of glass.
- No embolization
- No stress constraints on thrombus growth
- Platelets can only deposit in active cells. An active cell is one that borders either the boundary of the blood vessel wall or borders the boundary of the thrombus. Platelets attach when they reach any location in the cell.

- The accuracy of the solution is limited by the choice in time step. The time step was chosen small enough so that the thrombus formation did not have any visually qualitative variance at smaller time steps for the thrombus formation location and occlusive time.
- Forces, such as the lift force, are excluded from the model and are assumed to be included in the margination condition. This is a limitation in the model and may result in inaccuracies, especially for conditions that don't include margination.

Phenomenological Model Results

The results of the phenomenological model are presented in Figure 28. The figure displays computational cells that have completely occluded. The thrombus begins growing at the highest shear regions, as specified by the model algorithm. The thrombus continues to grow in the throat of the stenosis. There is some additional growth along the vessel wall, which is uniform in regions away from the stenosis. The growth continues outward from the apex of the stenosis, until it occludes the blood vessel near 320 s, corresponding to 5.3 minutes. There is very fast growth once the thrombus is midway to full occlusion. This can be seen by looking at the times associated with the figure. The times are increased incrementally by 80 seconds. However, an additional time point is inserted at 280 seconds to capture the shape of the growth as the thrombus nears occlusion.

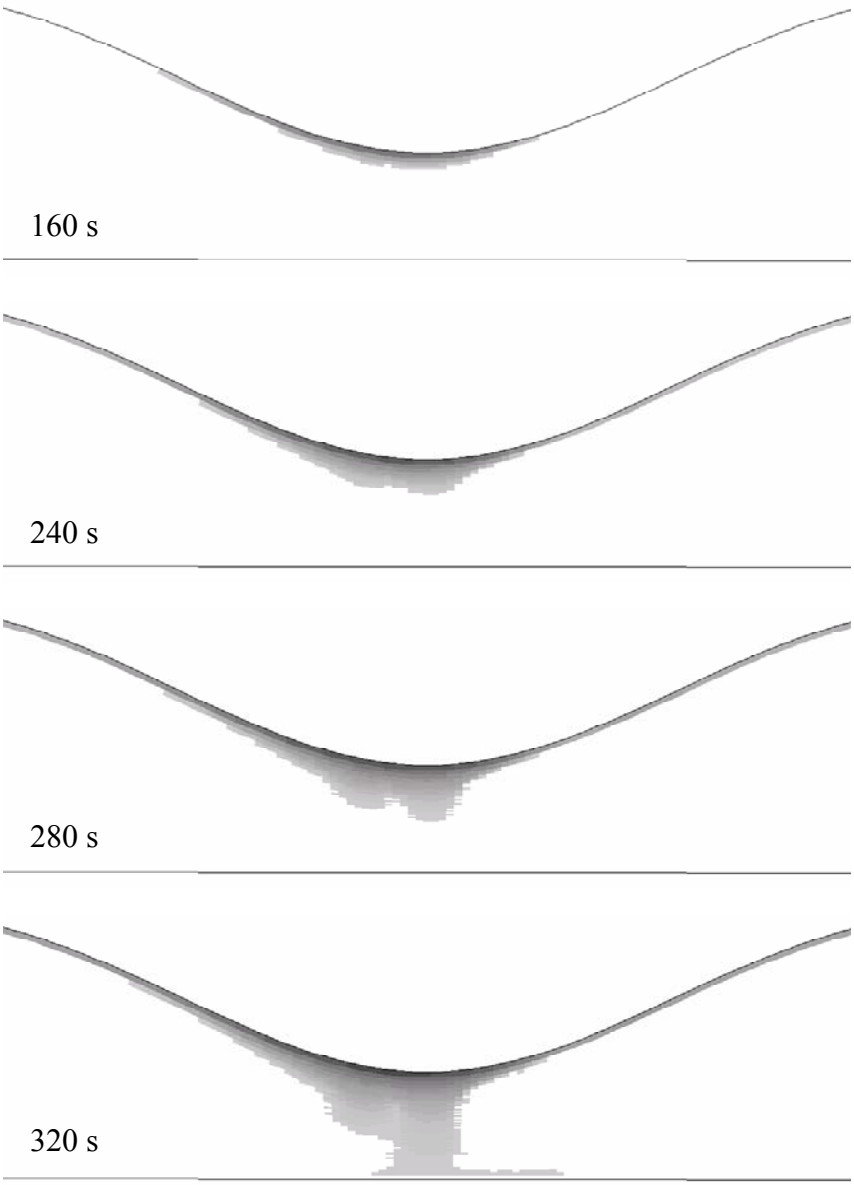

Figure 28: Time progression of thrombus formation based on the curve fitting condition from Figure 17. The contours are of the time progression of thrombus growth. The outer, light gray region is the most recent addition to the thrombus, while the darkest shade is the oldest thrombus. A condition of zero velocity is applied to regions that are considered blocked by thrombus.

The results match the location of the experimental vessel occlusion. However, there is increased thrombus size in the converging region for the experimental results, relative to what can be seen in the computational results, Figure 28. It takes slightly over five minutes for complete occlusion in the computational results, which matches very closely

with phase II of the experimental results. Therefore, the phenomenological model captures important features of the thrombus formation and can be used as a baseline for the mechanistic models that consider the contributing mechanisms to platelet deposition. A plot of platelet deposition with respect to time, for the phenomenological model, is presented in Figure 29. Platelet deposition begins very slowly. The deposition becomes approximately linear with respect to time for approximately 1.5 minutes, beginning after 1 minute. After a base layer of thrombus forms, deposition begins to accelerate and then becomes approximately linear with respect to time again for a little under another 1.5 minutes. The lumen diameter continues to decrease during this period, increasing the shear rate and decreasing the available surface area for deposition. The deposition rate returns to a lower value, again, after four minutes. It remains approximately constant until full occlusion around five minutes.

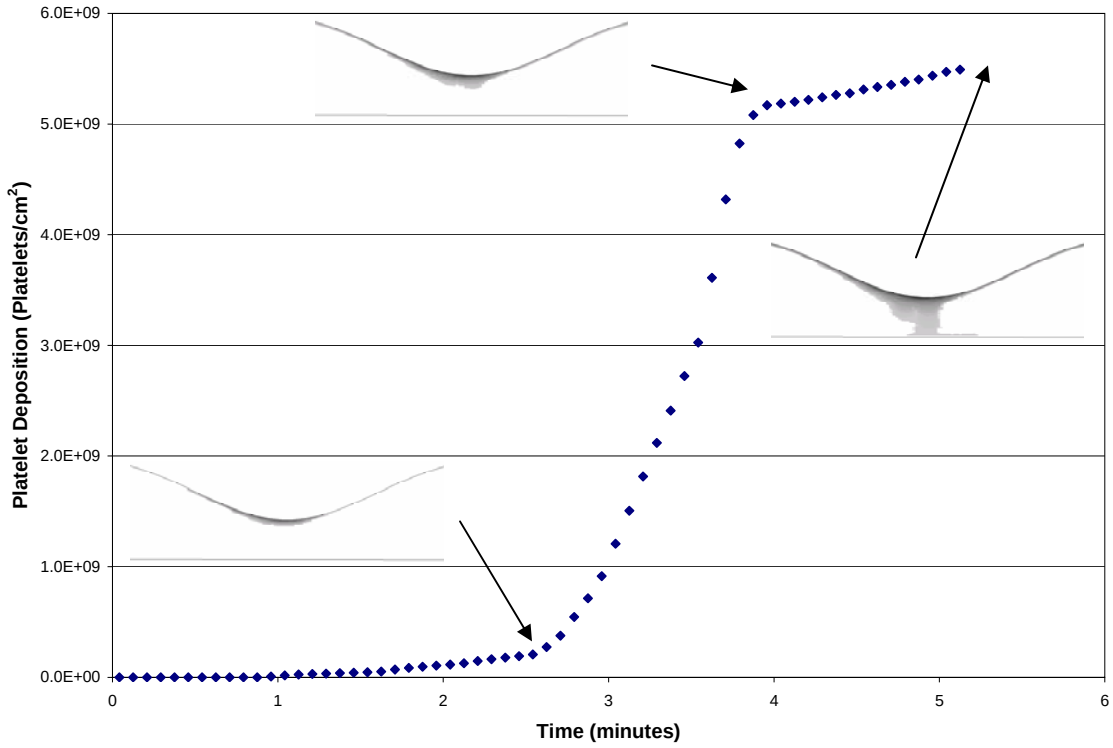

Figure 29: Phenomenological model of platelet deposition versus time plot.

Mechanistic Models of Platelet Deposition

The mechanistic model is used to consider how individual mechanisms may affect thrombus growth. Three mechanisms are considered: shear rate enhanced diffusivity, platelet margination, and shear rate dependent platelet adhesion. These are broad categories that self contain many additional mechanisms. However, these three categories are often the primary mechanisms that are considered for thrombotic models (Stubley, Strong et al. 1987; Wootton, Markou et al. 2001). Additional parameters, such as platelet activation and a drag force threshold for platelet attachment were also considered and are described in Appendix A.

Each run was allowed to reach a steady state condition before platelets were allowed to adhere. Steady state, here, means that the time averaged platelet concentration gradient did not change across the fully developed flow solution. The test cases were then allowed to run until the thrombus reached full occlusion. A sufficient number of continuous phase iterations were specified to run between discrete time steps to resolve the flow solution around the transporting platelets, before they were allowed to advance in the flow. The number was set at 10 iterations. Four different computational experiments were performed to evaluate how each of the three mechanisms used in the study affect thrombus growth. The computational experiments are listed in Table 4. They are listed in order of least complex to the most complex. This allows each new mechanism to build on the previous one.

Table 4: Computational experiments

Run	Description
1	Shear rate enhanced diffusivity
2	Shear rate enhanced diffusivity and margination
3	Shear rate enhanced diffusivity, margination, and adhesion shear threshold
4	Shear rate enhanced diffusivity, margination, and linear relation between adhesion and shear rate

Assumptions and Limitations

- Newtonian fluid: Approximation at the high flow rate and large vessel diameter used here.
- Flow is steady: Pulsatile flow has been shown to have secondary effects on convective transport (Basmadjian 1990) and diffusive transport (Fiechter 1998).
- Flow is laminar: Turbulence is only possible as the thrombus nears occlusion (Young and Tsai 1973). The addition of a turbulent model was found to have negligible effects on the platelet deposition for the studies used to simulate the experimental conditions.
- Flow is fully developed near the stenosis: A length of ten times the diameter was included between the inlet and the stenosis.
- Two-dimensional axisymmetric flow in the axial and radial direction: Approximation to the experimental flow.
- Adhered platelet volume fraction in a computational cell is 0.2 before thrombus grows to next cell: A change in the volume fraction threshold would affect the time scale of the computational results, but would not affect the relative time scales between the computational results. 0.2 was approximated as an "atomic packing factor" for platelets in a thrombus.
- The vessel wall is inelastic: The test specimen's wall was made of glass.
- Platelets have infinitely fast binding
- Platelet enhanced diffusivity is only shear rate dependent and not dependent on volume fraction
- Platelets are a modeled as point masses
- Platelets are allowed to pass through the occluded computational cells. However, there is one condition that is considered for the case of shear rate enhanced diffusivity and margination, in which the platelets are eliminated if the do not

deposit and reach a completely occluded cell. They do not reflect off the boundary or roll on the boundary, like they would in a physical system.

- No embolization
- Only stress constraint was a condition that a cell could not activate until the neighboring computational cell closer to the wall is activated. The condition thickened any outgrowth from the thrombus, essentially decreasing the stress at the base of the outgrowth
- Platelets can only deposit in active cells. An active cell is one that borders either the boundary of the blood vessel wall or borders the boundary of the thrombus. Platelets attach when they reach any location in the cell.

1. Shear Enhanced Diffusivity

Shear enhanced diffusivity was evaluated based on a study performed by (Zydney and Colton 1988). The randomized velocity fluctuation term used to model shear enhanced diffusivity was verified with predicted results. The verification is described in the methods section. Platelets were permitted to flow through the thrombus if they have not reached an active computational cell that permits adhesion. The results for shear enhanced diffusivity yielded thrombus growth ranging from the stenosis apex to approximately the midline of the converging region of the stenosis. There is minimal thrombus formation everywhere else along the vessel. This is illustrated in Figure 30. The highest deposition location corresponds to the highest wall shear rates, which can be reviewed in Figure 26. The thrombus continues to grow in the downstream direction from the points of highest wall shear rate. As the thrombus grows, the wall essentially grows and changes the location of highest wall shear rate. Flow separation begins to occur off of protruding thrombi, therefore, drastically lowering the wall shear rate in the

separation region, which may have previously been a high wall shear rate. The thrombus eventually occludes in the post-stenotic apex region.

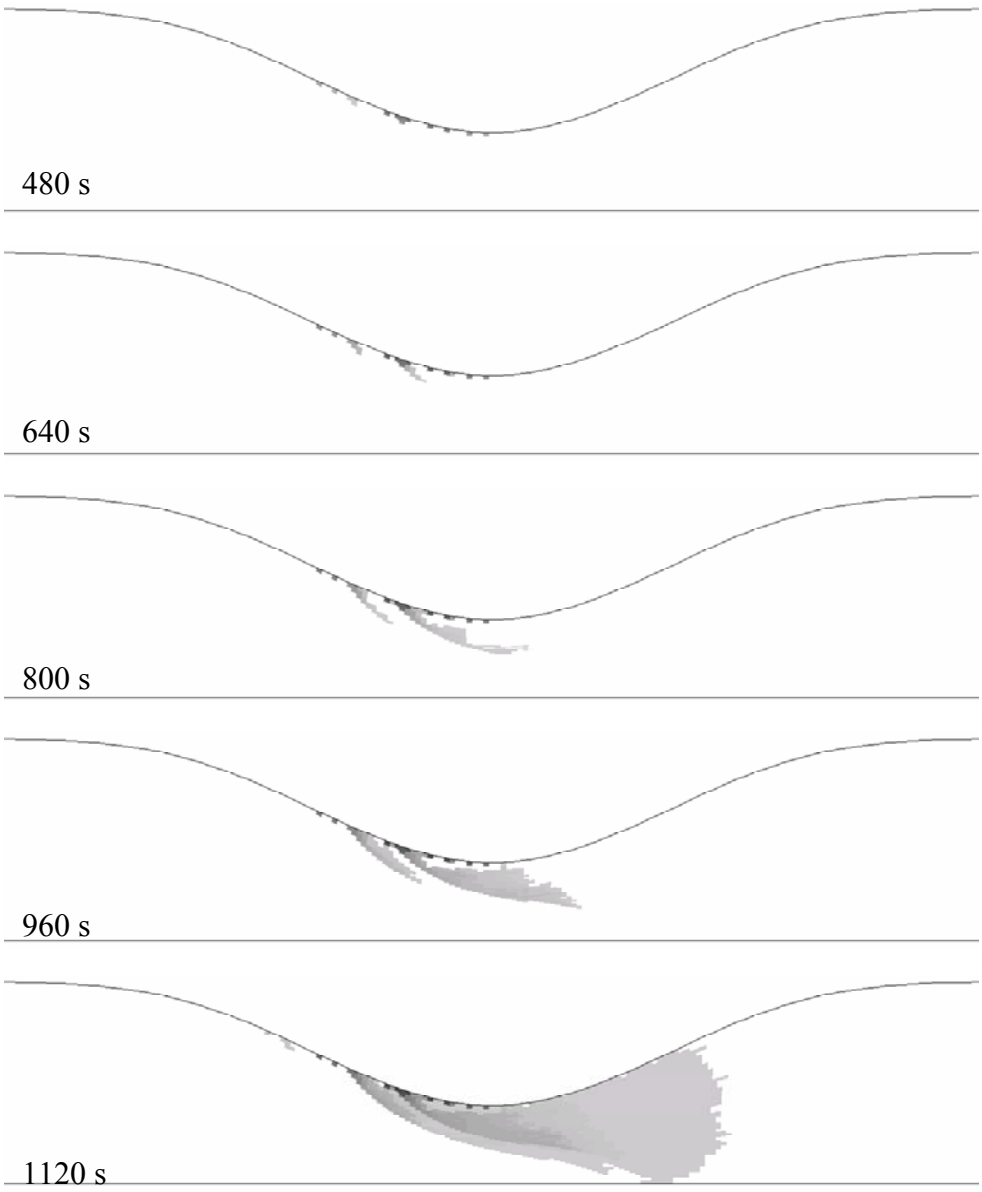

Figure 30: Shear enhanced diffusivity time progression of thrombus aggrandizement.

A plot of platelet deposition with respect to time, for the enhanced diffusivity model, is presented in Figure 31. Platelet deposition begins very slowly. The deposition becomes approximately linear with respect to time for approximately 10 minutes, beginning after 3 minutes. After a base layer of thrombus forms, deposition begins to

accelerate and a protrusion of thrombus extends into the flow. The lumen diameter continues to decrease during this period, increasing the shear rate and decreasing the available surface area for deposition. The curve flattens out momentarily and then the deposition begins to accelerate again. The entire curve is approximately second order.

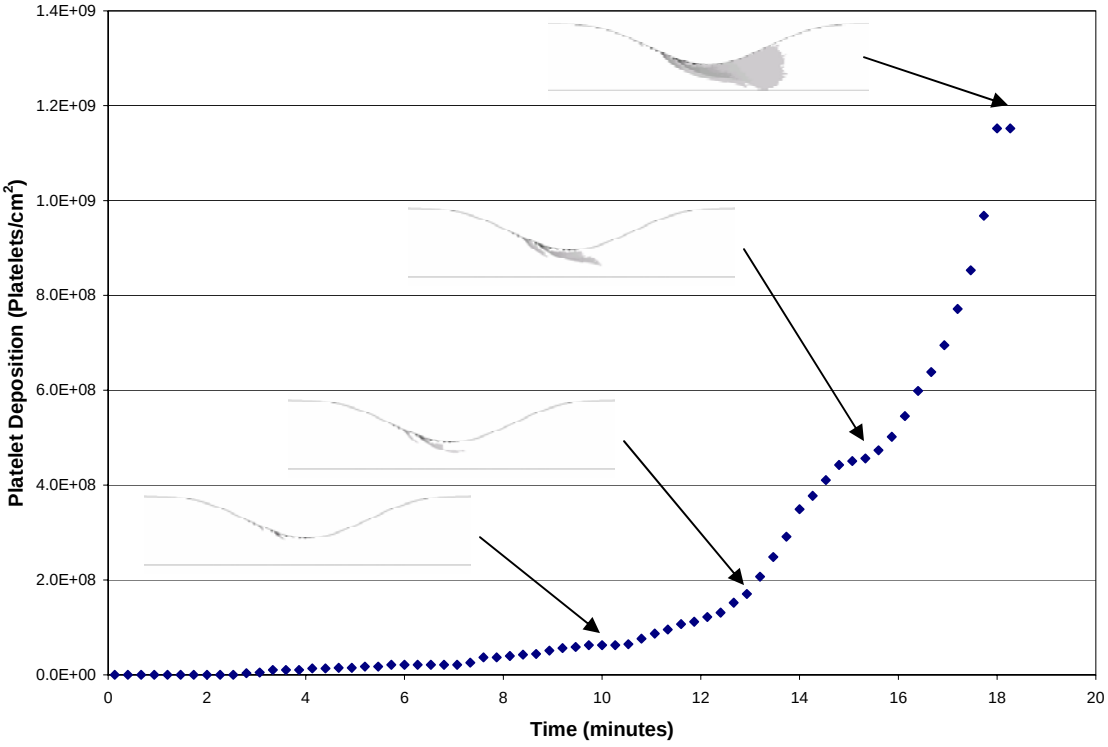

Figure 31: Enhanced diffusivity model of platelet deposition versus time plot.

2. Shear Enhanced Diffusivity and Margination

Shear enhanced diffusivity and shear dependent platelet margination were considered in this study. There was no shear dependence for adherence. Platelets were assumed to adhere once they enter an active computational cell. Multiple sub-studies were performed for the shear enhanced diffusivity and margination condition. The first considered platelet concentration with and without margination. The second considers thrombus growth using the same conditions applied to the shear enhanced diffusivity case. The third considers the elimination of platelets that enter a fully occluded computational cell, therefore prohibiting them from passing through a thrombus.

Concentration of Shear Enhanced Diffusivity and Shear Enhanced Diffusivity with Margination

It was instructive to consider the platelet concentration profile resulting from shear dependent dispersion before considering thrombus formation in the shear enhanced diffusivity with platelet margination case. It was predicted that increased platelet motion at high shear regions would cause increased concentrations in the regions of lower motion. This would cause platelets to move toward the central axis in a tubular vessel. The concentration profile after applying shear rate dependent effective diffusivity is shown in Figure 32 and is approximately the inverse of the concentration profiles predicted by (Eckstein, Bilsker et al. 1987; Aarts, van den Broek et al. 1988). It should be noted that the geometry is not streamlined like the other runs. However, the concentration profile of the streamlined geometry yields a similar result to the one shown here.

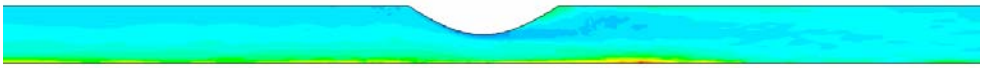

Figure 32: Concentration profile results from only shear dependent dispersion and no margination. The blue region has the lowest concentration of platelets. The largest concentration is along the central axis.

It can be seen from Figure 32 that the largest concentration of platelets occurs along the central axis of the vessel, where shear rate was the lowest. The lowest concentrations exist where the shear rate was found to be the largest, along the wall at the apex of the stenosis. The result can be compared with Figure 33, which includes margination. The concentration profile in Figure 33 appears to match with experimental profiles of (Eckstein, Bilsker et al. 1987; Aarts, van den Broek et al. 1988). A uniform cylindrical vessel was also used to verify predicted concentration results, as described and shown in the methods section.

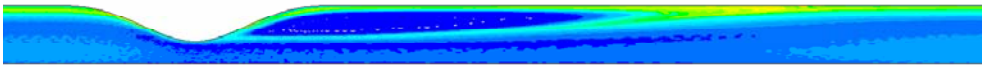

Figure 33: Concentration profile resulting from shear dependent dispersion and the addition of margination. The blue region has the lowest concentration of platelets. The largest concentration is along the wall of the vessel.

Shear Enhanced Diffusivity with Platelet Margination

The results of the shear enhanced diffusivity with platelet margination are presented in Figure 34. The time sequence looks very similar to the results seen for the case that only considered shear enhanced diffusivity. The thrombus begins to develop from the highest wall shear rate and continues to grow in the downstream direction. The thrombus completely occludes around 480 s, or approximately 8 minutes. Occlusion occurs slightly downstream of the stenosis apex.

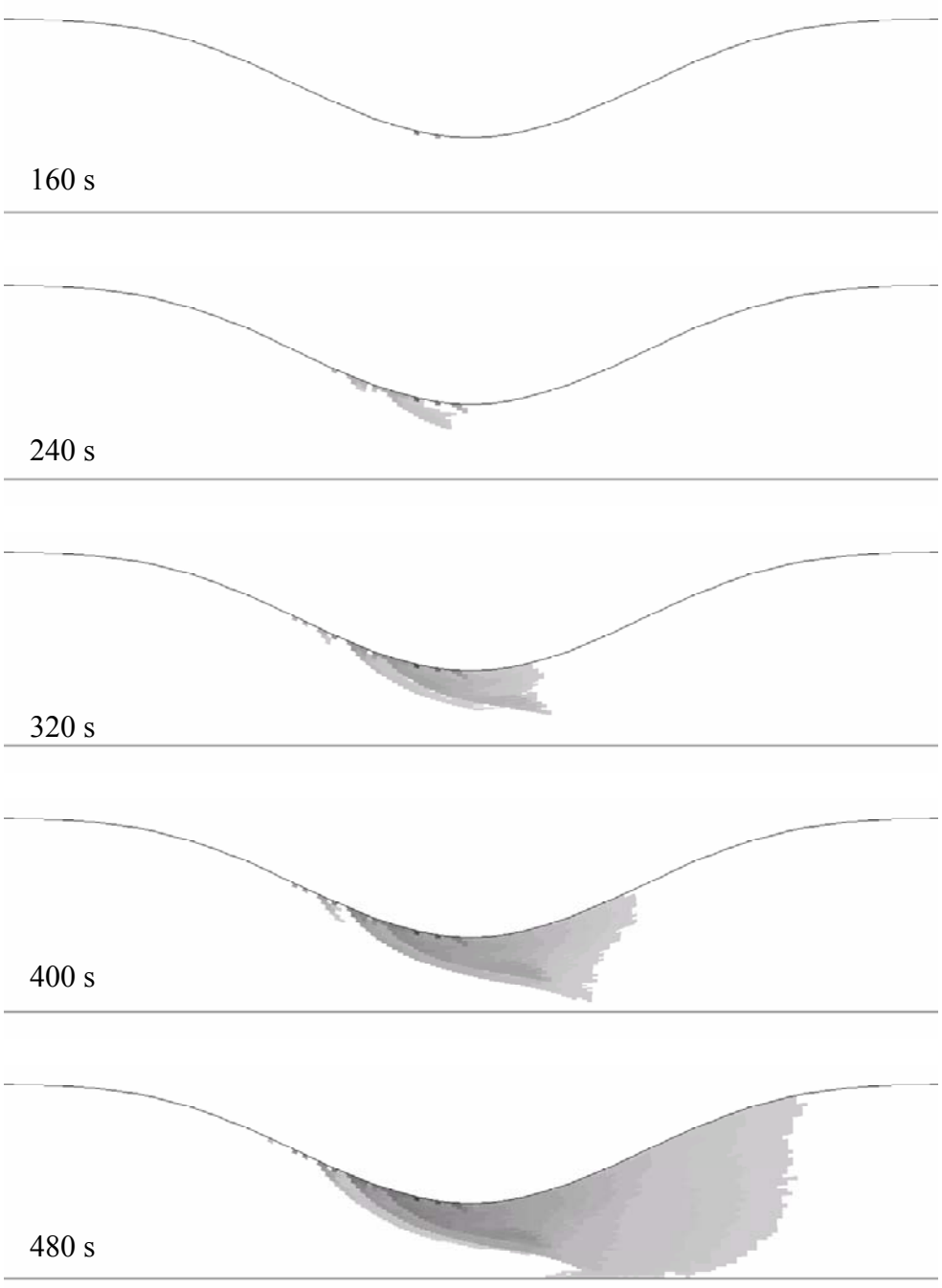

Figure 34: Shear enhanced diffusivity and platelet margination time progression of thrombus aggrandizement. The darkest shade in the figure corresponds the oldest thrombus, while the lighter shade is the newest region of thrombus.

A plot of platelet deposition with respect to time, for the shear enhanced diffusivity with margination model, is presented in Figure 35. Platelet deposition begins

very slowly, like in the other cases. There is a region of acceleration after 2 minutes. Then the curve becomes approximately linear until about 6.5 minutes, where deposition begins to accelerate again.

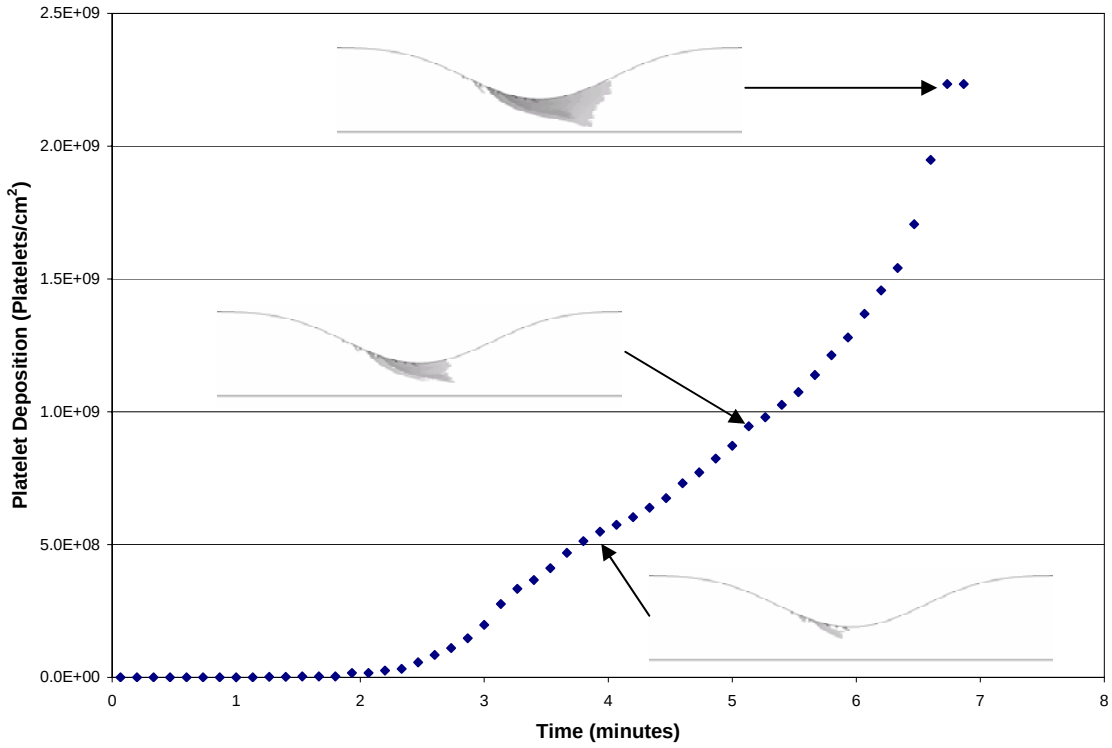

Figure 35: Enhanced diffusivity with Margination model of platelet deposition versus time plot.

Shear Enhanced Diffusivity with Platelet Margination and Prohibition of Platelet Transport Through Occluded Thrombus

An additional condition was applied to consider how deposition would change if platelets were not allowed to flow through the thrombus. Every other parameter is the same as the condition just described in the previous subsection, "Shear Enhanced Diffusivity with Platelet Margination." Thrombus, for the platelet prohibition condition, began to form slightly further upstream of the previous case. The thrombus formation is not as thick because platelets have minimal capability of transporting to the region behind a protruding thrombi. This is because platelets are not permitted to pass through a

thrombus if they do not deposit for this particular sub-study. The thrombus also takes significantly longer to occlude the blood vessel. The thrombus begins to thicken in the upstream direction, as the time sequence proceeds. Complete occlusion occurs at 2000 s, corresponding to 33.3 minutes.

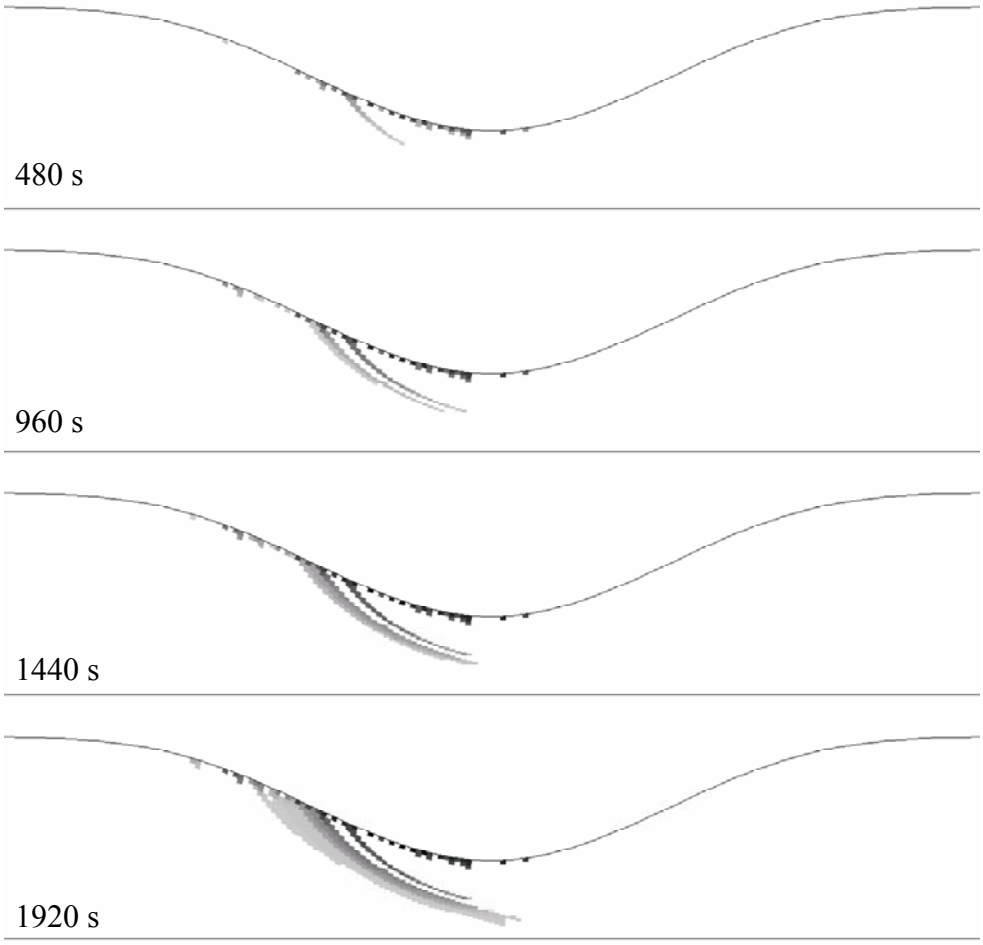

Figure 36: Shear enhanced diffusivity and platelet margination time progression of thrombus aggrandizement. The case does not permit the passage of non-depositing platelets to pass through the thrombus. The darkest shade in the figure corresponds the oldest thrombus, while the lighter shade is the newest region of thrombus.

3. Shear Enhanced Diffusivity, Margination, and Adhesion Shear Threshold

A shear threshold for adhesion was added to the enhanced diffusivity with margination model. Figure 37 illustrates that the most significant thrombus growth occurs in post-stenosis area. There is some additional growth along the throat of the stenosis, where the thrombus was allowed to grow from the apex, the only region where the wall shear rate exceeds 20000 s^{-1}.

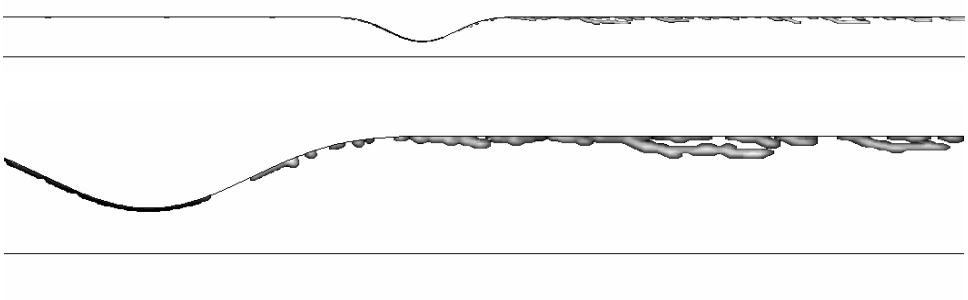

Figure 37: Shear enhanced diffusivity, platelet margination, and adhesion threshold condition thrombus aggrandizement. The darkest shade in the figure corresponds the oldest thrombus, while the lighter shade is the newest region of thrombus.

4. Shear Enhanced Diffusion, Margination, and Linear Relation Between Adhesion and Shear Rate

The resemblance between the phenomenological model and the experimental results indicates that there may be a linear relationship between platelet adhesion and shear rate for phase II of platelet deposition. The linear relationship was extended to the mechanistic model by considering a probability for platelet attachment based on the linear relation with shear rate, described in the methods. Higher shear rates result in a higher probability for platelet adherence. The results of the study are presented in Figure 38. The linear adhesion relationship appears to shift the thrombus growth further downstream. Growth still initiates near the highest shear rate. However, there is minimal growth upstream of this point for the linear adhesion case. Therefore, no further

protrusions of thrombus occur elsewhere along the stenosis. The occlusion time for this case is near 800 s, corresponding to 13.3 minutes.

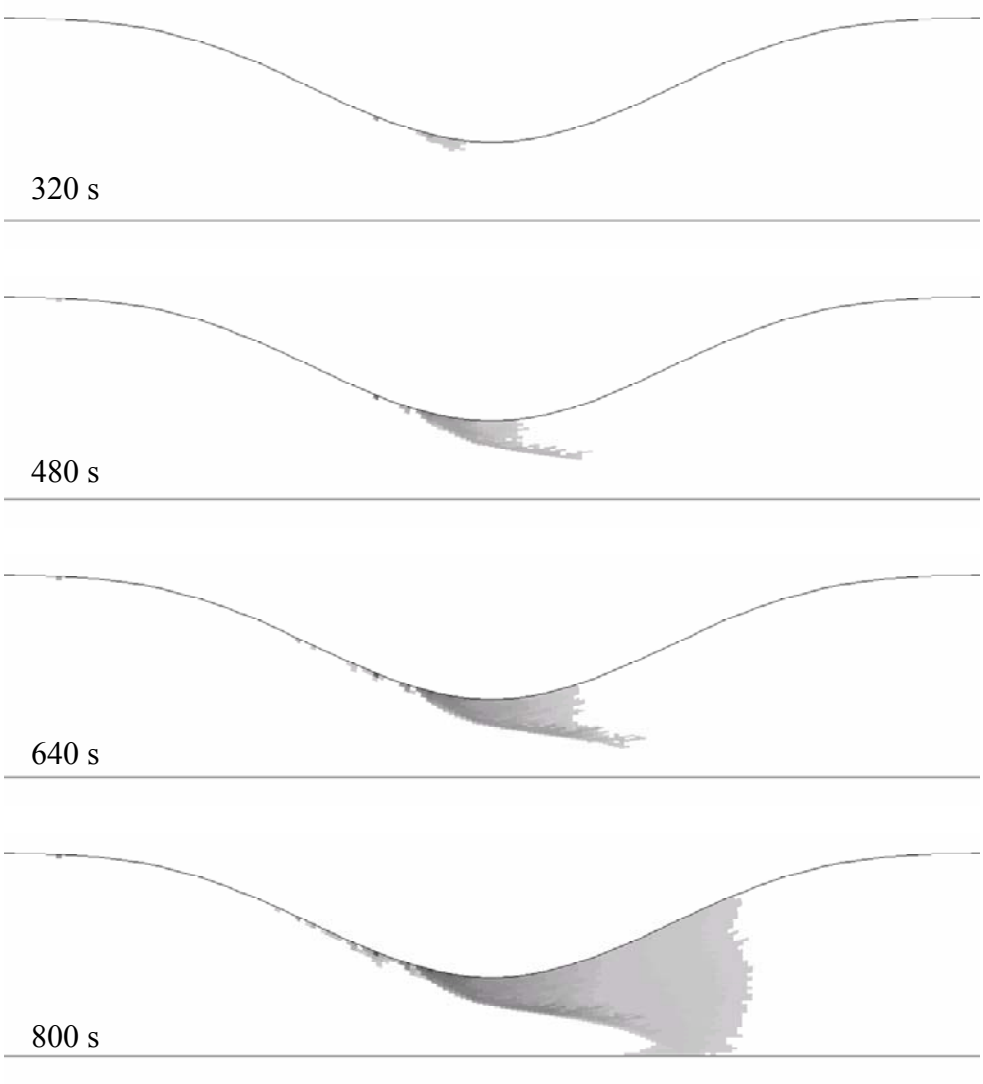

Figure 38: Shear enhanced diffusivity, platelet margination, and linear shear to adhesion relation time progression of thrombus aggrandizement. The darkest shade in the figure corresponds the oldest thrombus, while the lighter shade is the newest region of thrombus.

A plot of platelet deposition with respect to time, for the shear enhanced diffusivity with margination model, is presented in Figure 39. Platelet deposition begins very slowly. There is a region of acceleration after 4.5 minutes. Then the curve becomes approximately linear until about 10.5 minutes, where deposition begins to accelerate

rapidly.

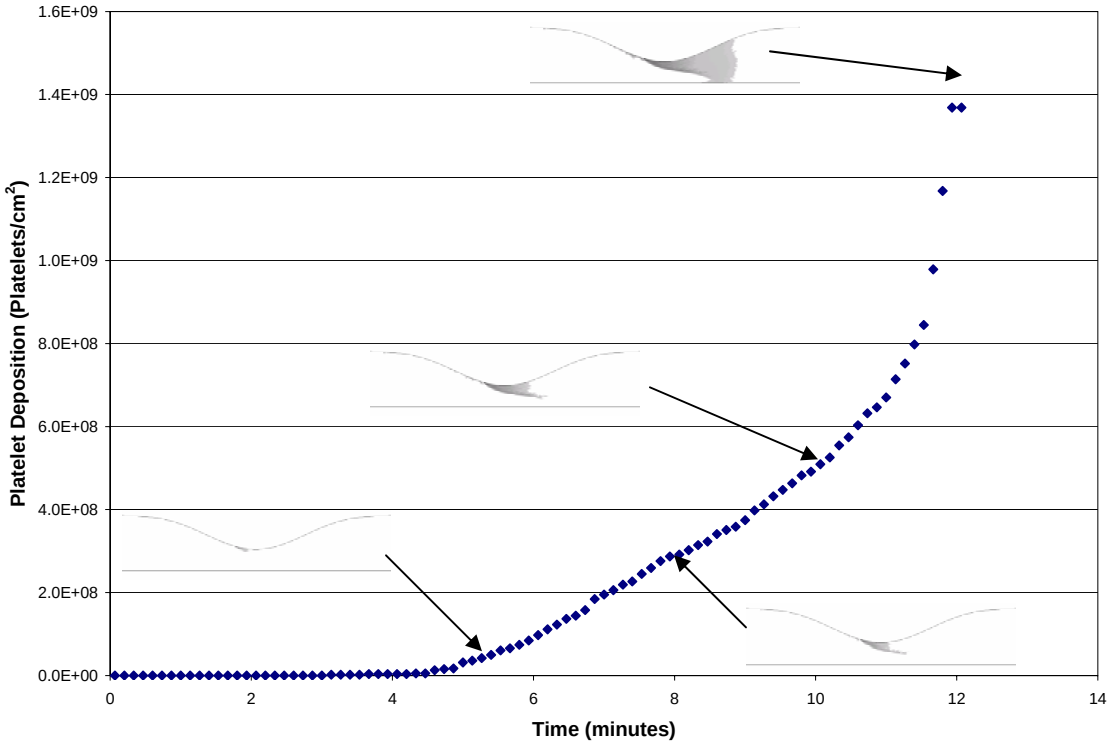

Figure 39: Enhanced diffusivity, Margination, and Adhesion model of platelet deposition versus time plot.

The shear rate linear dependent adhesion condition reduced occlusion time relative to shear enhanced diffusivity with margination. This was necessary from the definitions used to generate the linear relation between shear rate and adhesion probability. Adding adhesion probability can only disallow adhesion based on particular shear rates. Since, the shear enhanced diffusivity with margination case assumed all platelets at the wall deposited, then adding the adhesion probability can only reduce the occlusion time and possibly change the thrombus deposition location. It appeared from the results to only affect the rate of occlusion, and did not change the location.

Summary of Experimental Simulation Results

The results are summarized in this section to clarify a comparison of the three various mechanisms considered here for thrombus formation. A point in time is taken for each condition in the results based on approximately equal thrombus growth. These points are shown in Figure 40. The phenomenological model grows the fastest and has an occlusion time that corresponds with the experimental results. Enhanced diffusivity and margination also has an occlusion time that is near the experimental time of occlusion. Enhanced diffusivity, alone, takes the longest time to occlude the vessel. The location for thrombus occlusion that best corresponds with the experimental results is the phenomenological model. The second best correspondence is the effective diffusivity and margination model. All of the mechanistic models had similar growth patterns. Growth initiated near the highest wall shear rate, and then began to grow downstream. The phenomenological model also had slight downstream growth, as can be see from Figure 40, where the downstream bulge is slightly larger than the upstream bulge. It appears as though there may be a similar bulge in the experimental result presented in the figure. However, it is difficult to discern due to image quality.

Models of thrombus formation and aggrandizement would need to include mechanisms of platelet transport and adhesion. However, the results here indicate which parameters may need to be physically measured with accuracy. The rate of occlusion had significant dependence on margination. Therefore, if an accurate rate of occlusion was of interest in a future model, then margination should be considered an important mechanism to the model. If occlusion time is not the main interest, then accuracy of margination may not be as pertinent. The adhesion function is not as important for a case where transport limits the rate of thrombus deposition. However, there can be a condition where there are excess platelets at the thrombus reactive surface, in which case the

adhesion function may be very important. Enhanced diffusivity is an important mechanism for the case where transport limits the rate of platelet deposition.

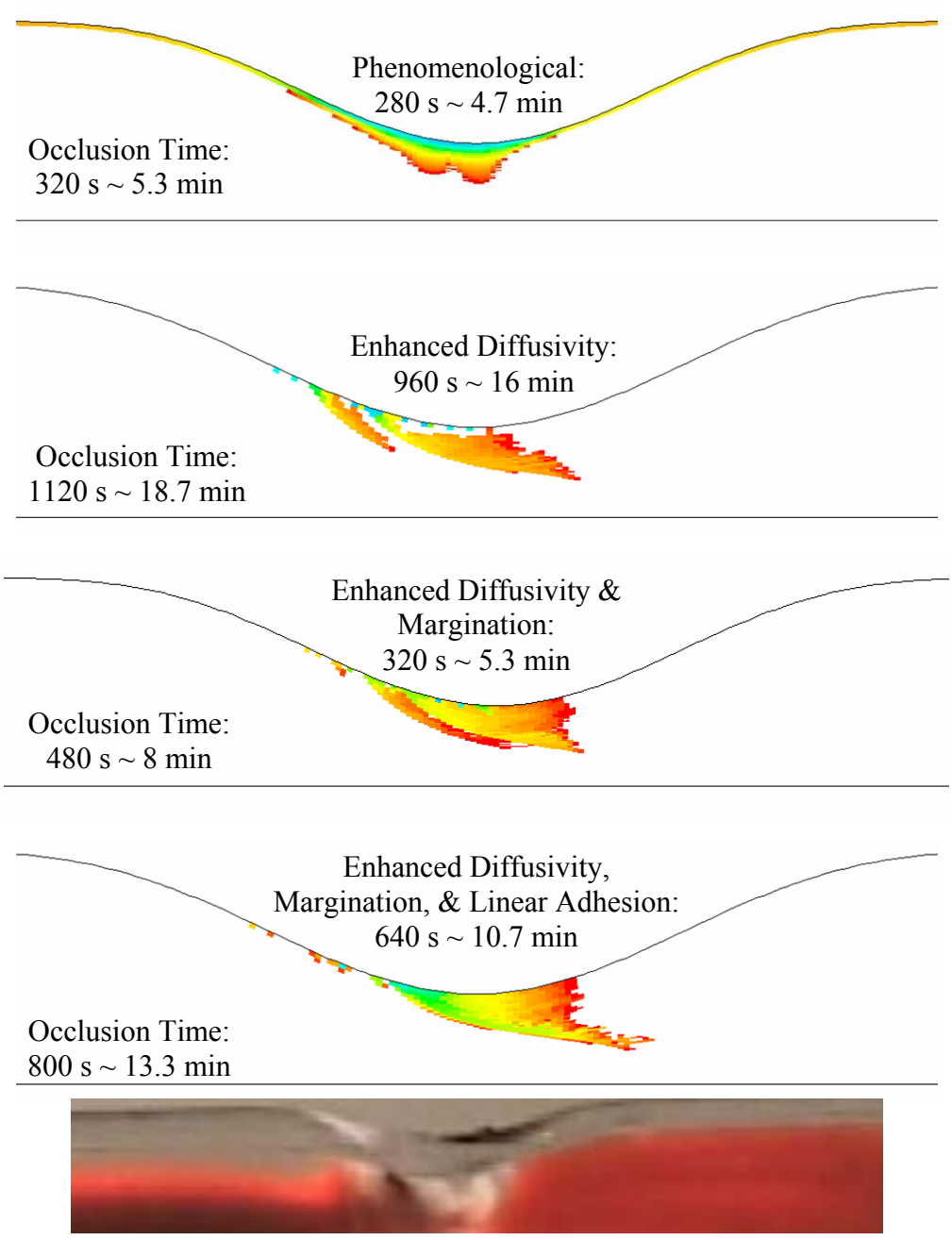

Figure 40: Summary of the experimental simulation results comparing models and mechanisms.

The phenomenological model was quantitatively capable of predicting occlusion time to within 0.2 minutes, while the closest occlusion time for the mechanistic model

was within 2.5 minutes. These values assume that the computational model only simulated the second phase of platelet deposition and that only the second phase timeframe could be compared. The various assumed phases are presented in Figure 41. However, a plot of platelet deposition versus time showed that the first phase may actually exist in the computational models in addition to the second phase of platelet deposition. This was concluded by evaluating the shape of the deposition curves; there is an accelerating phase of deposition, which develops into tends to a linear relation between deposition and time, except for possibly the case where shear enhanced diffusivity is only considered.

If the first two phases are assumed for the mechanistic model, then evaluation of the second phase yields a much better correlation with the empirical results. This explanation is illustrated in Figure 41; where the occlusion time for the model is presented in Equation 45, where τ is time.

Equation 45: Occlusion time

$$\tau_{i,\,final} - \tau_{i,initial,\,j}$$

where the i is either p for the empirical results or m for the mechanistic model and j is 1 for the initial time assuming only the second phase is modeled or 2 for the initial time assuming that two phases are modeled. The mechanistic shear enhanced diffusivity with margination case was within approximately 0.5 minutes of the occluding time for the results, assuming two phases are modeled. The phenomenological model was more difficult to decipher. It did not have a distinctive second phase. However, values of approximately a 4 minute difference, or a 2.7 minute difference could be estimated for a phase II of the phenomenological model.

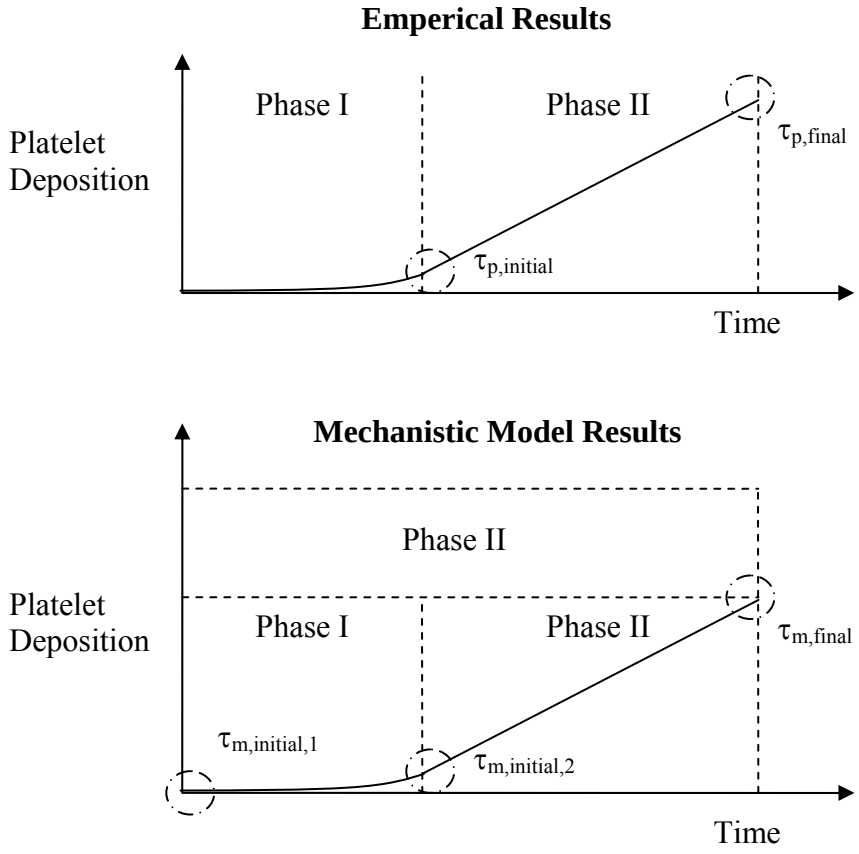

Figure 41: Predicted platelet deposition versus time plot with an illustration of the mechanistic model results.

The platelet deposition versus time plots generated for the mechanistic models are based on the assumption that the function for platelet adhesion to the wall does not change with time, agonists, or activation. The adhesion assumes every platelet that reaches the wall deposits, and is therefore representative of the maximum possible deposition. Therefore, the initiation of time in these plots may correspond to a point in the experiment where the equilibrium of these mechanisms has occurred. If the plots are plotted together, it is interesting to note that there appears to be a region of 8.5 minutes that the model does not capture, seen in Figure 42.

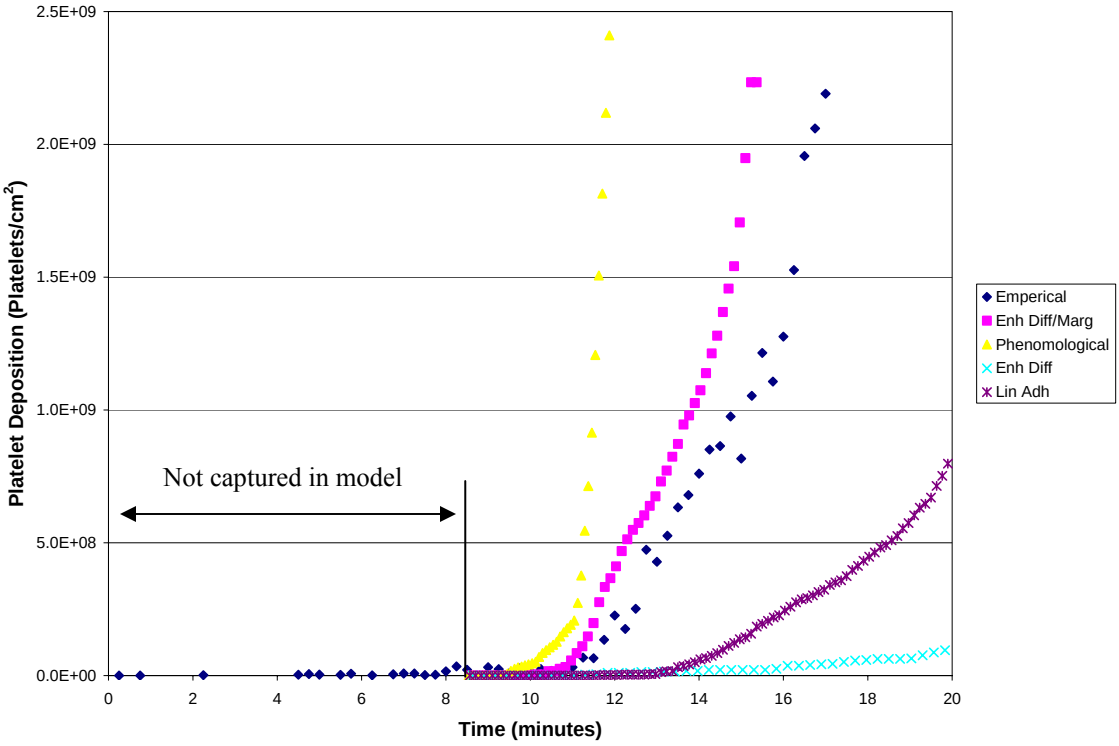

Figure 42: Plot summary of platelet deposition versus time. All model results are assumed to begin at 8.5 minutes. The axes are cutoff, so that the empirical model best fit in the graph. Therefore, the only two curves that fit fully on the plot are the empirical results and the enhanced diffusivity with margination model.

The results show that the model that best correlated with the empirical results was the enhanced diffusivity with margination model. There appears to be a very similar curve shape between that model and the empirical results. However, the empirical results may be leveling off slightly near occlusion, while the model accelerates deposition. The other models had significantly different slopes. The phenomenological model's deposition accelerated at approximately the same rate as the empirical results, but then continued to accelerate instead of becoming linear with time. The deposition plot is recreated in Figure 43. However, the initial points of phase II for the computational models were lined up approximately with the initial point of phase II for the empirical results. In addition all plots are shown until full occlusion. The enhanced diffusivity with

margination plot was still the closest match to the empirical results. In addition, the occlusion time based on phase II was the closest for the enhanced diffusivity with margination model.

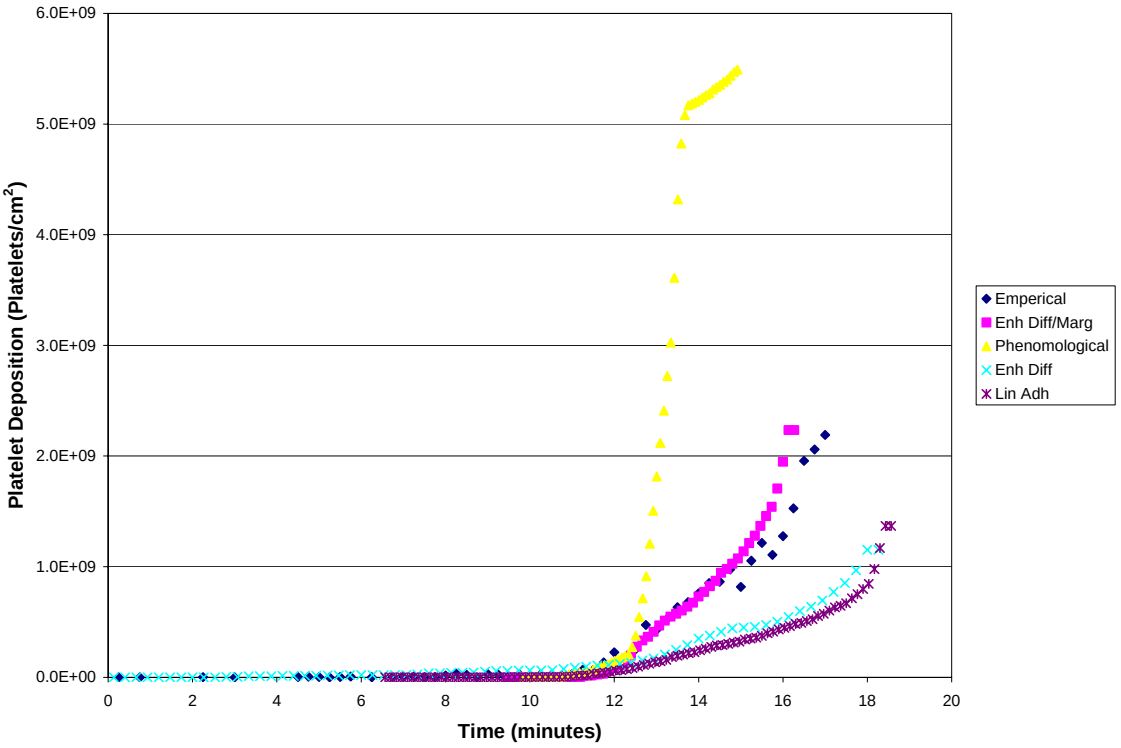

Figure 43: Plot summary of platelet deposition versus time. The model results were plotted so that the largest acceleration of platelet deposition is plotted at approximately the same time. The initial time point for the phenomenological model was set to 9.8 s, the enhanced diffusivity model at 0 s, the enhanced diffusivity with margination at 9.4 s, and the enhanced diffusivity, margination, and linear adhesion model was set at 6.5 s.

A final platelet deposition versus time plot is presented in Figure 44, which has a normalized platelet deposition scale. The time scale and curve locations are the same as what was given in Figure 43. The deposition scale was normalized to the maximum deposition for the specific curve. The surface area calculation to obtain platelets per unit length squared is not precise. It is obtained by taking an area along the stenosis wall where the most significant deposition occurs. The methods used for the previous plots consider the same technique that (Flannery 2005) used to obtain his plots and is kept constant, therefore relative comparisons should not be affected by the scaling. The scaled

plot has very similar trends to the previous plots. The scaled plot indicates that the enhanced diffusivity with margination case is still the closest match to the empirical results. The second closest deposition to time slope is the enhanced diffusivity, alone, case. The phenomenological deposition rate is too fast, and the linear adhesion case has a slow deposition rate, that becomes too fast as the thrombus nears occlusion.

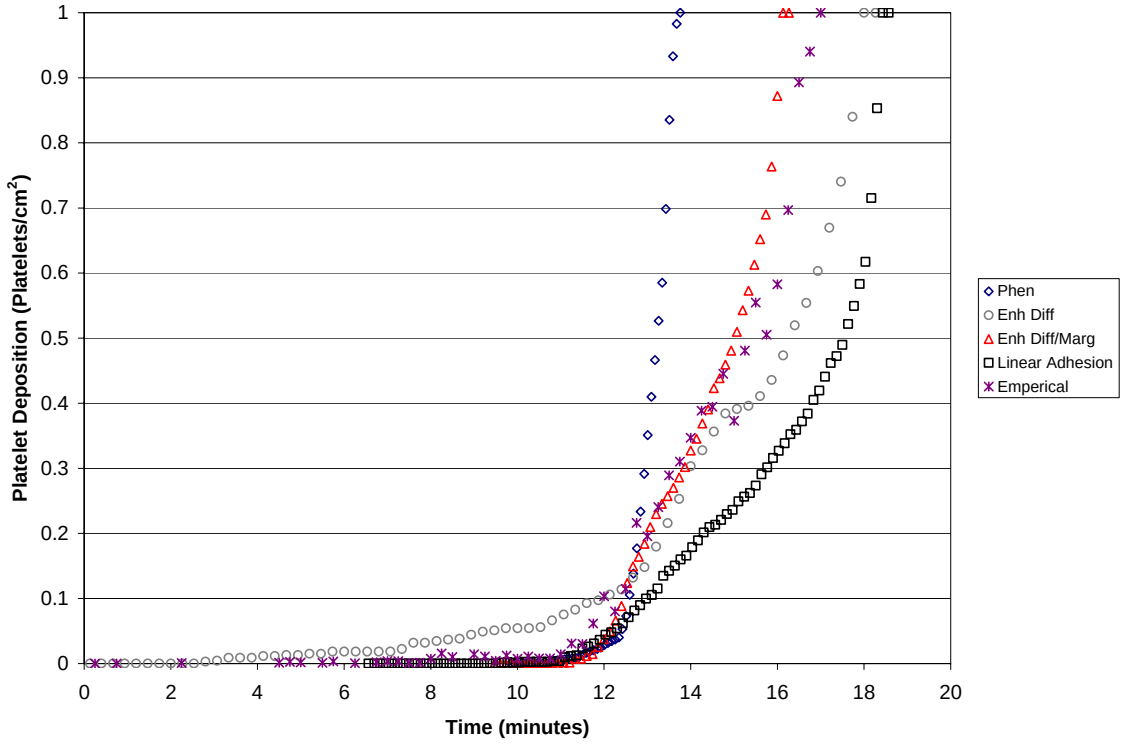

Figure 44: Plot summary of platelet deposition versus time with a normalized platelet deposition scale. The model results were plotted so that the largest acceleration of platelet deposition is plotted at approximately the same time. The initial time point for the phenomenological model was set to 9.8 s, the enhanced diffusivity model at 0 s, the enhanced diffusivity with margination at 9.4 s, and the enhanced diffusivity, margination, and linear adhesion model was set at 6.5 s.

The platelet deposition versus time plots are indicative of the effects of the various conditions. The accelerating region of the enhanced diffusivity case extended over a longer period of time, increasing the occlusion time by 3 fold from the case of enhanced diffusivity with margination. Margination appeared to decrease the length of time for the acceleration portion of the deposition curve, and also made the deposition slope more linear than the shear enhanced diffusivity case. The accelerating phase may

be occurring once a protrusion disturbs the flow, deflecting the streamlines. This could allow convection related mechanisms to contribute to deposition because flow may be impinging on the protrusion. Platelets may carry enough momentum to continue through the streamlines to the site of protrusion. Otherwise, the only platelet transport mechanism is assumed to be diffusion related phenomenon. Margination increases the number of platelets near the wall and thus the number of platelets that may be affected by the protrusion, therefore could amplify the effect. A plot was not generated for the adhesion threshold condition because it did not yield thrombus in a location that resembled the empirical results. The case where adhesion probability was a linear function of shear rate resulted in a deposition curve that was very similar to the case that only considered enhanced diffusivity.

Mechanistic Models of Platelet Deposition Extrapolation

The phenomenological model and shear enhanced diffusivity mechanistic condition matched the closest with the experimental results. These models were considered for the same vessel geometry at a upstream Reynolds number that is approximately five times larger than the Reynolds number used in the experiment. The Reynolds number evaluated here is 220, corresponding to the Reynolds number found in the coronary arteries. A complete study that separates all possible combination of mechanistic conditions is presented in Appendix A.

Each run was allowed to reach a steady state condition before platelets were allowed to adhere. Steady state, here, means that the time averaged platelet concentration gradient did not change across the fully developed flow solution. The test cases were then allowed to run until the thrombus reached full occlusion. A sufficient number of continuous phase iterations were specified to run between discrete time steps to resolve the flow solution around the transporting platelets, before they were allowed to advance in the flow. The number was set at 10 iterations. Two different computational experiments were performed to evaluate the extension of the model used to simulate the experimental results. In addition, a case of no mechanistic conditions is considered. Platelets were allowed to transport based on turbulent dispersion. When the platelets reached an active computational cell, the platelets were considered to adhere. The turbulent dispersion is considered here, because the flow regime is now assumed to be in a transition turbulent regime (Young and Tsai 1973), allowing turbulent dispersion particle transport. This was not appropriate for the laminar case that was used to simulate the experiment. All three computational experiments are listed in Table 5.

Table 5: Computational experiments

Run	Description
1	Phenomenological Model
2	Shear Enhanced Diffusivity and Margination
3	No Shear Rate Condition

Assumptions and Limitations

- Newtonian fluid: Approximation at the high flow rate and large vessel diameter used here.
- Flow is steady: Pulsatile flow has been shown to have secondary effects on convective transport (Basmadjian 1990) and diffusive transport (Fiechter 1998).
- Flow is neither laminar or turbulent: The turbulent transition region exists near the throat of the stenosis (Young and Tsai 1973).
- Flow is fully developed near the stenosis: A length of ten times the diameter was included between the inlet and the stenosis.
- Two-dimensional axisymmetric flow in the axial and radial direction: Approximation to the experimental flow.
- Adhered platelet volume fraction in a computational cell is 0.2 before thrombus grows to next cell: A change in the volume fraction threshold would affect the time scale of the computational results, but would not affect the relative time scales between the computational results. 0.2 was approximated as an "atomic packing factor" for platelets in a thrombus.
- The vessel wall is inelastic: The test specimen's wall was made of glass.
- Platelets have infinitely fast binding
- Margination drift term doesn't vary with thrombus growth
- Platelet enhanced diffusivity is only shear rate dependent and not dependent on volume fraction

- Platelets are a modeled as point masses
- Thrombus can only grow in the radial and downstream direction
- Platelets are either chosen to be eliminated when they reach a cell that has reached its platelet fraction limit, or they are allowed to pass through the cell. They do not reflect off the boundary or roll on the boundary, like they would in a physical system.
- No embolization
- Only stress constraint on thrombus is for no upstream growth. The thrombus may bend or break in a physical system.
- Platelets can only deposit in active cells. An active cell is one that borders either the boundary of the blood vessel wall or borders the boundary of the thrombus. Platelets attach when they reach any location in the cell.

1. Phenomenological Model

The phenomenological for the Re of 220 was generated the same way as the model used for the experimental simulation. The results are presented in Figure 45. The thrombus begins to growing in a similar manner to the case that simulated the experiment. However, the growth was much sharper and much more sudden. 30 s elapsed with minimal growth, but then the thrombus complete occluded with 2 additional seconds. The thrombus occlusion appears to occur at the peak wall shear rate.

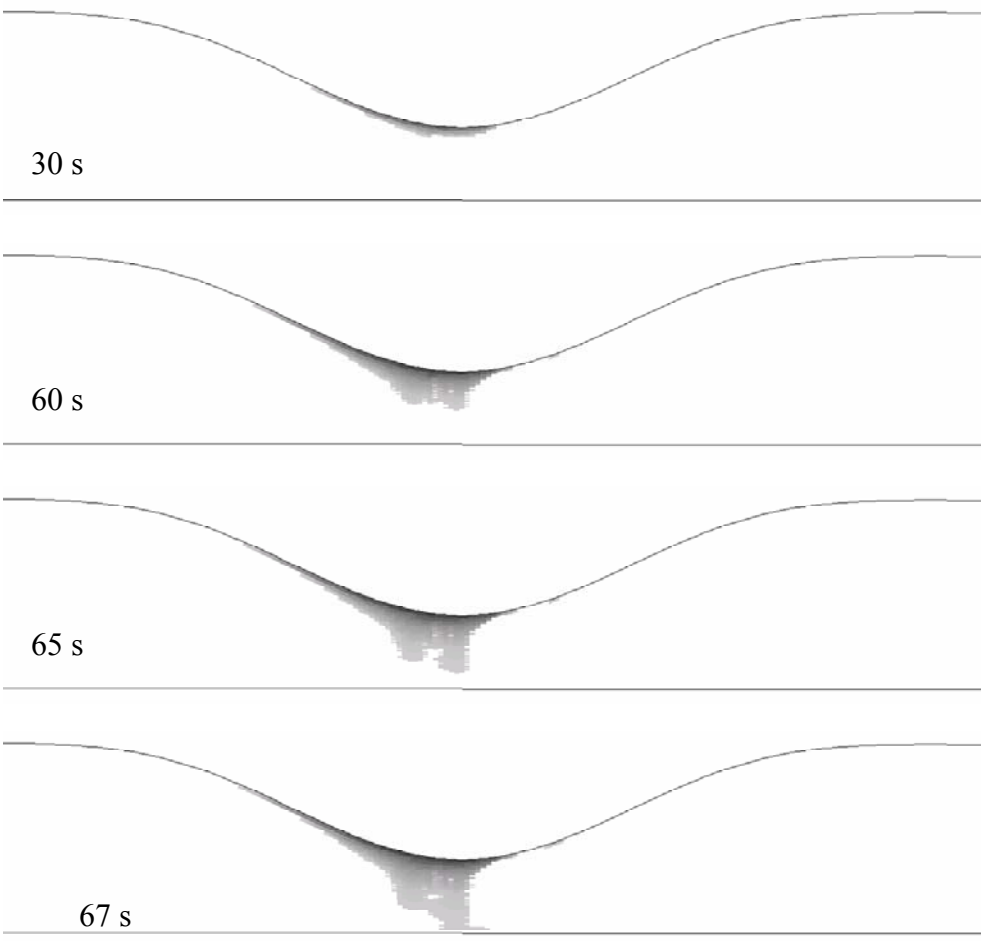

Figure 45: Time progression of thrombus formation for the phenomenological model. It is based on the curve fitting condition from Figure 17.

2. Shear Enhanced Diffusivity and Margination

Shear enhanced diffusivity and margination was reconsidered for the higher Reynolds number because this case was the mechanistic condition that most closely resembled the experimental results. The results for this study are illustrated in Figure 64. Thrombus grows in the converging region near approximately 20000 s^{-1}. The thrombus then continues to grow from the initial protrusion, until full occlusion in the converging region of the stenosis.

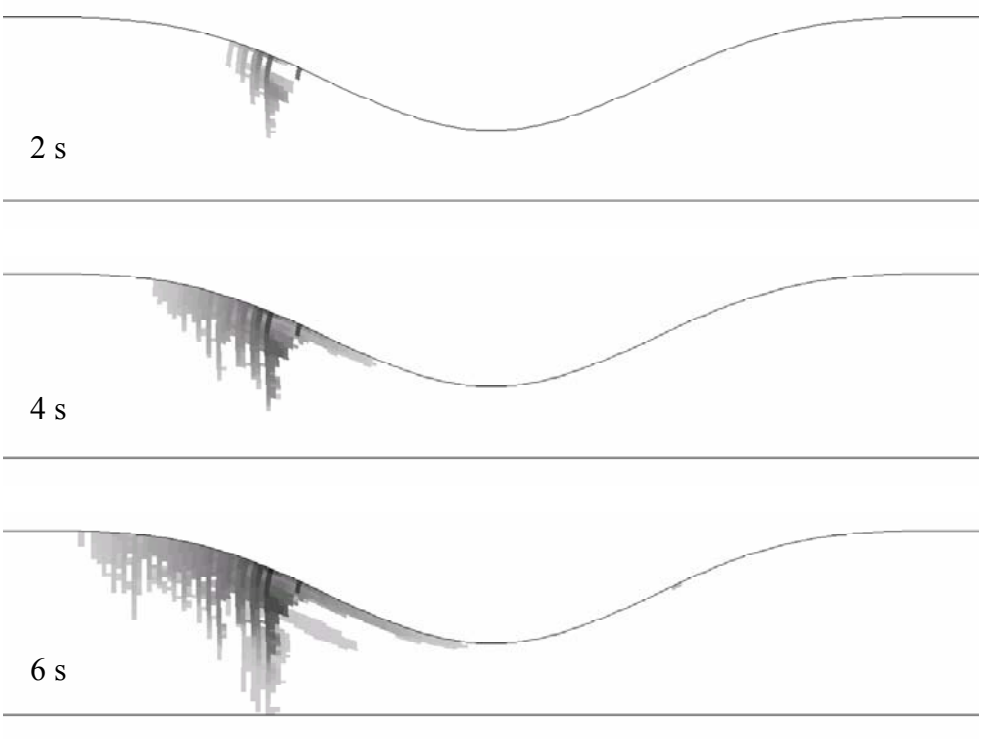

Figure 46: Time progression of thrombus aggrandizement for shear dependent dispersion and shear dependent margination. The condition for 0 velocity was applied for cells that were considered to be occluded by the thrombus. The red or darker color is the most recent time, while blue is the oldest portion of the thrombus. The information can also be extracted from the time sequence presented here.

3. No Shear Rate Condition

A computational experiment was performed to determine where thrombus would likely grow in the case that there is no shear rate dependency for deposition or particle transport, other than turbulence. Shear independent margination was applied to simulate near wall effects, excluding shear rate terms. Diffusive particle motion was governed by the methods described in the turbulence portion of the methods section. Particles have some random motion as dependent on turbulent velocity fluctuations. A different random motion is applied when a particle travels out of an eddy, or when it is not in an eddy. The results show deposition occurs in the region where the flow reattaches after separating near the stenosis apex.

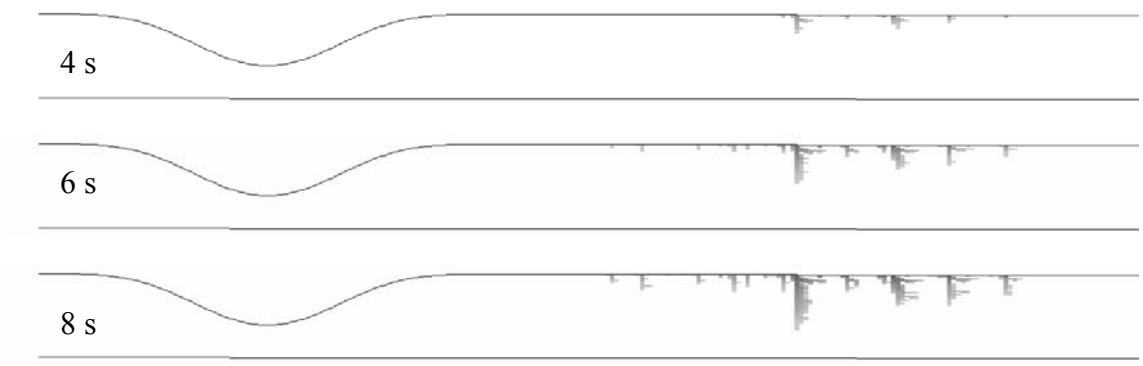

Figure 47: Time progression of thrombus formation when no shear conditions are applied.

CHAPTER

4. DISCUSSION

Stochastic Discrete Phase Model

Two possible computational models have been developed that simulate an occluding thrombus using computational fluid mechanics. The location and phase II time for occlusion determined from the models were within the bounds seen in the experiments. Separate mechanisms involved in the process of thrombus formation were considered and evaluated. It was determined from the results that transport related phenomena are sufficient for predicting thrombus location and occlusion time. The deposition curve for the transport phenomena based model matched very closely with the empirical curve. A shear dependent mechanism was found to be necessary for thrombus formation at the throat of the stenosis. Otherwise, thrombus forms in the post-stenotic region. The results indicate that it is unnecessary and undesirable to determine adhesion as a function of shear rate. Additional experimental studies may verify this. This study may be one of the first to consider the dynamic growth of thrombus to full occlusion through a numerical simulation. The evaluation of the results has triggered many new questions and may focus future experimental work to better understand the mechanisms involved in thrombus formation.

The phenomenological and mechanistic models were both qualitatively verified with the occluding thrombus location of the empirical results (Flannery 2005), meaning that the occlusion occurred within the apex region of the stenosis. The phenomenological model was quantitatively capable of predicting occlusion time after initiation of the second phase to within the range seen experimentally (Flannery 2005). The mechanistic shear enhanced diffusivity and margination case was within approximately the range of the experimental results (Flannery 2005), assuming two phases are modeled and time is

calculated from the initiation of the second phase. The time for occlusion was well within the ranges seen by (Wootton, Markou et al. 2001) who evaluated deposition at lower shear rates. It would be necessary to consider a decrease in deposition at very high shear rates to obtain phase III in the mechanistic model. Otherwise, the current model continually increases the rate of deposition in relation to shear rate.

The phenomenological model was based on one parameter, shear rate, and therefore is an attractive model to obtain a quick estimate of platelet deposition. It however, would need to be validated for each new situation because it is solely based on a linear correlation. In addition, it does not give insight into the physical system. The mechanistic model is capable of providing more insight into the physical system. In the mechanistic model, shear enhanced diffusivity appeared to be sufficient for obtaining thrombus in the apex of the stenosis for the experimental simulation. The addition of margination increased the concentration of platelets near the wall, which increased the frequency that a platelet will reach the wall, and thus increased the rate of platelet transport to the wall. Margination did not affect the location of thrombus formation significantly, even though it corrected the nonuniform concentration profile along the wall to better resemble the physical system seen in (Eckstein, Bilsker et al. 1987; Aarts, van den Broek et al. 1988). The correction was previously detailed in the concentration plots, Figure 27 and 28, of the "Results" section for "Shear Enhanced Diffusivity with Margination."

Two shear dependent adhesion probability functions were considered which augmented the shear enhanced diffusivity with margination case. The first considered an on/off threshold relation, which resulted in thrombus growth in the post-stenotic region. This is the only region that had shear rates below 1000 s^{-1}, while there was negligible surface area that was above 20000 s^{-1}. Since these results do not correlate with the empirical results, it is assumed that there is not a distinct cutoff for adhesion at 20000 s^{-1}. Adhesion could not have an on/off relationship associated with 1000 s^{-1} and 20000 s^{-1}

based on work by (Badimon, Badimon et al. 1986; Sakariassen, Joss et al. 1990; Markou, Hanson et al. 1993). The simplest adhesion function of shear rate, a linear function, was also considered. The linear dependence slowed down the deposition rate at any given location as necessary since it lowers the probability of adhesion as shear rates decrease. It also altered the deposition versus time curve. It is possible that a linear adhesion dependence on shear rate occurs up to a particular shear rate and then levels off to a constant. This is suggested in (Wootton, Markou et al. 2001), where the curve may level off near 10000 s^{-1}, based on the results of (Barstad, Kierulf et al. 1996).

The occlusion time for the coronary artery simulations may not represent the physical nature of thrombus aggrandizement because at such high shear rates the drag force on an individual platelet would be very large, which either could cause a decrease in adhesion, or an increase in platelet embolization. The exceptionally fast times for occlusion do not match the order of magnitude of occlusion time for any experimental studies considered in this thesis (Markou, Hanson et al. 1993; Wootton, Markou et al. 2001; Flannery 2005). Shear rates in these experimental models do come near the ones studied in the coronary simulation when the thrombus nears occlusion. Flannery's deposition versus time plots do not indicate an occluding time of seconds once these high shears are reached. This is indicative that deposition rate would not continue increasing with shear rate. Deposition at high shear rate conditions may lower from what is predicted in the model from broken bonds or a limiting dependence on shear rate for one or more of the mechanisms considered in this study. In addition, very high shear rate conditions may change the thrombus deposition rate limiting mechanism. The rate limiting mechanism in the experimental simulation was assumed to be platelet transport. However, as the number of platelets reaching the wall in a given time increases, the rate limiting mechanism could change to adhesion of the platelets.

A model with no shear dependent terms resulted in thrombus formation in the post-stenotic region and not in the throat for the coronary study. Growth in the post-

stenotic region was not seen in our experimental results, but it was seen in (Schoephoerster, Oynes et al. 1993) and was consistent with a suggested location for the most activated platelets (Raz, Einav et al. 2007). Schoephoerster et. al. used platelet rich plasma (PRP). PRP would eliminate margination effects from RBCSs (Matas, Morris et al. 2004). In addition, the concentration of PRP platelets was low enough to effectively lower the shear enhanced diffusivity mechanism. Therefore, use of PRP may lower the effect from the transport mechanisms studied in this thesis, and only leave the shear rate dependent adhesion platelet receptor mechanism. The number of platelets deposited at the apex was lower than any other location in the PRP study. This may indicate that shear dependent adhesion does not play a major role in determining the location of the thrombus formation in whole blood. If shear dependent adhesion was the major factor, then thrombus would have been expected to grow at the apex of the stenosis based on the other studies of thrombus formation over a stenosis. A factor that could negate this argument is that the experiments performed by Schoephoerster et. al. included a flow loop. Therefore, platelets may activate without adherence in one cycle, but then may remain activated and adhere differently in the next cycle. Therefore, the results may be skewed and additional experimentation would need to be performed to confirm the effect of shear rate dependent adhesion through the use of platelet rich plasma. Their system was also at a lower shear rate, but does match the shear rates considered by (Badimon and Badimon 1989; Sakariassen, Joss et al. 1990) who found the highest amount of deposition at the stenosis apex with whole blood.

Limitations and Justifications of Study

Platelet adhesion was lumped into a probability factor. In reality there are numerous factors involved with platelet adhesion. However, the factors all result in a probability for a platelet at the wall to adhere under a given condition. Margination was included as a probability for diffusive direction. This simulates the physical system

because as a platelet moves further from a vessel wall, there is more likelihood that it will collide with a red blood cell, which dominates the collision. Platelets that do reach a high concentration of red blood cells have a equal likelihood of moving in any direction. This was included in the margination term, where the direction of collision was randomized after a platelet passes the "initial edge region" of red blood cells. The randomized motion of platelets, termed the shear enhanced diffusivity, was theoretically described in the "Introduction, Biorheology" section. It is based on a phenomenological relation evaluated by (Zydney and Colton 1988) and represents the physical system based on particle to particle interactions.

The models evaluated in this study are limited in many ways. One of the most significant physical constraints that was relatively neglected is the inclusion of stress conditions on the growth of the thrombus. The thrombus was allowed to grow as a thin membrane without either bending or fracturing. The immersed boundary method should be capable of converging even for the high deformation that could occur with thrombus protrusions. The occlusion times determined based on the models used in the experiment could be underestimated because of the availability for structural protrusion growth. Additionally, platelets were allowed to pass through occluded thrombus in most cases studied in this thesis. This has some physical basis because stagnant flow behind a thrombus protrusion could result in red thrombus formation. In addition, the protrusions would likely bend and form new structures as the thrombus grows because of the high fluid forces, while still allowing growth on top of the structure.

The allowance for platelet transport through the thrombus could skew the deposition relative to time plots. However, these plots would be equally skewed, so the relative differences between the plots should not change significantly. In addition, when the deposition scale on the plots is normalized, then the effects from allowing platelets to pass through the thrombus should be negligible, when comparing the computational results to the experiment. One other physical event that is neglected is the inclusion of

any drag force expression prohibiting platelets from adhering. A simulation of the coronary arteries should include pulsatile flow because the Womersley parameter is three. This was neglected in the coronary artery study in this thesis based on simplicity and the results from (van Breugel, Sixma et al. 1988; Basmadjian 1990; Fiechter 1998). However, modeling methods are different, and therefore, the assumption might not have the same validity for the methods used in this study. This is a limitation on the results presented in the coronary simulation.

Additionally the gradient of shear along the stenosis may have an effect on platelet deposition based on platelet transport. This is not taken into account in this thesis. The enhanced diffusivity study (Zydney and Colton 1988) and the platelet margination study (Aarts, van den Broek et al. 1988) did not consider the variation in shear, and assumed constant shear rates. However, studies have been performed that considered pulsed shear rates with respect to time. (van Breugel, Sixma et al. 1988) found that the frequency of the pulse did not significantly affect platelet deposition. However, this study used a roller pump upstream of the region of interest; therefore results may be affected by early platelet activation. Therefore, the exclusion of a shear rate gradient from the model is an imposed limitation; however it is assumed that the gradient would only have secondary effects.

Another limitation of the study is the exclusion of near wall forces, and the lift force. It was assumed that the radial motion of platelets was controlled by the applied enhanced diffusivity and margination conditions. The motion from enhanced diffusivity was primarily resisted by the drag force. The exclusion of radial forces is a limitation of the study. This may result in inaccuracies, especially in the cases that do not consider platelet margination. Platelet margination was used to control the platelet concentration, which develops based on force balances and collisions in the fluid.

The condition for platelet attachment may be another limitation of the study. Platelets were considered attached once they entered an active computational cell,

considered to be the thrombus edge. However, results may have some dependence on the grid sizing. Larger grid size would result in the allowance of platelets to attach to the thrombus, which are further from the wall than a platelet entering an active computational cell of smaller grid size. The actual platelet distance from the wall should be used in future models to avoid affecting the results by having varying grid size in the flow domain. This calculation is not always straightforward, unless the computational coordinates conform along the wall boundary and adjust as the thrombus grows. A code similar to the one used to account for a growing wall in the platelet margination condition could also be used to determine the platelet to wall distance.

Significance in the Field of Thrombosis

The studies performed here may have significant impact in the field of thrombosis because few researchers focus their attention on the mechanisms of transport phenomena near a forming thrombus. This study indicates that transport phenomena may be very important in the process of thrombotic occlusion. The focus of many researchers has been on shear rate dependent adhesion and the different mechanisms involved in the adhesion process. However, adhesion's dependence on shear rate still has not been well defined and there are often mechanisms of platelet transport that confound in the determination of adhesion's dependence on shear rate. The use of CFD allows one to separate the different transport mechanisms from the probability for platelet adhesion. It may be difficult to separate transport phenomena from adhesion phenomena in experimental work, but it is relatively simple through numerical analysis. This is one of the advantages to studying biological phenomena through numerical analysis instead of through physical experimentation. The results indicate that platelet transport to a reactive surface may be the rate limiting factor for thrombus growth.

If the rate of thrombus growth is limited by the rate of transport to a reactive surface, then the problem of modeling thrombus formation may be simplified by avoiding

the complexities of modeling adhesion mechanisms. Adhesion mechanisms change with shear rate (Savage, Saldívar et al. 1996; Ruggeri 2002; Ruggeri, Orje et al. 2006), agonist transport, and time, among others. The specifics of these mechanisms are not well quantified. The results of this study indicate that shear enhanced diffusivity and margination may be sufficient to obtain a thrombus similar to what has been experimentally seen by others (Badimon, Badimon et al. 1986; Sakariassen, Joss et al. 1990; Markou, Hanson et al. 1993; Wootton, Markou et al. 2001; Flannery 2005). A powerful clinical resolution to thrombosis may exist if complete thrombotic occlusion can be averted by controlling the transport of platelets to the wall. If minimal platelets travel to the wall, then there is a minimal source of platelets for adhesion at the wall.

Platelet transport to the wall can be thwarted by reducing the hematocrit below a level of 10% because the red blood cells would likely no longer aggregate to the center of the blood vessel (Minsoo, Chongyoup et al. 1999). In addition, if the particle Reynolds number was large enough (>~0.2), then higher levels of hematocrit (0.2-0.3) may still retard the amount of platelets transporting to the wall (Minsoo, Chongyoup et al. 1999). Lowering the hematocrit may affect the oxygen carrying ability of the blood if it is too low. However, if the oxygen carrying ability is sufficient, then lowering hematocrit may be one possible way to resolve thrombotic occlusion. It may even be possible to locally filter out high hematocrit near atherosclerotic areas. The challenge with filtering out high hematocrit include keeping the shear rates low enough to avoid activating platelets and to still maintain appropriate oxygen levels for the local tissue. However, both the carotid and the coronary arteries oxygen supply are very important to survival, and both arteries are problematic atherosclerotic areas. There may be other methods that could lead to the reduction in platelet transport to the wall. However, more studies should be done to prove that reducing platelet transport to the wall could actually avert thrombotic occlusion.

Another interesting finding based on the mechanistic models of the experimental and coronary simulations was that thrombus formed around 20000 s^{-1} for the cases where shear enhanced diffusivity was implemented. This was associated with the apex of the stenosis for the experimental simulation and was slightly before the midline of the converging region for the coronary artery based model. The threshold may vary with geometry or may be a residual of the computational model. Coincidently, 20000 s^{-1} was also determined by (Ruggeri, Orje et al. 2006) to be a threshold at which platelets adhering through the GPIbα-VWF mechanism will begin a persistent adherence for minutes. At lower shear rates, the GPIbα-VWF mechanism only transiently adheres, and thus allows platelets to roll. A longer period of binding increases the probability that a platelet will activate, before the bond is released. Therefore, 20000 s^{-1} may be a characteristic shear rate threshold that supports occlusive thrombus formation. Therefore, if a technique were available to lower the shear rate on an atherosclerotic lesion, then there may be another resolution to complete thrombotic occlusion. The most obvious technique would be to use angioplasty. However, there may be less invasive methods to lower the shear rate low enough for to avoid shear rates around 20000 s^{-1} and above.

The models developed in this study may also be a source of predicting heart attacks by predicting the location and occluding time of thrombus formation, depending on a patient's blood, geometric, and flow characteristics. In addition, the results indicate that a shear rate of 20000 s^{-1} may be a criterion for prophylactic intervention, instead of the current method, which considers the degree of stenosis. A 60% reduction in area stenosis would result in different shear rates if it existed in the coronary arteries compared to the carotid arteries. Prediction may be as simple is determining where the thrombus would form. For example if it forms in the post-stenotic region, then the thrombus may have characteristics more like red thrombus, which may have less bonding strength between platelets for resisting the high shear stresses that exist as the thrombus grows in an artery (Savage, Saldívar et al. 1996). Predicting the risk of thrombus may

also be as simple as determining the time for thrombotic occlusion. If the time is sufficiently large, then the thrombus may be less likely to completely occlude the artery (Markou, Hanson et al. 1993; Wootton, Markou et al. 2001). Wootton predicted that occlusion times predicted below 30 minutes would likely lead to full thrombotic occlusion, while larger times are associated with a decreased likelihood for occlusion. This corresponds with the current experiment in our lab (Flannery 2005), where thrombotic occlusion occurs within 30 minutes.

CHAPTER

5. CONCLUSIONS AND FUTURE WORK

Conclusions

Two models of thrombus growth to complete occlusion were developed. The results of the mechanistic model indicated that platelet transport phenomena may be sufficient to develop thrombus growth at the apex of a stenosis, as seen experimentally. Occlusion time and deposition rate were also consistent with the experimental results for the model based on transport mechanisms. Therefore, transport phenomena may be the rate limiting step in thrombus growth, which would suggest that shear dependent adhesion rate may be extraneous for thrombus occlusions in arterial stenoses.

Future work

- Flow platelet rich plasma through the laboratory experiment. This would eliminate the effects of red blood cells on platelet transport, which should essentially eliminate platelet margination, and possibly shear enhanced diffusivity. Then thrombus should form only through shear rate dependent adhesion and may have some additional effects from shear rate dependent tubular pinch. This would allow the shear rate dependent adhesion term to be more easily extracted. The model predicts that thrombus should form in the post-stenotic region and would take significantly longer to reach full occlusion.
- Increase the flow rate through the current experimental setup to see if the thrombus location changes to the converging region, as indicated in the coronary simulation of the mechanistic model. The current experimental results appear to already have significant thrombus growth in the converging region, but do not occlude there.

- Base future experimental results on the growing thrombus wall shear rate, instead of the initial wall shear rate to determine a more exact relationship between the wall shear rate and thrombus growth. This can be done through image analysis and would prelude to how the thrombus growth is affected when the thrombus nears full occlusion. The model indicates that the wall shear rate may increase by an order of magnitude during the growth process.
- A fluid structure interaction (FSI) computational model should be considered for the growing thrombus. The immersed boundary method may be one useful way to include the structural interaction to determine how the thrombus responds to the stresses that develop as it grows.
- A discrete phase model that includes particle collisions instead of margination and effective diffusivity based assumptions. Collisions would need to model all particle to particle interaction that would cause a particle to change direction from its current direction. Such motion can be determined from a macroparticle study and then scaled up to represent individual computational cells of the larger scale model that includes the stenosis.
- Determine a method to run the experiment, so that there are always available platelets for adherence next to the thrombus reactive wall. This would represent a case that platelet bonding is the rate limiting step, and therefore a adhesion dependence term on flow conditions could be extracted from the results.

APPENDIX A

SYSTEMATIC COMPARISON OF SHEAR RATE DEPENDENT MARGINATION, ENHANCED DIFFUSIVITY, AND ADHESION

An 85% reduction by area stenosis is used here to computationally evaluate thrombus formation. It is instructive to consider the flow patterns near the stenosis before thrombus is evaluated. Pathlines, colored by velocity magnitude contours, are illustrated in Figure 48. Flow is from left to right, as it is for all following figures in the results section. The flow separates just after the apex of the stenosis. The separated flow reattaches 8 mm from the stenotic peak. 8 mm corresponds to a data extrapolation for a 89% stenosis by area at a Reynolds number near 200 (Young and Tsai 1973). This increases the confidence in the turbulent model that is used in this study. Other turbulent models showed earlier reattachment.

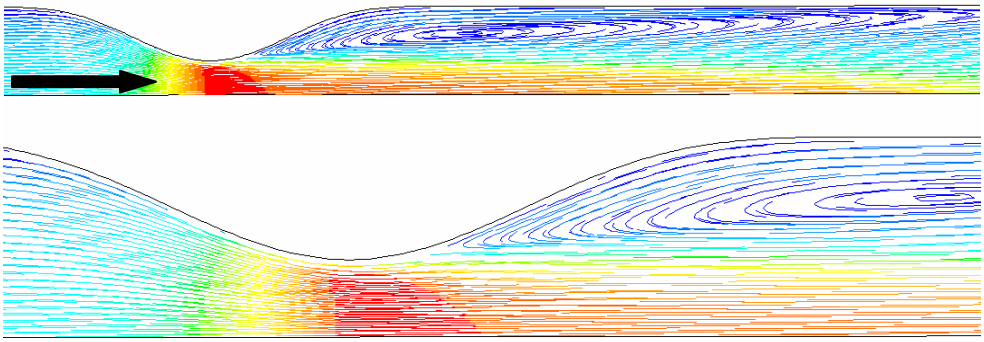

Figure 48: Pathlines in the coronary flow colored by the velocity magnitude. The peak velocity is at the apex with low velocity in the recirculation region and near the wall due to the no-slip boundary condition.

A contour plot of the shear rate, also known as the strain rate is presented in Figure 49. The methods used in the model are highly dependent on shear rate, and therefore it is important to understand how it varies in the flow field. The shear rate increases near the

converging region of the stenosis and is highest at the wall. The high shear rate begins to extend from the wall once the flow starts separating. The post-stenotic region has an increased level of shear that dissipates away from the stenotic apex.

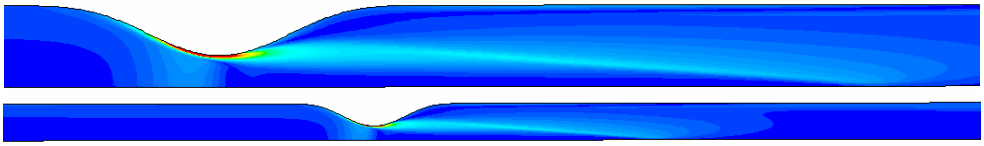

Figure 49: Strain rate contour plots across the stenotic region. The red or darkest region corresponds with the highest shear rate. The values can be taken from Figure 25.

A plot of the wall shear rate is shown in Figure 25 to supplement the flow field contour plot of shear rate, given in Figure 24. Figure 25 displays a higher shear rate near the entrance of the flow, as the velocity profile changes from a uniform profile to a parabolic profile. The flow enters the stenotic region at a position of 15 mm, displaying increasing shear rate. The shear rate peaks slightly before the center of the stenosis, 17 mm, and begins to decrease thereafter. It reaches a value of 0 s^{-1} slightly before 25 mm, which is indicative of the flow reattachment point.

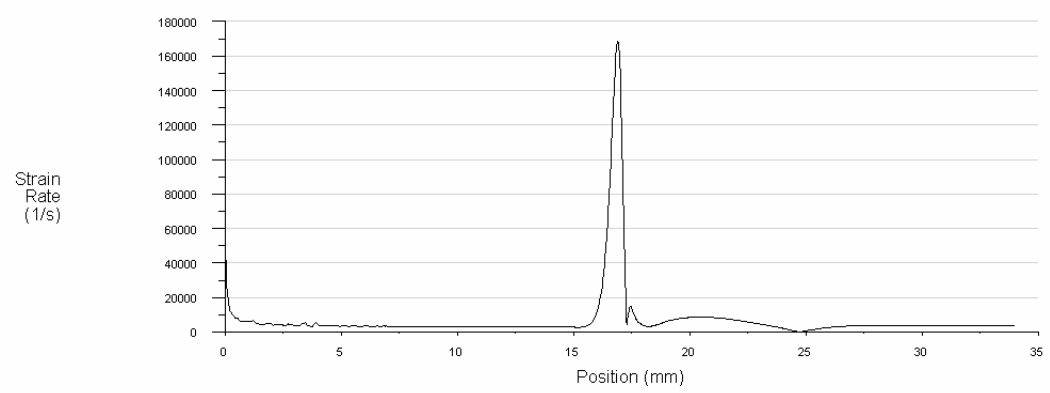

Figure 50: Wall strain rate across the entire flow field.

A magnified view of the wall shear rate plot at the stenosis is presented in Figure 26. The peak shear rate occurs slightly before the apex of the stenosis, 17 mm, and then dips down in the recirculation region.

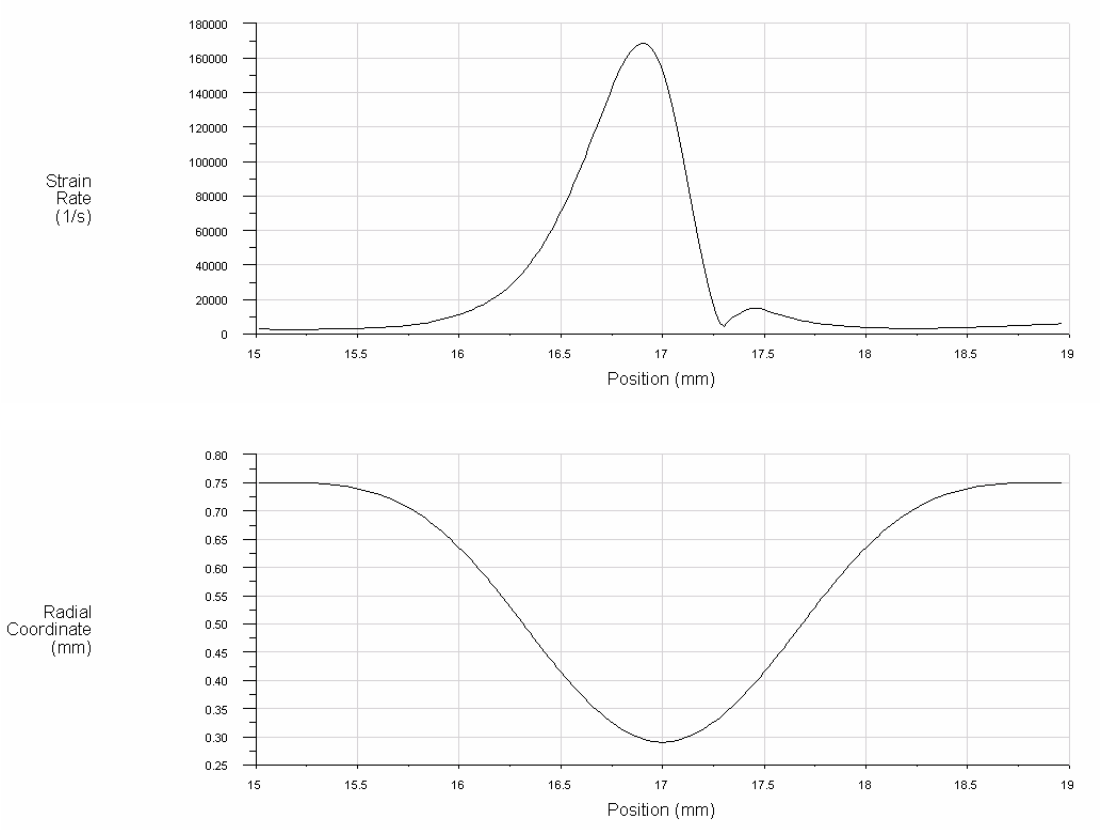

Figure 51: Magnified region around the stenosis. The wall shear rate is plotted relative to axial distance. The radial coordinate of the wall is also plotted across the axial position.

The pressure drop is also evaluated across the stenosis, Figure 52 matches closely with the data taken by (Young and Tsai 1973). The pressure rises again to its second peak at the flow reattachment point of ~25mm.

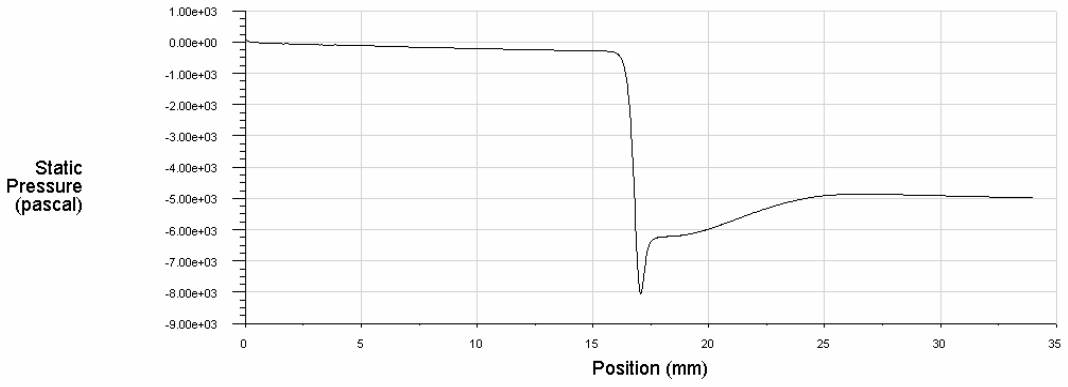

Figure 52: Static pressure distribution along the wall of the vessel.

Each run was allowed to reach a steady state condition before, platelets were allowed to adhere. Steady state, here, means that the time averaged platelet concentration

gradient did not change across the fully developed flow solution. The test cases were then allowed to run until thrombus reached full occlusion. A sufficient number of continuous phase iterations were specified to run between discrete time steps. The number was set at 10 iterations. This was necessary so that the shear rate and flow solution near the porous region (active computational cells) was allowed to reach a new value after platelets deposit, decreasing the porosity of the computational cell. Ten different computational experiments were performed to estimate the dominating shear rate effects. The computational experiments are described in Table 4. The first run is intended to be used as a baseline for comparison with the other runs. Runs 2-8 are intended to be used for comparisons of the varying shear rate effect on thrombus growth. Run 9 evaluates a linear relationship between adhesion and shear rate. Flow is from left to right in every figure in the results section. It is noted that all of the computational experiments resulted in a very rapid occlusion time, which would not occur physically. It is assumed that this is a result of the assumption that platelets instantly adhere when they reach an active computational cell prone for adhesion.

Table 6: Computational experiments

Run	Description
1	Phenomenological Model
2	No shear dependence
3	Shear Enhanced Diffusivity
4	Shear Dependent Margination
5	Shear Threshold Dependent Adhesion
6	Shear Enhanced Diffusivity and Margination
7	Shear Enhanced Diffusivity and Adhesion
8	Shear Dependent Margination, and Adhesion
9	Shear Enhanced Diffusivity Margination, and
10	Shear Enhanced Diffusivity, Margination, and Linear Dependent Adhesion

An additional constraint was applied to the thrombus formation for the coronary simulation to yield realistic results. Trial runs of the thrombus growth resulted in strings of thrombus growing upstream. An example is shown in Figure 53. The particular run only had shear rate dependent enhanced diffusivity. A constraint of disallowing growth

in the upstream direction was applied for subsequent runs. The justification is that the strings of thrombus would fold on themselves or embolize off due to high stress at the base of the strings. The overall solution should not be affected significantly because the fastest occlusion would be due to growth in the radial direction.

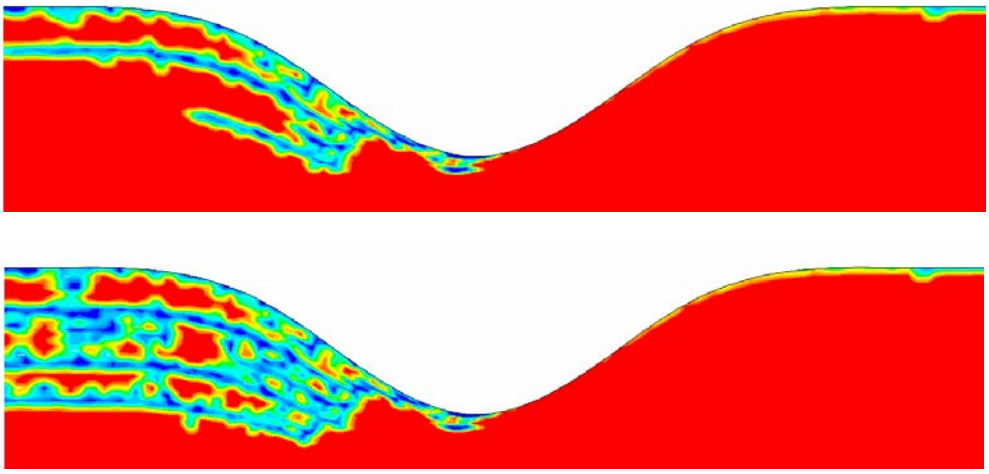

Figure 53: Strings of thrombus forming upstream

Another test run considered adhesion of platelets only when the drag force on the platelet was below a particular value. This resulted in a cessation of growth in the radial direction, once the thrombus reached a critical height. An example of the cessation is illustrated in Figure 54.

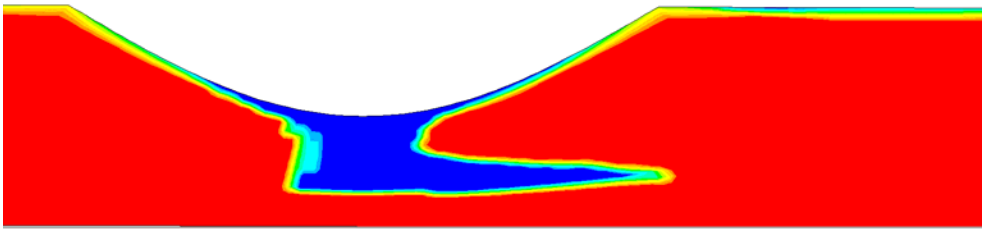

Figure 54: Constraint of platelet drag force threshold

This yielded a shape similar to what has been referred to as a fibrin tail, as described in the introduction. However, there was no further growth in the radial direction,

assumingly because the velocity reached a value that caused the drag force on individual platelets to reach the applied threshold.

Assumptions and Limitations

- Newtonian fluid: Approximation at the high flow rate and large vessel diameter used here.
- Flow is steady: Pulsatile flow has been shown to have secondary effects on convective transport (Basmadjian 1990) and diffusive transport (Fiechter 1998).
- Flow is neither laminar or turbulent: The turbulent transition region exists near the throat of the stenosis (Young and Tsai 1973).
- Flow is fully developed near the stenosis: A length of ten times the diameter was included between the inlet and the stenosis.
- Two-dimensional axisymmetric flow in the axial and radial direction: Approximation to the experimental flow.
- Adhered platelet volume fraction in a computational cell is 0.2 before thrombus grows to next cell: A change in the volume fraction threshold would affect the time scale of the computational results, but would not affect the relative time scales between the computational results. 0.2 was approximated as an "atomic packing factor" for platelets in a thrombus.
- The vessel wall is inelastic: The test specimen's wall was made of glass.
- Platelets have infinitely fast binding
- Margination drift term doesn't vary with thrombus growth
- Platelet enhanced diffusivity is only shear rate dependent and not dependent on volume fraction
- Platelets are a modeled as point masses
- Thrombus can only grow in the radial and downstream direction

- Platelets are either chosen to be eliminated when they reach a cell that has reached its platelet fraction limit, or they are allowed to pass through the cell. They do not reflect off the boundary or roll on the boundary, like they would in a physical system.
- No embolization
- Only stress constraint on thrombus is for no upstream growth. The thrombus may bend or break in a physical system.
- Platelets can only deposit in active cells. An active cell is one that borders either the boundary of the blood vessel wall or borders the boundary of the thrombus. Platelets attach when they reach any location in the cell.

1. Phenomenological model

A contour plot of the occluding thrombus for the phenomenological model is illustrated in Figure 55. The results show that the fastest deposition occurs near the peak of the stenosis. The location of thrombus growth is similar to what was seen in the experiments. The time for occlusion was much faster than what was seen by (Flannery 2005), which was approximately 320 s. Therefore, the computational results were off by a factor of 6. However, the shear rate in the experiment was approximately a fifth of what was calculated for the stenosis used here.

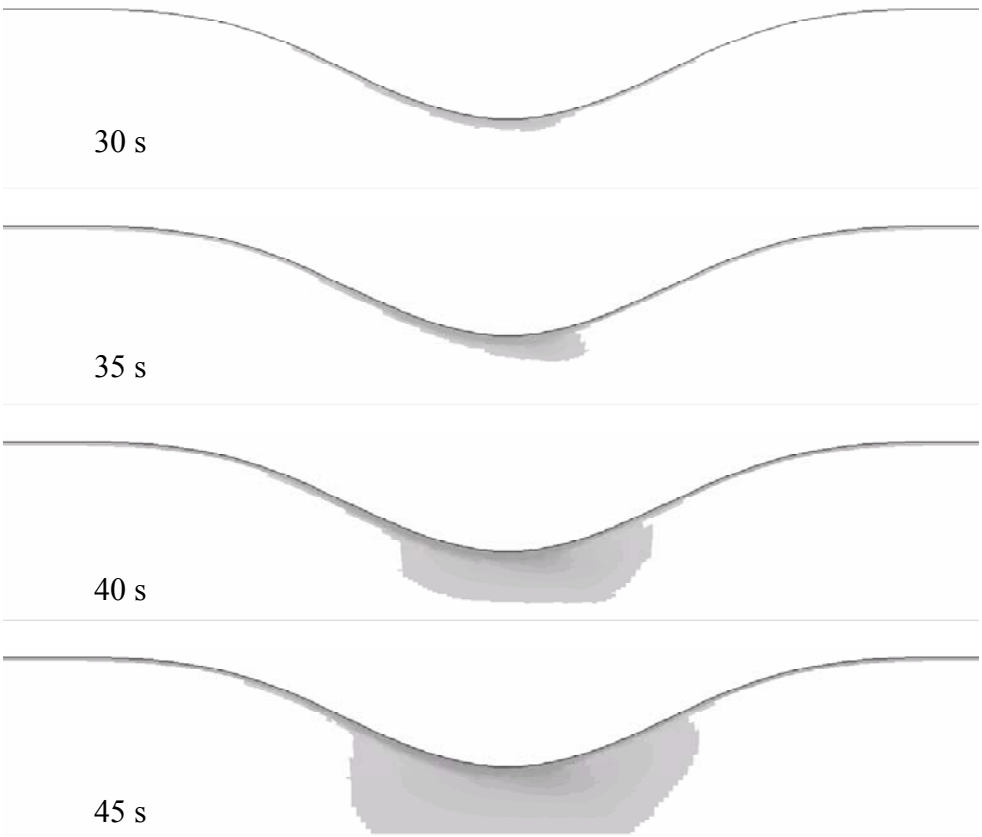

Figure 55: Time progression of thrombus formation for the phenomenological model. The contours are of the time progression of thrombus growth. The outer, light gray region is the most recent addition to the thrombus.

Some flow was allowed to pass through the thrombus based on the porous condition of the computational cells. Therefore, another case considered the condition that the thrombus region was completely blocked. Therefore, another computational run was implemented where the velocity in an occluded cell was set to zero. This could result in computed shear rates that more closely reflect reality. The time progression of the thrombus growth due to this condition is presented in Figure 58.

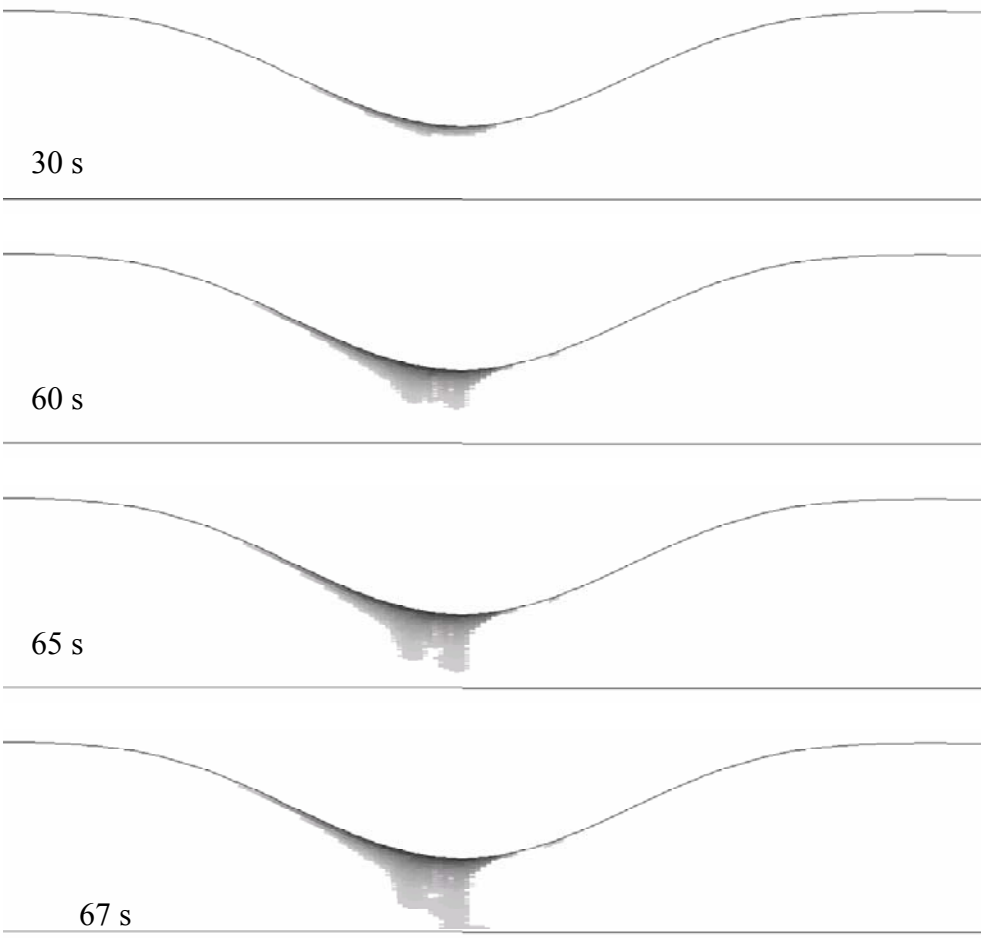

Figure 56: Time progression of thrombus formation for the phenomenological model. A condition of zero velocity is applied to regions that are considered blocked by thrombus.

Figure 55 and Figure 56 yield different thrombus growth results. Both figures show the largest amount of growth near the apex of the stenosis. The rest of the flow region has no significant thrombus growth in either trial. The trial where velocity was set to zero resulted in increased growth upstream of the stenosis apex, relative to the trial where the velocity was not adjusted. Figure 55 shows the opposite, where there is increased growth in the post-stenotic region. Figure 56 is a closer match to the experimental results, shown earlier. The zero velocity condition decreases the solution convergence.

The platelet deposition for a particular computational cell was calculated based on Equation 46. The deposition based on this equation is calculated here and again for the shear rate dependent diffusivity and margination. The deposition plot is used to extract out information about how adhesion may be shear rate dependent and how it would need to change the solution of margination and effective diffusivity so that the results of adhesion, margination, and effective diffusivity correlate with the results found here.

Equation 46: Computation for platelet deposition

$$\frac{\text{Platelets}}{\text{m}^2 - s} = 0.8 \frac{A_{\text{comp cell}}}{A_p \Delta t_{\text{comp cell occlusion}} SA_{\text{outer face}}}$$

A value of .8 was used because 80% of the computational cell volume is consumed by platelets when the computational cell is considered to be occluded. A plot of the deposition is illustrated in Figure 57: Phenomenological model plot of calculated platelet deposition based on the curve fit data.. The plot yields a linear fit equal to $4723000\ \dot{\gamma} + 3.108 \times 10^{10}$ Platelets/m^2-s. This is not an exact match to the imposed value given as $600749\ \dot{\gamma} + 5 \times 10^{9}$ Platelets/m^2-s. The discrepancy is likely due to the resolution of time increment used for this study. The time increment was taken at 0.1. A smaller time increment would yield more accurate results.

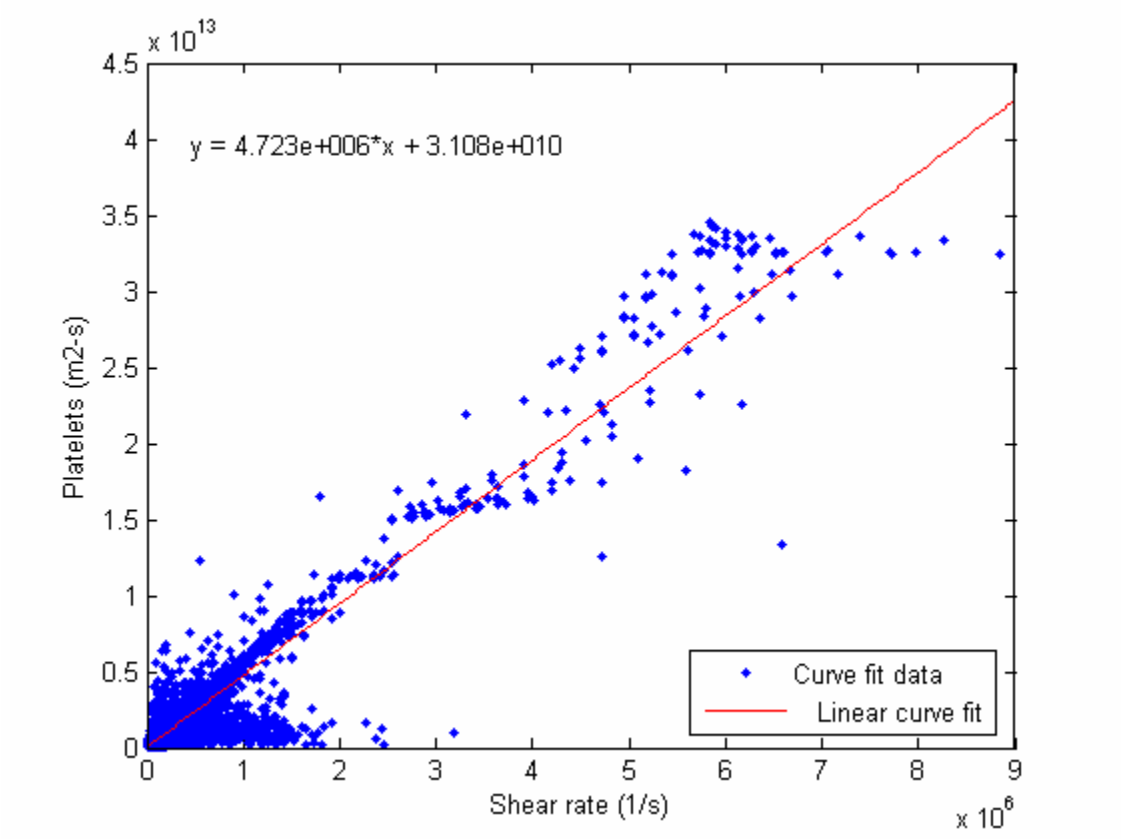

Figure 57: Phenomenological model plot of calculated platelet deposition based on the curve fit data.

2. No Shear Dependence

A computational experiment was performed to determine where thrombus would likely grow in the case that there is no shear rate dependency for deposition or particle transport, other than turbulence. Shear independent margination was applied to simulate near wall effects, excluding shear rate terms. Turbulent diffusive particle motion was governed by the methods described in the turbulence portion of the methods section. Particles have some random motion as dependent on turbulent velocity fluctuations. A different random motion is applied when a particle travels out of an eddy, or when it is not in an eddy. The results show deposition occurs in the region where the flow reattaches after separating near the stenosis apex.

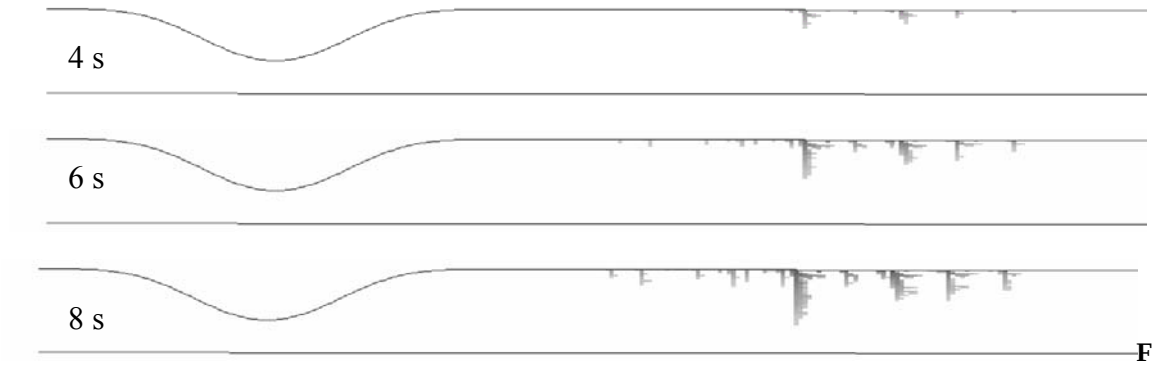

Figure 58: Time progression of thrombus formation when no shear conditions are applied.

3. Shear Enhanced Diffusivity

Shear enhanced diffusivity was added in this study, with shear independent margination. The results yield deposition where the stenosis first begins converging. There is minimal thrombus formation everywhere else along the vessel. This is illustrated in Figure 59. Platelets were allowed to flow through the thrombus in this study if they have not reached an active computational cell. For a cell to be active it must have a porosity between 0.8, the minimum, and 1, the maximum.

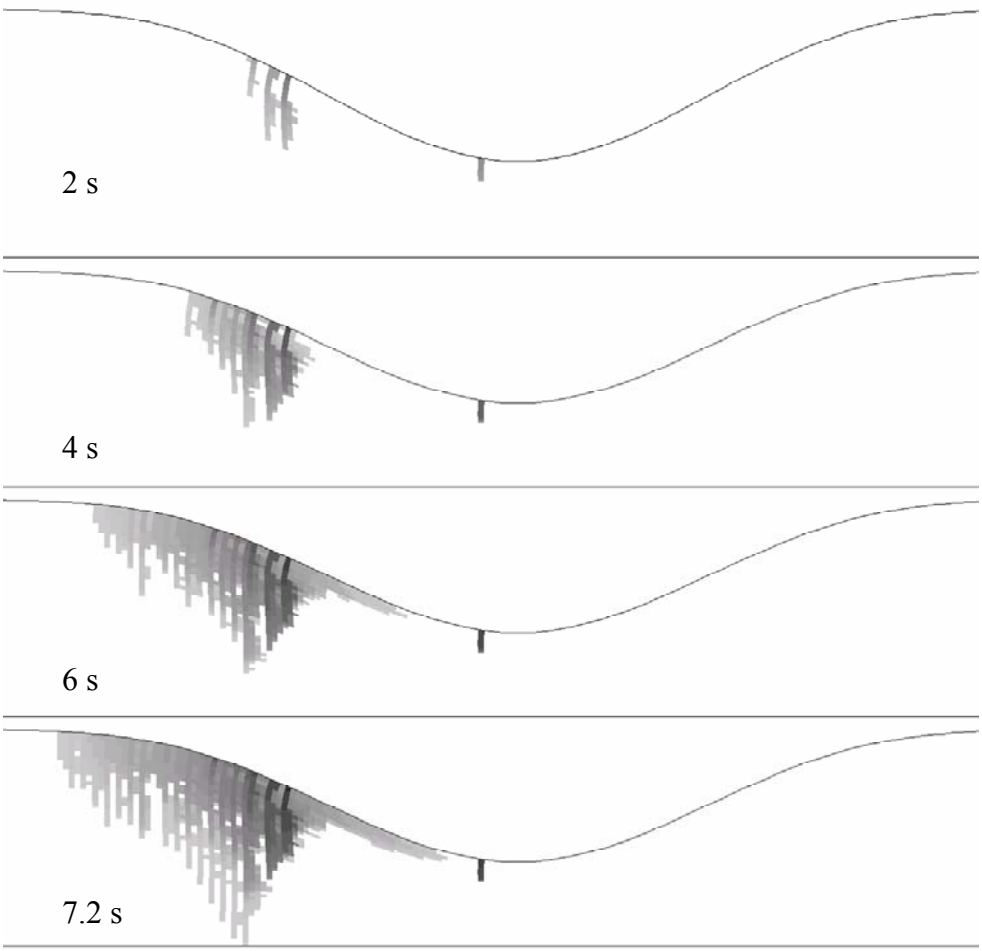

Figure 59: Time progression of thrombus aggrandizement for shear enhanced diffusivity with shear independent margination.

4. Shear Dependent Margination

The margination definition used in this study is based on shear rate dependent effective diffusivity. Therefore, the shear rate based effective diffusivity was set to a constant to maintain the ability of applying margination. The thermal diffusivity of platelet motion is too small for any significant motion, and therefore, a shear rate of 3000 s^{-1} was taken to exist over the whole flow region when calculating effective diffusivity. This increases the rate of platelet transport by three to four orders of magnitude. Therefore, the time scale in this study will be off, but deposition location, should be approximately the same if effective diffusivity was set at the thermal value. Shear

dependent margination was calculated from actual shear rates and not 3000 s^{-1}. Margination was included by directing the effective diffusive motion based on probability. Thrombus growth for shear enhanced margination is illustrated in Figure 60.

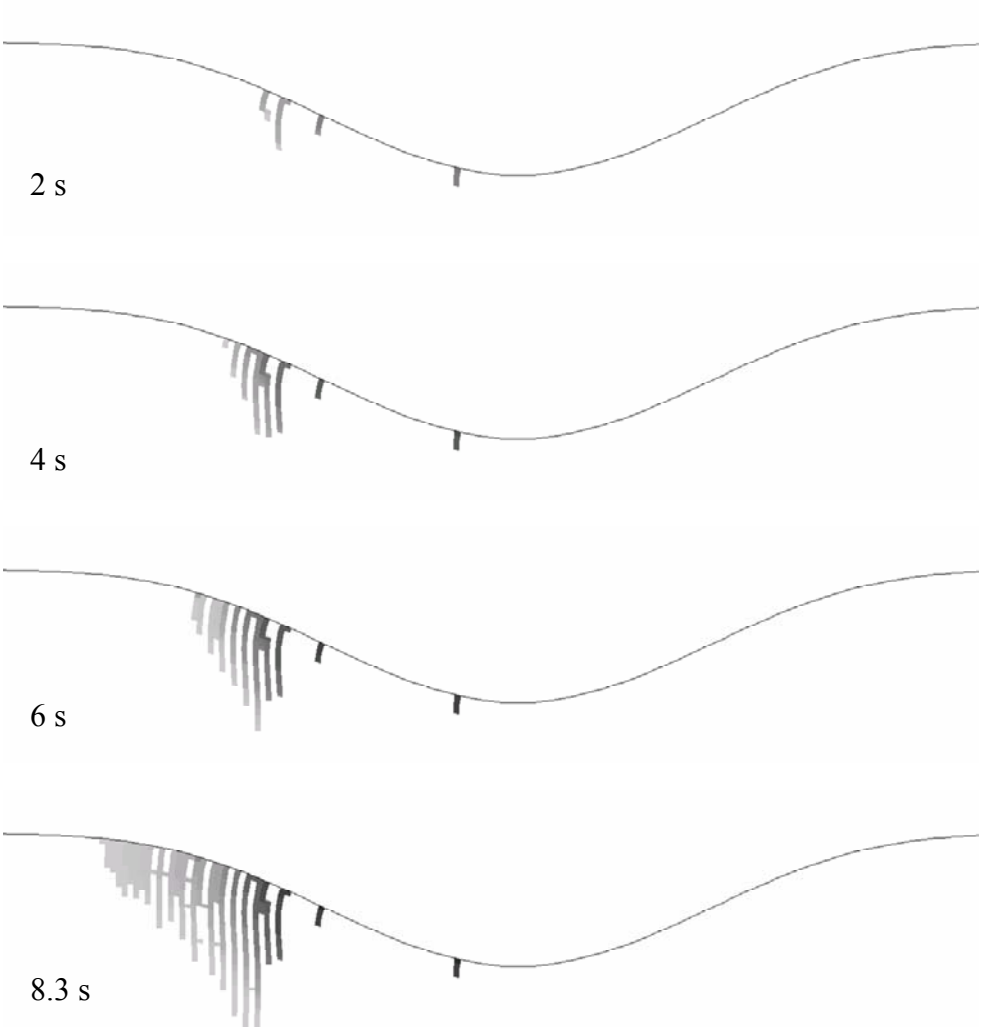

Figure 60: Time progression of thrombus aggrandizement with shear dependent margination and constant platelet diffusivity. Time may be off by 3-4 orders of magnitude.

The thrombus began growing along the converging region and at the stenosis apex. However, streamlines began to deflect away from the apex as the thrombus in the converging region grew. Therefore, growth only continued in the converging region.

5. Shear Threshold Dependent Adhesion

Shear dependent adhesion was applied by considering platelet adhesion at shear rates less than 1000 s^{-1} or greater than 20000 s^{-1}. The only point along the vessel wall that has a shear rate below 1000 s^{-1} is at the flow reattachment point. No other shear dependent conditions were applied. Turbulent motion was considered for adding particle motion, however as seen from the "no shear dependent" study, there would be minimal motion near the high shear region. A concentration profile based on the turbulent condition is shown in Figure 61 to confirm that there would be few platelets that would approach the wall in the high shear rate regions. Therefore, the shear rate based effective diffusivity was set to a constant of 3000 s^{-1} to simulate constant particle motion, just like the previous study for shear dependent margination.

Figure 61: Concentration profile resulting from shear dependent adhesion. The blue/darkest gray region has the lowest concentration of platelets. The largest concentration is along the wall of the vessel.

The choice of constant shear rate for the shear rate based diffusivity could affect the location of deposition. Figure 62 illustrates where platelets begin adhering for a constant shear rate based diffusivity of 3000 s^{-1}. Therefore, times may be off by three to four orders of magnitude from the case that transport could only occur through thermal diffusivity. The results show deposition in the converging region that is closer to the apex than the other studies.

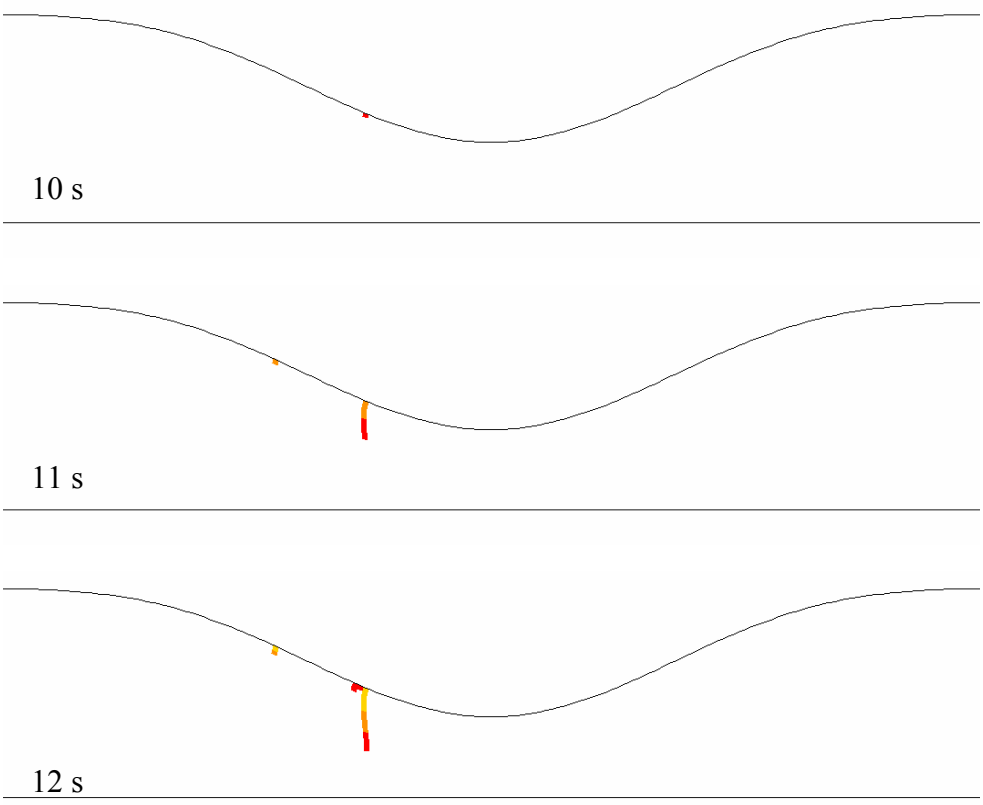

Figure 62: Time progression of thrombus aggrandizement for shear threshold dependent adhesion. Times may be off by three to four orders of magnitude.

6. Shear Enhanced Diffusivity and Margination

Shear dependent dispersion and shear dependent margination were considered in this study. There was no shear dependence for adherence. Multiple studies were performed for this case. The first considered deposition without application of the zero velocity specification in occluded computational cells, as explained in the curve fit section of the results. The unaltered porous technique is shown in Figure 63. Deposition begins along the converging region of the stenosis, up to the apex. As time progresses, the thrombus begins to increase growth more toward the base of the converging section of the stenosis. Platelets in this figure were allowed to flow through the thrombus in this study if they have not reached an active computational cell. For a cell to be active it must

have a porosity between 0.8, the minimum, and 1, the maximum. There was a small amount of deposition upstream of the stenosis, where adhesion is first considered permissible.

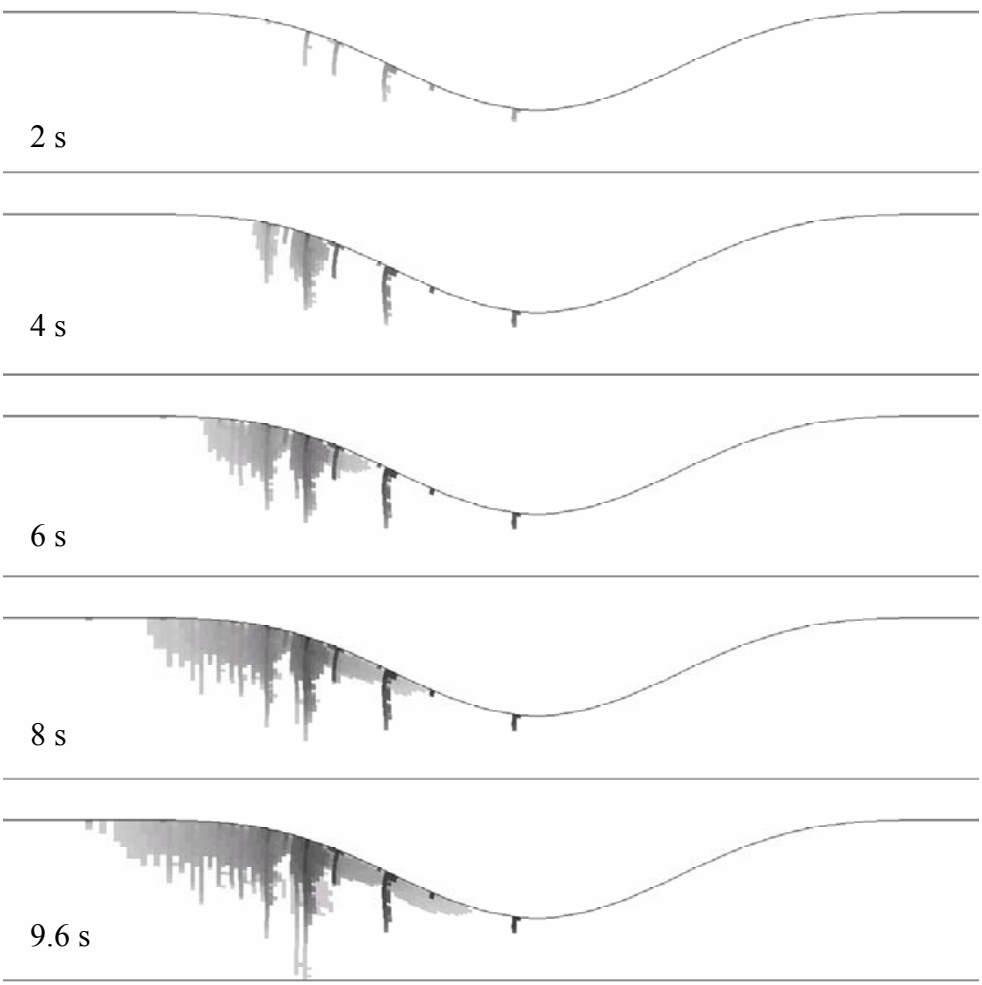

Figure 63: Time progression of thrombus aggrandizement for shear enhanced diffusivity and shear dependent margination.

The zero velocity condition was added to regions of thrombus to account for complete blockage of flow. The results of this condition are shown in Figure 64. The results are similar to Figure 63, but with less growth toward the apex of the stenosis. As with Figure 63, Figure 64 also includes the capability for platelets to pass through fully occluded computational cells. This would account for the protrusions on the downstream side of the thrombus.

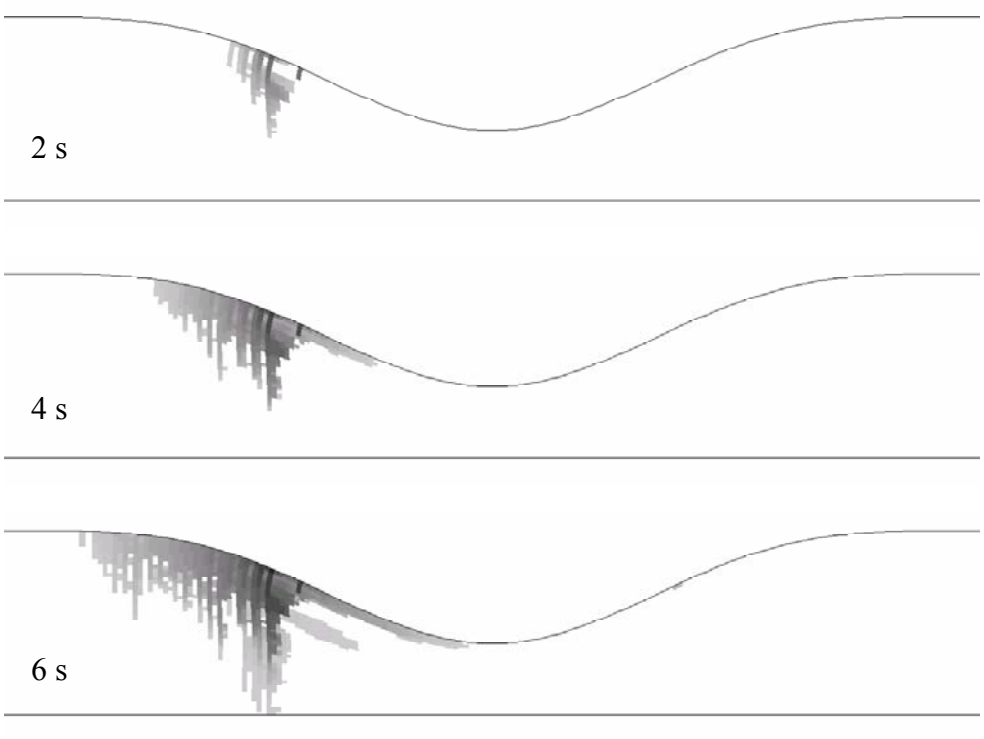

Figure 64: Time progression of thrombus aggrandizement for shear enhanced diffusivity and shear dependent margination. The condition for zero velocity was applied for cells that were considered to be occluded by the thrombus.

The next condition considered for shear enhanced diffusivity and shear dependent margination is the deletion of a platelet when it reaches the thrombus site. This condition results in a similar location of thrombus, but with a smaller base, shown in Figure 65. This is inherent based on the constrictions of thrombus growth. Platelets that pass by the thrombus must do so by going around the thrombus. Therefore, there would be few platelets that reach the downstream base of a forming thrombus.

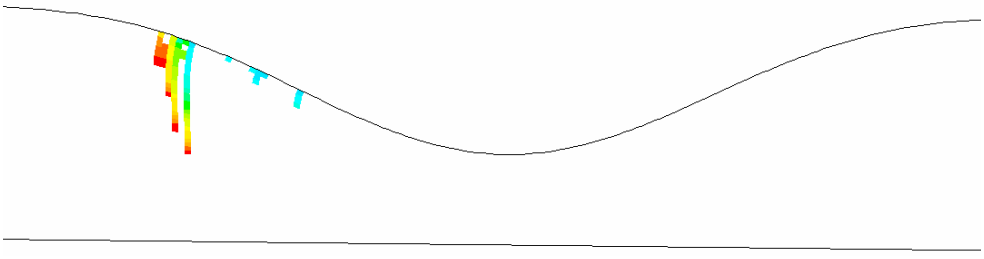

Figure 65: Thrombus aggrandizement for shear enhanced diffusivity and shear dependent margination. The condition for zero velocity was applied for cells that were considered to be occluded by the thrombus. Platelets were not allowed to pass through the forming thrombus. The time is taken at 3 s.

The pathlines based on the same flow are shown in Figure 66. The pathlines show flow recirculation in the post-thrombus region. The thrombus alters the stenosis region by making it more like a blunt object in cross flow, thereby deflecting streamlines over the stenosis apex.

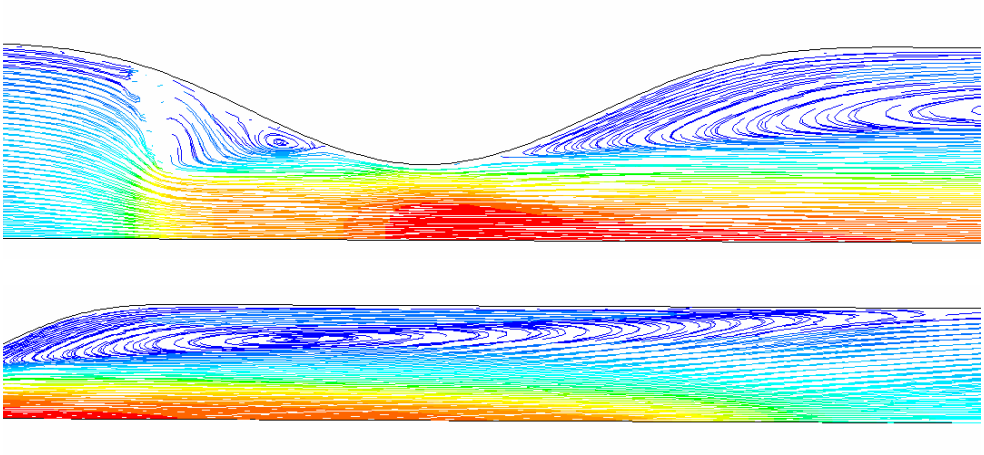

Figure 66: Pathlines of the fluid with contours based on velocity magnitude. The darkest red/gray is the region of the highest velocity, as seen at the apex. The recirculation region and downstream region is at the lowest velocity.

A plot of platelet deposition relative to shear rate is shown in Figure 67. There is much more scatter in this plot, relative to the deposition plot developed for the phenomenological model. The increased scatter is expected because the previous plot was essentially self-fulfilling, where the deposition was prescribed *a priori* to the simulation. This plot shows randomized deposition at low shear rates. The linear regression curve is only included to contrast with the previous plot in Figure 57. It does show that the trend of the data suggests increased deposition at higher shear rates. Shear rate effects on platelet enhanced diffusivity and margination is developed further from the wall than where platelets actually adhere. Therefore, the scatter of the plot would increase from this phenomena too, because the shear rates measured are taken at the point of platelet deposition.

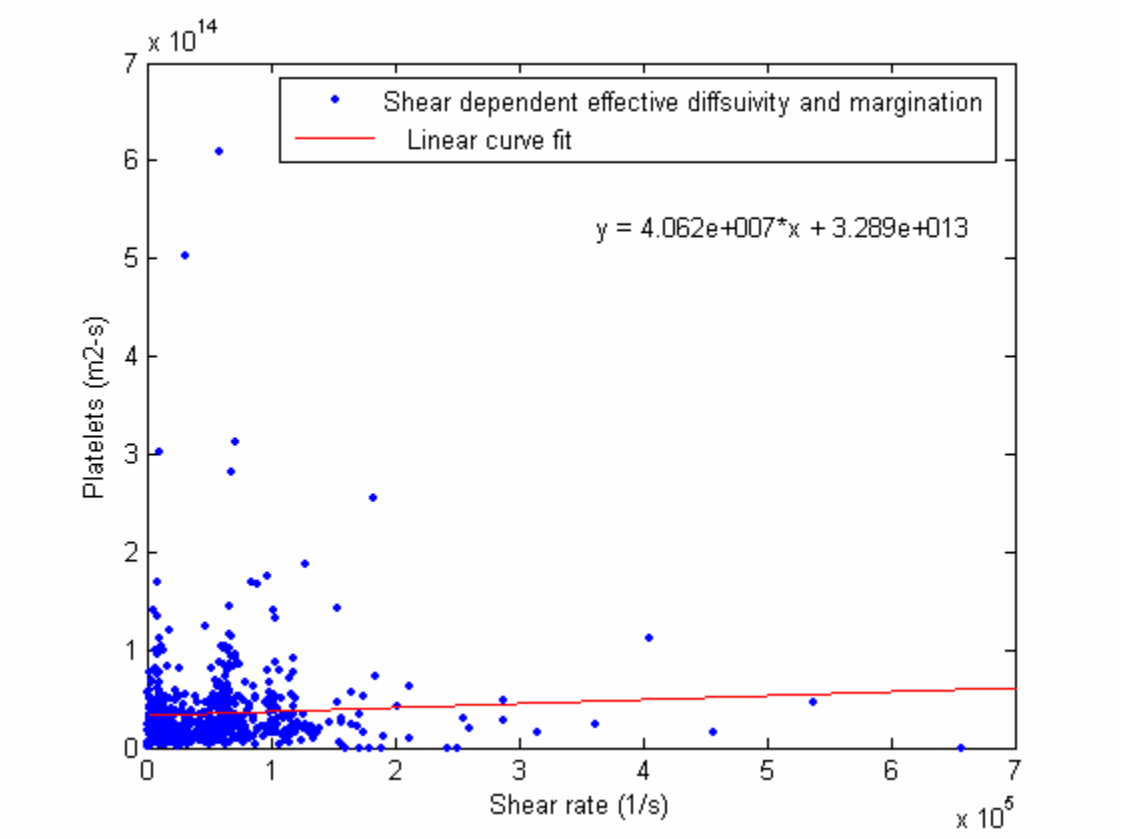

Figure 67: Plot of calculated platelet deposition based on the results of considering shear dependent margination and shear dependent effective diffusion.

7. Shear Enhanced Diffusivity and Adhesion

The case studied here considers shear dependent dispersion and shear dependent adhesion. Two conditions are considered. The first is the inclusion of shear independent margination, while the second excludes all margination. In addition, the first case does not include the zero velocity specification for occluded computational cells, while the second case does include the zero velocity specification. Both cases permit particles to pass through the thrombus. The time progression of thrombus aggrandizement for the first condition is illustrated in Figure 68. Platelets begin accumulate in the converging region of the stenosis. As time progresses, the thrombus begins to grow radially from the initial thrombus adherence point. There is relatively minimal growth along the wall past the initial adhesive point. There would likely be less deposition in this region if platelets were not allowed to pass through the thrombus.

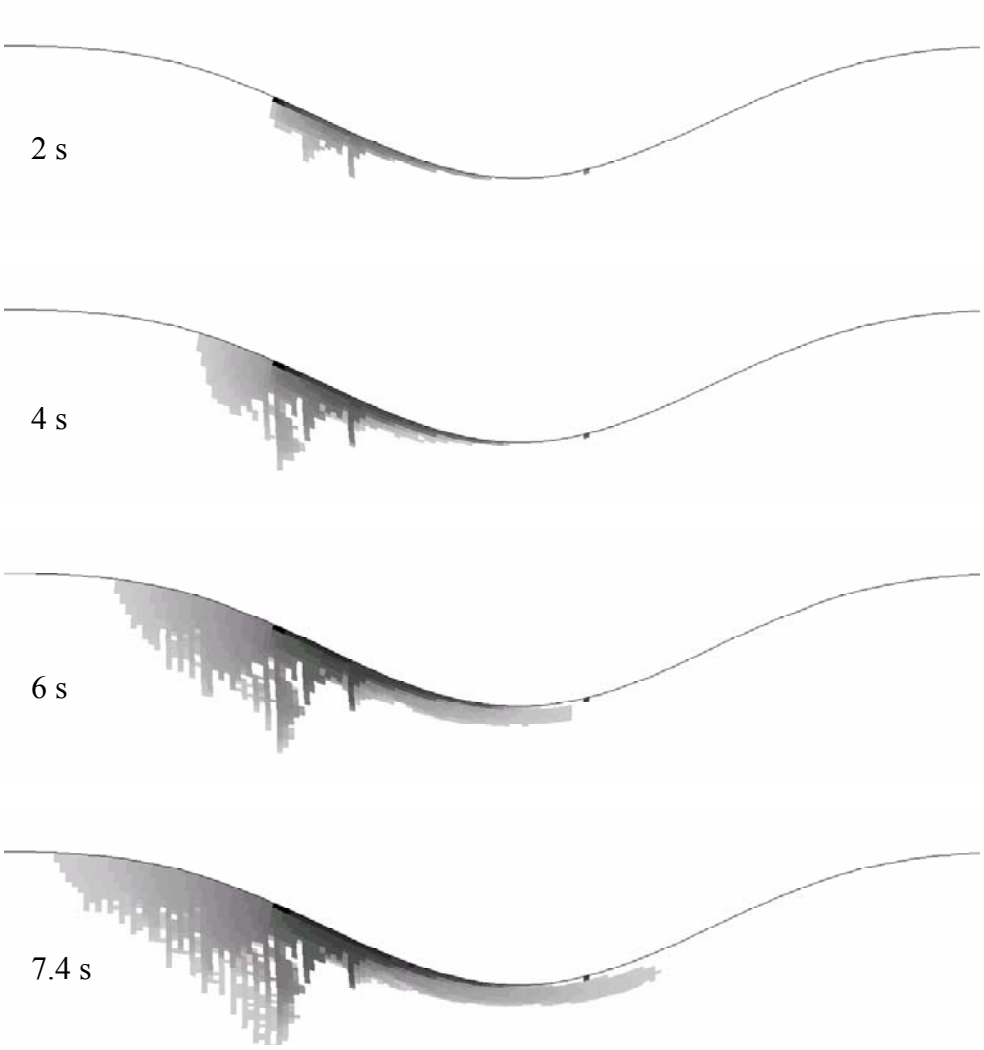

Figure 68: Time progression of thrombus aggrandizement for shear dependent dispersion and shear dependent adhesion. The red or darker color is the most recent time, while blue is the oldest portion of the thrombus. The information can also be extracted from the time sequence presented here.

The second condition considered the zero velocity condition for occluded computational cells, in addition to no margination. The condition is illustrated in Figure 69. Thrombus begins to form at the base of the converging region. This location is the same as Figure 68, and is approximately the point where the shear rate threshold is reached for 20000 s^{-1}. The location of can be compared to wall shear rate through Figure 51. However, the midline of the converging region also corresponds with the location of adherence when only shear dependent enhanced diffusivity was considered. A case of no margination was considered to contrast with the other cases in this study. The results are shown in Figure

69. The thrombus begins to form up from one location and was found to remain localized in the one location.

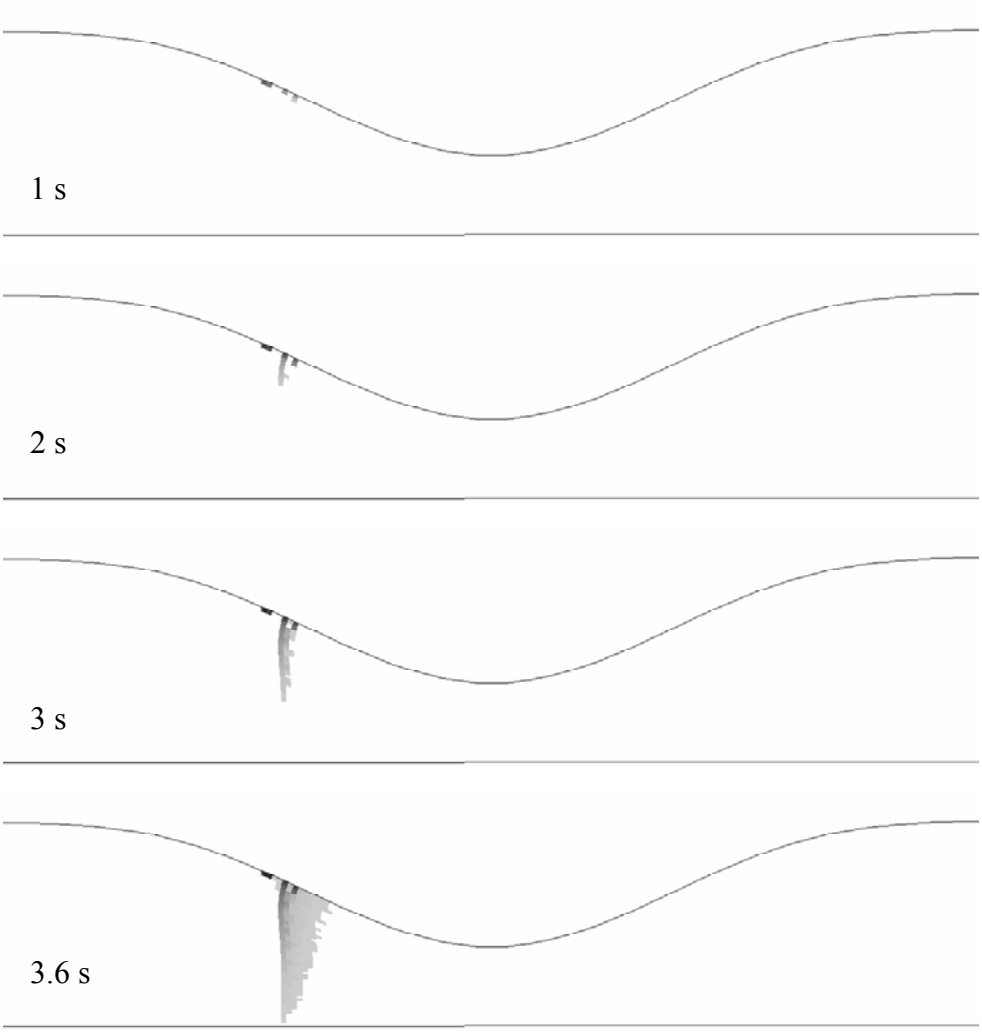

Figure 69: Time progression of thrombus aggrandizement for shear enhanced diffusivity and shear threshold dependent adhesion. The case does include the zero velocity condition for occluded computational cells, but does not include any margination.

8. Shear Dependent Margination and Adhesion

Shear dependent margination and adhesion was not necessary to consider because results of shear dependent margination could be extrapolated here. Thrombus due to margination began growing in the converging region. The same thrombus would form here, but would be constrained to grow in a region less than 10000 s^{-1}.

9. Shear Enhanced Diffusivity, Margination, and Adhesion

This case studies shear dependent diffusivity, margination, and adhesion. Two conditions were considered here. One considered platelet deposition without the application of the zero velocity condition for a occluded computational cells, while the other did consider platelet deposition based on the zero velocity condition. Both trials allowed platelets to pass through occluded computational cells. The trial that excluded the zero velocity condition is illustrated in Figure 70. From the figure it can be seen that the growth begins from the midline of the converging region and extends outward in all directions. A layer of thrombus develops across the apex. There is a faster growth rate in the upstream direction out of the wall, than in the downstream direction. This can be seen by contrasting the contours at the different time points. The growth continues radially from the area of inception. The rate of growth begins to increase as the thrombus nears occlusion, peaking at the point of occlusion.

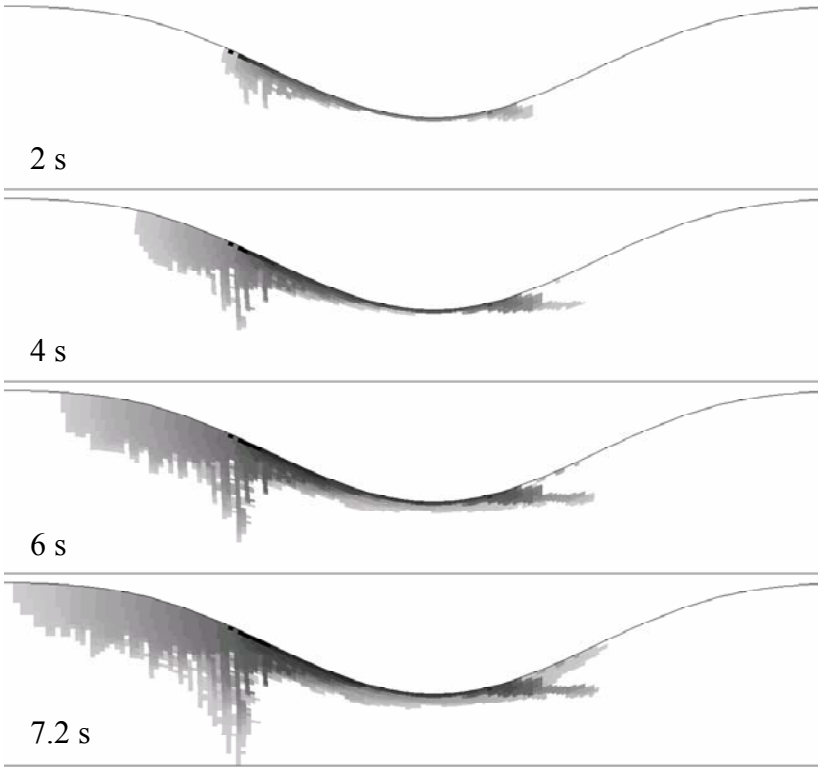

Figure 70: Time progression of thrombus aggrandizement for shear enhanced diffusivity, margination, and adhesion. The condition case does not consider the zero velocity condition for occluded computational cells.

Next the condition of zero velocity in occluded computational cells is considered. These results are displayed in Figure 71. Thrombus initiates near the midline of the converging region again. However, for this case the thrombus only grows in the radial and downstream directions. The thrombus occludes the vessel from the protrusion projecting from the initial occluded cell. The growth near the apex of the stenosis appears to grow faster radially than what was seen in Figure 70.

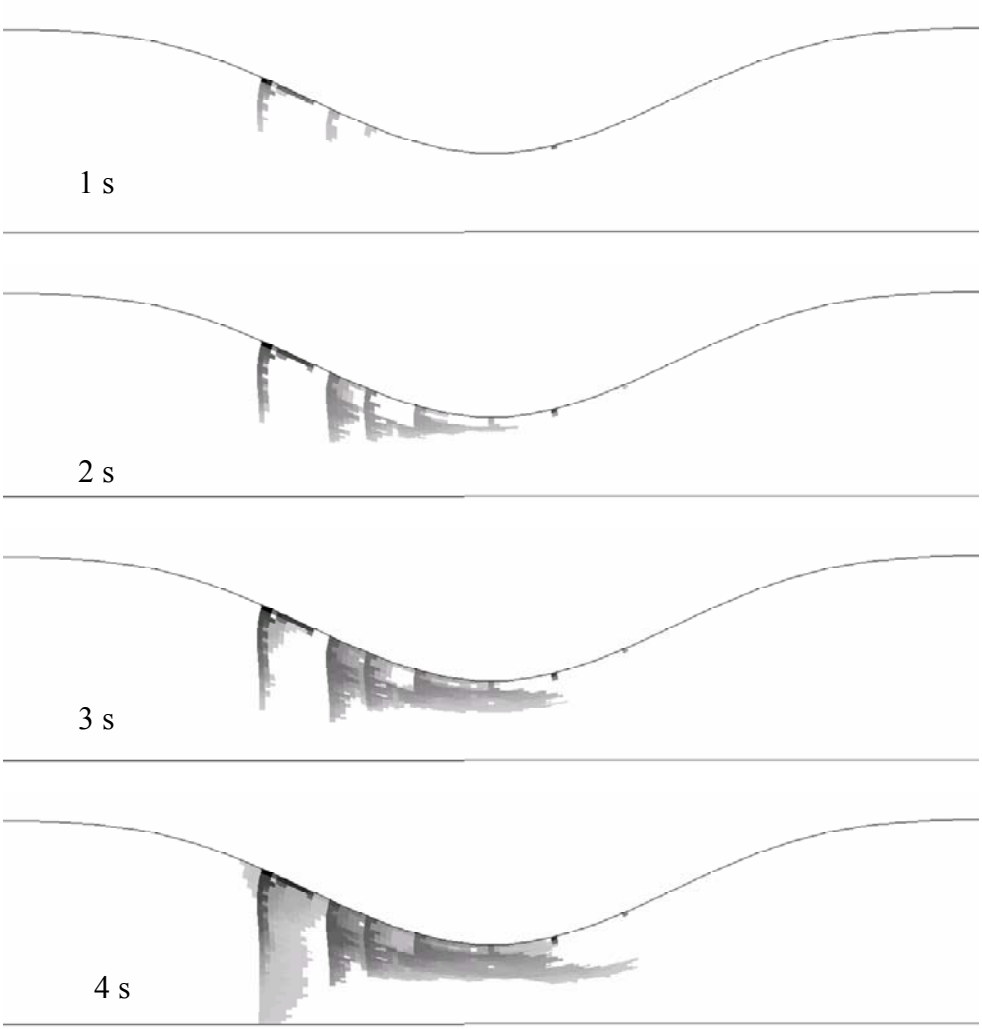

Figure 71: Time progression of thrombus aggrandizement for shear enhanced diffusivity, margination, and adhesion. The condition included the zero velocity condition for occluded computational cells.

10. Shear Enhanced Diffusivity, Margination, and Linearly Dependent Adhesion

All of the previous cases that have been considered have shown occlusion in the converging region of the stenosis. This may indicate that adhesion is more favorable at higher shear rates, in order to match experimental results. This is first considered by specifying the probability of platelet adherence to be associated with a linear relationship to shear. The equation used for the relationship is Equation 47. A random value is taken from a uniform distribution ranging from zero to one, and if the value is lower than the probability, the platelet will adhere.

Equation 47: Probability for platelet adherence.

$$p = \frac{600749\ \dot{\gamma} + 5\times10^{9}}{600749\ \left(\dot{\gamma}_a\right) + 5\times10^{9}}$$

Where p is the probability, $\dot{\gamma}$ is the shear rate, $\dot{\gamma}_a$ is a specified constant. The specified constant's relevance is that it controls at which shear rate, the probability is equal to one. The linear equation was taken from the curve fitting data of (Flannery 2005). The constant was set at 75000, resulting in thrombus formation in the converging region and the apex Figure 72. The thrombus first occluded at the throat of the stenosis. The conditions in the figure included a zero velocity condition for occluded computational cells. Platelets were not allowed to pass through an occluded thrombus region.

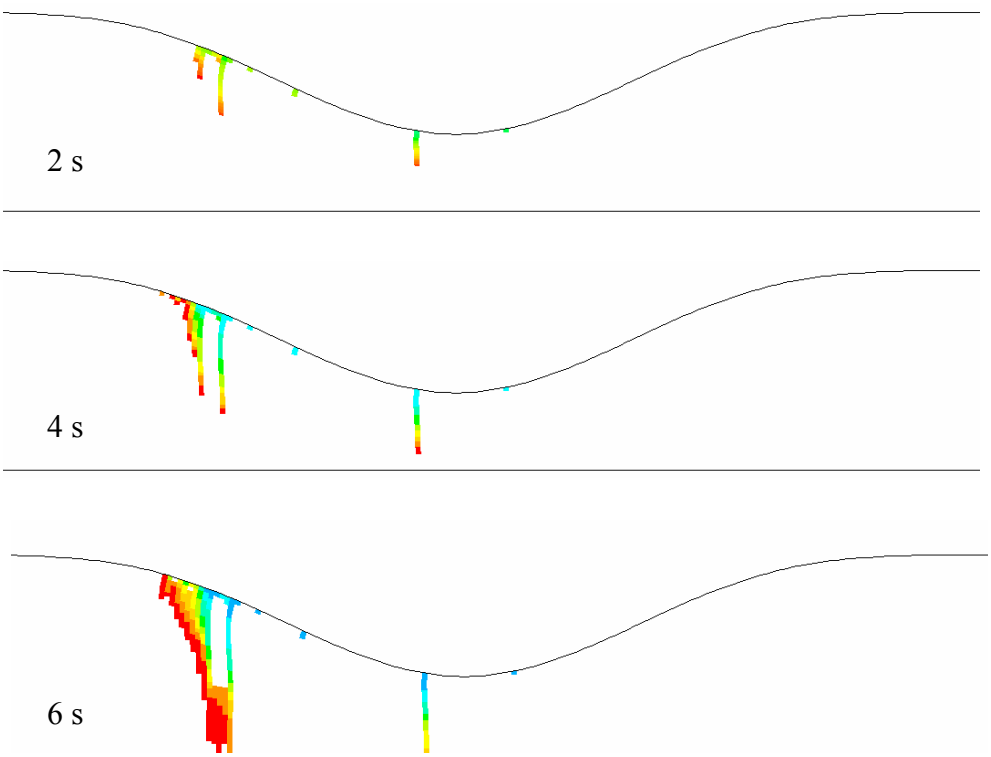

Figure 72: Thrombus time progression for shear enhanced diffusivity, margination, and a linear dependence on shear rate for adhesion. The condition included the zero velocity condition for occluded computational cells. Platelets were not allowed to pass through an occluded thrombus region The red or darker color is the most recent time, while blue is the oldest portion of the thrombus. The information can also be extracted from the time sequence presented here.

APPENDIX B

USER-DEFINED FUNCTIONS USED IN FLUENT

Phenomenological Model

```
#include "udf.h"
#include "dpm.h"
#include "surf.h"
#include <math.h>
#include "math.h"
#include "stdlib.h"
#include "time.h"
#define TSTART 0.0 /* field applied at t = tstart */
/*Define porosity from 0-1 in the computational domain based on user
defined memory (C_UDMI(0))*/
DEFINE_PROFILE(poros,t,i)
{
      real porosity;
      real x[ND_ND];
      real y;
      cell_t c;
      begin_c_loop(c,t)
      {
            C_CENTROID(x,c,t);
            y=x[1];
            porosity = C_UDMI(c,t,0);   /*Assign porosity based on
particle deposition*/
            F_PROFILE(c,t,i)= porosity;
      }
      end_c_loop(c,t)
}
/*Adjusts the velocity to zero, if a computaional cell is considered to
be completely occluded*/
DEFINE_ADJUST(adjus,d)
{
      Thread *t;
      cell_t c;
      real x[ND_ND];
      real plat=0.;
      Particle *p;
      int n;
      thread_loop_c(t,d)
      {
            begin_c_loop(c,t)
            {
                  if (C_UDMI(c,t,0)==.08)
                  {
                        C_U(c,t)=0;
                        C_V(c,t)=0;
                  }
            }
            end_c_loop(c,t)
      }
```

```
}
/*Function to update the porosity based on the shear rate conditions*/
DEFINE_EXECUTE_AT_END(end_ex)
{
      Domain *d;
      Thread *t, *t1, *t0, *t2, *tx;
      face_t f1, fx, fy, fy2, fy3;
      real cen, cen2, cen3;
      cell_t c, c0, c1;
      real x1, x2, w, v, k, area,g;
      real x[ND_ND], a[ND_ND];
      Particle *p;
      Tracked_Particle *tp;
      int n, cnt, plat;
      d = Get_Domain(1);   /* mixture domain if multiphase */
      srand(time(NULL));
      Alloc_Storage_Vars(d, SV_DPM_PARTICLE_BIN, SV_NULL);
      bin_particles_in_cells(d);
      thread_loop_c(t,d)
      {
            if (FLUID_THREAD_P(t))
            {
                  begin_c_loop(c,t)
                  {
                        C_UDMI(c,t,6)=C_UDMI(c,t,6)+.01; /*Time*/
                        if (C_UDMI(c,t,1)>1) /*Active cell*/
                        {
                              C_UDMI(c,t,5)=C_UDMI(c,t,5)+.01; /*Time
since cell activation*/
                              C_CENTROID(x,c,t);
                              C_UDMI(c,t,0)=C_UDMI(c,t,0)-
(((600749*C_UDMI(c,t,3)+5e9)*C_UDMI(c,t,4))*.01*.000000000000000008)/(C
_VOLUME(c,t)*2*3.14); /*Phenomenological porosity based on (Flannery
2005)*/
                              if (C_UDMI(c,t,0)<.2) /*Porosity
threshold*/
                              {
                                    C_UDMI(c,t,0)=.08;
                                    C_UDMI(c,t,1)=.5; /*Deactivate
cell*/
                                    C_UDMI(c,t,7)=C_UDMI(c,t,6); /*Time
of occlusion*/                              }
                        /* If porosity is less than some limit, then
neighboring cells also experience deposition*/
                        if ((C_UDMI(c,t,0)<.1)&&(C_UDMI(c,t,2)!=2))
                        {
                              C_UDMI(c,t,2)=2; /*Avoids repitition of
making neighbor cells porous*/
                              c_face_loop(c, t, n)
                              {
                                    f1=C_FACE(c,t,n);
                                    t1=C_FACE_THREAD(c,t,n);
                                    if (!BOUNDARY_FACE_THREAD_P(t1))
                                    {
                                          c1=F_C0(f1,t1);
                                          t2=THREAD_T0(t1);
                                          if ((C_UDMI(c1,t2,1)!=.5))
```

```
                                        {
                                              C_UDMI(c1,t2,1)=2;
/*Cell has been initialized*/

      C_UDMI(c1,t2,3)=C_STRAIN_RATE_MAG(c,t);
                                        }
                                        c1=F_C1(f1,t1);
                                        t2=THREAD_T1(t1);
                                        if ((C_UDMI(c1,t2,1)!=.5))
                                        {
                                              C_UDMI(c1,t2,1)=2;
/*Cell has been initialized*/

      C_UDMI(c1,t2,3)=C_STRAIN_RATE_MAG(c,t);
                                        }
                                    }
                                }
                            }
                            }
                        }
                        end_c_loop(c,t)
                  }
      }
      Free_Storage_Vars(d, SV_DPM_PARTICLE_BIN, SV_NULL);
}
DEFINE_ON_DEMAND(mem_init)
/*Used to initialize the user defined memory to specific values*/
{
      cell_t c;
      Domain *d;
      Domain *dom;
      Thread *t;
      face_t f, f1, f2, f3, fx;
      Thread *t2, *t1, *t0, *tx, *t3;
      cell_t c0;
      cell_t c1;
      real x[ND_ND];
      real a[ND_ND];
      real cen, cen2, cen3, area;
      int id, n, goo;
      d=Get_Domain(1);
      /* Allocate memory */
      Alloc_Storage_Vars(d, SV_DPM_PARTICLE_BIN, SV_NULL);
      bin_particles_in_cells(d);
      /* Free Memory */
      thread_loop_c (t,d)
      {
            begin_c_loop (c,t)
            {
                  C_UDMI(c,t,0)=1;
                  C_UDMI(c,t,1)=0;
                  C_UDMI(c,t,2)=0;
                  C_UDMI(c,t,4)=0;
                  C_UDMI(c,t,5)=0;
                  C_UDMI(c,t,6)=0;
                  C_UDMI(c,t,7)=0;
                  C_UDMI(c,t,8)=0;
```

```
                  C_UDMI(c,t,9)=0;
                  C_CENTROID(x,c,t);
                  cen3=100000;
                  goo=0;
                  /*Determine the cell to wall distance.  Only works
            when turbulence is turned on*/
                        c_face_loop(c, t, n)
                        {
                              f1=C_FACE(c,t,n);
                              t1=C_FACE_THREAD(c,t,n);
                              if ((!BOUNDARY_FACE_THREAD_P(t1)))
                              {
                                    c1=F_C0(f1,t1);
                                    t2=THREAD_T0(t1);
                                    cen=C_WALL_DIST(c1,t2);
                                    c1=F_C1(f1,t1);
                                    t2=THREAD_T1(t1);
                                    cen2=C_WALL_DIST(c1,t2);
                                    if ((cen2<cen)&&(cen2<cen3))
                                    {
                                          fx=f1;
                                          tx=t1;
                                          cen3=cen2;
                                    }
                                    if ((cen<cen2)&&(cen<cen3))
                                    {
                                          fx=f1;
                                          tx=t1;
                                          cen3=cen;
                                    }
                              }
                              else
                              {
                                    fx=f1;
                                    tx=t1;
                                    cen3=0;
                              }
                        }
                        F_AREA(a,fx,tx);
                        F_CENTROID(x,fx,tx);
                        C_UDMI(c,t,4)=NV_MAG(a)*2*3.14;/*Surface area
of computational cell for deposition calculation*/
                        C_UDMI(c,t,9)=NV_MAG(a)/x[1];/*2-D SA of cell*/
            }
            end_c_loop (c,t)
      }
      /*Initialize wall conditions or active cells*/
      t3 = Lookup_Thread(d,5);
      begin_f_loop(f3,t3)
      {
            F_CENTROID(x,f3,t3);
            if ((x[0]>.003)&&(x[0]<.03))
            {
                  c0=F_C0(f3,t3);
                  t0=THREAD_T0(t3);
                  {
                  C_UDMI(c0,t0,0)=1.-(1.7e-10);
```

```
                  C_UDMI(c0,t0,1)=2;
                  C_UDMI(c0,t0,5)=0;
                  C_UDMI(c0,t0,3)=C_STRAIN_RATE_MAG(c0,t0);
                  }
            }
      }
      end_f_loop(f3,t2)
            Free_Storage_Vars(d, SV_DPM_PARTICLE_BIN, SV_NULL);
}
DEFINE_ON_DEMAND(conc_cnt)
/*Used to calculate deposition*/
{
      cell_t c;
      Domain *d;
      Domain *dom;
      Thread *t;
      face_t f, fx, fy, fy2, fy3;
      face_t f1;
      face_t f2;
      Thread *t2;
      Thread *t1;
      Thread *t0;
      Thread *tx;
      cell_t c0;
      cell_t c1;
      real x[ND_ND];
      real a[ND_ND];
      int id, n, goo;
      real cen, cen2, cen3, area;
      d=Get_Domain(1);
      thread_loop_c (t,d)
      {
            begin_c_loop (c,t)
            {
                  C_CENTROID(x,c,t);
                  if ((C_UDMI(c,t,4)>0))

      C_UDMI(c,t,8)=100000000000000000*C_VOLUME(c,t)*2*3.14/(C_UDMI(c,t
,4));
                  if ((C_UDMI(c,t,9)>0))

      C_UDMI(c,t,9)=162974661726*(C_VOLUME(c,t)/x[1])/(C_UDMI(c,t,9));
            }
            end_c_loop (c,t)
      }
}
```

MECHANISTIC MODELS OF PLATELET DEPOSITION

```
#include "udf.h"
#include "dpm.h"
#include "surf.h"
#include <math.h>
#include "math.h"
```

```
#include "stdlib.h"
#include "time.h"
#define TSTART 0.0 /* field applied at t = tstart */
/*Define porosity from 0-1 in the computational domain based on user
defined memory (C_UDMI(0))*/
DEFINE_PROFILE(poros,t,i)
{
      real porosity;
      real x[ND_ND];
      real y;
      cell_t c;
      begin_c_loop(c,t)
      {
            C_CENTROID(x,c,t);
            y=x[1];
            porosity = C_UDMI(c,t,0);   /*Assign porosity based on
particle deposition*/
            F_PROFILE(c,t,i)= porosity;
      }
      end_c_loop(c,t)
}
/*Adjusts the velocity to zero, if a computaional cell is considered to
be completely occluded*/
DEFINE_ADJUST(adjus,d)
{
      Thread *t;
      cell_t c;
      real x[ND_ND];
      real plat=0.;
      Particle *p;
      int n;
      thread_loop_c(t,d)
      {
            begin_c_loop(c,t)
            {
                  if (C_UDMI(c,t,0)<.1)
                  {
                        C_U(c,t)=0;
                        C_V(c,t)=0;
                  }
            }
            end_c_loop(c,t)
      }
}
/*Determine enhanced diffusivity and margination for platelets*/
DEFINE_EXECUTE_AT_END(end_ex)
{
      Domain *d;
      Thread *t;
      cell_t c;
      real x1, x2, w, r, v, g, k;
      real x[ND_ND];
      Particle *p;
      Tracked_Particle *tp;
      int n, cnt, plat;
      d = Get_Domain(1);   /* mixture domain if multiphase */
      srand(time(NULL));
```

```
      Alloc_Storage_Vars(d, SV_DPM_PARTICLE_BIN, SV_NULL);
      bin_particles_in_cells(d);
      thread_loop_c(t,d)
      {
            if (FLUID_THREAD_P(t))
            {
                  begin_c_loop(c,t)
                  {
                        cnt=0;
                        plat=0;
                        /*Random numbers from Gaussian distribution*/
                        begin_particle_cell_loop(p,c,t)
                        {
                                    plat=plat+1;
                                    w=3;
                                    while((w>=1))
                                    {

      x1=((double)rand()/((double)RAND_MAX + (double)1.0));

      P_USER_REAL(p,3)=pow(pow((x1),2),.5);

      x2=((double)rand()/((double)RAND_MAX + (double)1.0));
                                          x1=2*x1-1;
                                          x2=2*x2-1;
                                          w=x1*x1+x2*x2;
                                    }
                                    w=pow(((-2*log(w))/2),.5);
                                    P_USER_REAL(p,0)=w*x1;
                                    /*if
((C_STRAIN_RATE_MAG(c,t)>10000)&&(P_USER_REAL(p,4)>0))*/
                                    {

      /*P_USER_REAL(p,4)=.00023+P_USER_REAL(p,4);*/

      /*P_USER_REAL(p,4)=.00023*.035*C_STRAIN_RATE_MAG(c,t)+P_USER_REAL
(p,4);*/
                                    }
                        }
                        end_particle_cell_loop(p,c,t)
                        C_CENTROID(x,c,t);

      /*C_UDMI(c,t,4)=.0000025*pow((plat/(C_VOLUME(c,t)/x[1])),2)+C_UDM
I(c,t,4);
                        C_UDMI(c,t,5)=C_UDMI(c,t,5)+1;*/

      C_UDMI(c,t,7)=C_UDMI(c,t,7)+3.14*.25*.0000025*.0000025*(plat/(C_V
OLUME(c,t)/x[1])); /*Cell concentration*/
                        C_UDMI(c,t,8)=C_UDMI(c,t,8)+1;/*Count*/
            v=pow(((0.101931915117668)*C_STRAIN_RATE_MAG(c,t)+3.71285E-
22),.5); /*Maximum velocity fluctuation*/
                        if ((C_UDMI(c,t,5)>0)&&(C_UDMI(c,t,0)>.1))
                                    C_UDMI(c,t,5)=.00023+C_UDMI(c,t,5);
/*Time that cell is active*/
                        C_UDMI(c,t,9)=C_UDMI(c,t,9)+.00023; /*Time*/
                        begin_particle_cell_loop(p,c,t)
                        {
```

```
                              if (x[0]<.004)

      P_VEL(p)[0]=(P_USER_REAL(p,0))*v*1000+P_VEL(p)[0]; /*Randomized
velocity near inlet to disperse particles*/
                              else

      P_VEL(p)[0]=(P_USER_REAL(p,0))*v+P_VEL(p)[0]; /*Axial velocity
fluctuation*/
/*Margination calculations*/
                              if (C_UDMI(c,t,2)>0)
                                    r=x[1]/(C_UDMI(c,t,2)+x[1]);
                              else
                                    r=1;
                              k=300;
                              g=(1-k/380+k*pow(r,14)*(1-r));
                              if (pow(g,2)>0){
                                    g=.01*(14*k*pow(r,13)-
15*k*pow(r,14))/g+(C_STRAIN_RATE_MAG(c,t)*0.000005);
                                    P_USER_REAL(p,5)=g;}
                              else
                                    g=0;
      if((P_USER_REAL(p,3)<g)&&(P_USER_REAL(p,3)<.8))
                              {

      P_USER_REAL(p,0)=pow(pow((P_USER_REAL(p,0)),2),.5);
                              }
                              if((-P_USER_REAL(p,3)>g)&&(g<0)&&(-
P_USER_REAL(p,3)>-.7))
                              {
                                    P_USER_REAL(p,0)=-
pow(pow((P_USER_REAL(p,0)),2),.5);
                              }
                              /*Radial velocity fluctuation*/
                              if (x[0]<.004)
                              {

      P_VEL(p)[1]=1000*(P_USER_REAL(p,0))*v;

      /*P_VEL(p)[1]=100*(P_USER_REAL(p,0))*P_VEL(p)[1]/P_USER_REAL(p,0)
;*/
                              }
                              else
                              {

      P_VEL(p)[1]=(P_USER_REAL(p,0))*v+P_VEL(p)[1];

      /*P_VEL(p)[1]=(P_USER_REAL(p,0))*P_VEL(p)[1]/(P_USER_REAL(p,0));*
/
                              }
                        }
                        end_particle_cell_loop(p,c,t)
                  }
                  end_c_loop(c,t)
            }
      }
      Free_Storage_Vars(d, SV_DPM_PARTICLE_BIN, SV_NULL);
}
```

```
DEFINE_ON_DEMAND(mem_init)
/*Used to initialize the user defined memory to specific values*/
{
      cell_t c;
      Domain *d;
      Domain *dom;
      Thread *t;
      face_t f, f1, f2, f3, fx;
      Thread *t2, *t1, *t0, *tx, *t3;
      cell_t c0;
      cell_t c1, c3;
      real x[ND_ND], x1[ND_ND], x2[ND_ND];
      real a[ND_ND];
      real cen, cen2, cen3, area;
      int id, n, goo, n2;
      d=Get_Domain(1);
      /* Allocate memory */
      Alloc_Storage_Vars(d, SV_DPM_PARTICLE_BIN, SV_NULL);
      bin_particles_in_cells(d);
      /* Free Memory */
      thread_loop_c (t,d)
      {
            begin_c_loop (c,t)
            {
                  C_UDMI(c,t,0)=1;
                  C_UDMI(c,t,1)=0;
                  C_UDMI(c,t,2)=0;
                  C_UDMI(c,t,4)=0;
                  C_UDMI(c,t,5)=0;
                  C_UDMI(c,t,6)=0;
                  C_UDMI(c,t,7)=0;
                  C_UDMI(c,t,8)=0;
                  C_UDMI(c,t,9)=0;
                  C_CENTROID(x,c,t);
                  cen3=0;
                  /*Determine distance from wall parameters*/
                  c_face_loop(c, t, n)
                        {
                              f1=C_FACE(c,t,n);
                              t1=C_FACE_THREAD(c,t,n);
                              if ((!BOUNDARY_FACE_THREAD_P(t1)))
                              {
                                    c1=F_C0(f1,t1);
                                    t2=THREAD_T0(t1);
                                    cen=C_WALL_DIST(c1,t2);
                                    c1=F_C1(f1,t1);
                                    t2=THREAD_T1(t1);
                                    cen2=C_WALL_DIST(c1,t2);
                                    if ((cen2>cen)&&(cen2>cen3))
                                    {
                                          fx=f1;
                                          tx=t1;
                                          cen3=cen2;
                                          n2=n;
                                    }
                                    if ((cen>cen2)&&(cen>cen3))
```

```
                        {
                              fx=f1;
                              tx=t1;
                              cen3=cen;
                              n2=n;
                        }
                  }
                  else
                  {
                        if (x[1]<.0001)
                        {
                        fx=f1;
                        tx=t1;
                        cen3=1000000;
                        n2=9;
                        }
                  }
            }
            C_UDMI(c,t,4)=n2;
            C_UDMI(c,t,2)=C_WALL_DIST(c,t);
      }
      end_c_loop (c,t)
}
/*Apply wall conditions*/
t3 = Lookup_Thread(d,5);
begin_f_loop(f3,t3)
{
      F_CENTROID(x,f3,t3);
      if ((x[0]>.008))
      {
            c0=F_C0(f3,t3);
            t0=THREAD_T0(t3);
            {
            C_UDMI(c0,t0,0)=1.-(1.7e-10);
            C_UDMI(c0,t0,1)=2;
            C_UDMI(c0,t0,3)=C_STRAIN_RATE_MAG(c0,t0);
            }
      }
      c0=F_C0(f3,t3);
      t0=THREAD_T0(t3);
      n2=C_UDMI(c0,t0,4);
      f1=C_FACE(c0,t0,n2);
      c1=c0;
      t2=t0;
      c3=c;
      t1=C_FACE_THREAD(c0,t0,n2);
      C_CENTROID(x1,c0,t0);
      while (n2<6)
      {
            c1=F_C1(f1,t1);
            t2=THREAD_T1(t1);
            if (c1==c3)
            {
                  c1=F_C0(f1,t1);
                  t2=THREAD_T0(t1);
            }
            n2=C_UDMI(c1,t2,4);
```

```
                    if (n2<6)
                    {
                    C_CENTROID(x2,c1,t2);
                    C_UDMI(c1,t2,2)=x1[1]-x2[1];
                    f1=C_FACE(c1,t2,n2);
                    t1=C_FACE_THREAD(c1,t2,n2);
                    c3=c1;
                    }
              }
      }
      end_f_loop(f3,t2)
            Free_Storage_Vars(d, SV_DPM_PARTICLE_BIN, SV_NULL);
}
DEFINE_ON_DEMAND(conc_cnt)
/*Calculations after runs*/
{
      cell_t c;
      Domain *d;
      Domain *dom;
      Thread *t;
      face_t f, f1, f2, f3, fx;
      Thread *t2, *t1, *t0, *tx, *t3;
      cell_t c0;
      cell_t c1, c2;
      real x[ND_ND], x1[ND_ND], x2[ND_ND];
      real a[ND_ND];
      real cen, cen2, cen3, area;
      int id, n, goo, n2;
      d=Get_Domain(1);
      /* Allocate memory */
      Alloc_Storage_Vars(d, SV_DPM_PARTICLE_BIN, SV_NULL);
      bin_particles_in_cells(d);
      /* Free Memory */
      /*t3 = Lookup_Thread(d,5); */
      thread_loop_c (t,d)
      {
            begin_c_loop (c,t)
            {
                  if (C_UDMI(c,t,1)>1)
                  {

                        n2=C_UDMI(c,t,4);
                        f1=C_FACE(c,t,n2);
                        t1=C_FACE_THREAD(c,t,n2);
                        if(!BOUNDARY_FACE_THREAD_P(t1))
                        {
                              c1=F_C1(f1,t1);
                              c2=c;
                              t2=THREAD_T1(t1);
                        }
                        /*if (c1==c)
                        {
                              c1=F_C0(f1,t1);
                              t2=THREAD_T0(t1);
                        }  */
                        C_UDMI(c1,t2,1)=3;
                        C_CENTROID(x1,c,t);
```

```
                        /*while (!BOUNDARY_FACE_THREAD_P(t1))
                        {
                              c1=F_C1(f1,t1);
                              t2=THREAD_T1(t1);
                              if ((c1==c)||(c1==c2))
                              {
                                    c1=F_C0(f1,t1);
                                    t2=THREAD_T0(t1);
                              }
                              C_CENTROID(x2,c1,t2);
                              C_UDMI(c1,t2,2)=x1[1]-x2[1];
                              n2=C_UDMI(c1,t2,4);
                              f1=C_FACE(c1,t2,0);
                              t1=C_FACE_THREAD(c1,t2,0);
                              c2=c1;
                        }  */
                  }
      }
            end_c_loop (c,t)
      }
      /*thread_loop_c (t,d)
      {
            begin_c_loop (c,t)
            {
                  if (C_UDMI(c,t,8)>0)
                  {
                        C_UDMI(c,t,4)=C_UDMI(c,t,7)/C_UDMI(c,t,8);
                        C_UDMI(c,t,6)=C_UDMI(c,t,4)/C_UDMI(c,t,5);
                  }
            }
            end_c_loop (c,t)
      }*/
            Free_Storage_Vars(d, SV_DPM_PARTICLE_BIN, SV_NULL);
}
DEFINE_DPM_SCALAR_UPDATE(particlemass,c,t,initialize,p)
/*Function to stop particle motion and generate porosity based particle
deposition*/
{
      face_t f1, fx, fy, fy2, fy3;
      Thread *t1;
      Thread *t2;
      cell_t c1, c3;
      int n, n2;
      real she;
      real x[ND_ND], x1[ND_ND];
      real cen, cen2, cen3;
      if(P_POS(p)[0]>.033)
      {
            p->stream_index=-1;
      }
      else
      {
      if (initialize)
      {
      }
      else
      {
```

```
            if((C_UDMI(c,t,1)>.1)&&(C_UDMI(c,t,1)<1))
                  p->stream_index=-1;
            if((C_UDMI(c,t,1)>1))
            {
                  if (P_USER_REAL(p,4)==0)
                  {
                        /*P_USER_REAL(p,4)=.00023;*/
                        P_VEL(p)[1]=0;
                        P_VEL(p)[0]=0;
                  }
                  /*if
((P_USER_REAL(p,4)>4000000)||(C_UDMI(c,t,3)>20000)||(C_UDMI(c,t,3)<1000
))*/ /*Adhesion threshold condition*/
                  /*if
(P_USER_REAL(p,3)<=pow(600749*C_UDMI(c,t,3)/95112350000+.0525694,1))*/
/*Linear adhesion condition*/
                  {
                        {
                              C_CENTROID(x,c,t);
                              /*C_UDMI(c,t,0)=C_UDMI(c,t,0)-
((58.599*C_UDMI(c,t,3)+571208)/10000)*(6.5e-17)/((4e-
6)*C_UDMI(c,t,5));*/
                              if (C_UDMI(c,t,5)==0)
                                    C_UDMI(c,t,5)=.000000001;

      /*C_UDMI(c,t,4)=(P_N(p)*.25*3.14*.0000025*.0000025)/(C_VOLUME(c,t
)/x[1])+C_UDMI(c,t,4);*/
                              C_UDMI(c,t,0)=C_UDMI(c,t,0)-
(P_N(p)*.25*3.14*.0000025*.0000025)/(C_VOLUME(c,t)/x[1]);
                              if (C_UDMI(c,t,0)<.4)
                              {
                                    C_UDMI(c,t,0)=.08;
                              }
                              else
                              {
                                    p->stream_index=-1;
                              }
                              /* If porosity is less than some limit,
then neighboring cells also experience deposition*/
                              if
((C_UDMI(c,t,0)<.1)&&(C_UDMI(c,t,1)>1))
                              {
                                    /*If drag force of a particle is
under a critical limit*/
                                    /*if
((.75*DragCoeff(p)*C_R(c,t)*(pow(pow(pow(pow(P_POS(p)[0],2)+pow(P_POS(p
)[1],2)+pow(P_POS(p)[2],2),.5)-
pow(pow(C_U(c,t),2)+pow(C_V(c,t),2)+pow(C_W(c,t),2),.5),2),.5))/(P_RHO(
p)*P_DIAM(p)))<(3000000.))*/
                                    /*if (C_UDMI(c,t,3)>20000.)*/
                                    {

                                          /*cen=100000;
                                          cen2=100000;
                                          cen3=0;
                                          c_face_loop(c, t, n)
                                          {
```

```
                                        f1=C_FACE(c,t,n);

      t1=C_FACE_THREAD(c,t,n);
                                        if
(!BOUNDARY_FACE_THREAD_P(t1))
                                        {

      F_CENTROID(x,f1,t1);
                                              if (x[0]<cen)
                                              {
                                                    cen=x[0];
                                                    fx=f1;
                                              }
                                              if (x[1]<cen2)
                                              {
                                                    cen2=x[1];
                                                    fy=x[1];
                                              }
                                              if (x[1]>cen3)
                                              {
                                                    cen3=x[1];
                                                    fy2=x[1];
                                              }
                                        }
                                  }
                                  if (cen<.017)
                                        fy3=fy2;
                                  else
                                        fy3=fy;
                                  if (fx==fy3)
                                        cen=x[0];*/
                                  f1=C_FACE(c,t,0);
                                  t1=C_FACE_THREAD(c,t,0);
                                  if
(!BOUNDARY_FACE_THREAD_P(t1))
                                  {
                                  c1=F_C1(f1,t1);
                                  t2=THREAD_T1(t1);
                                  if (c1==c)
                                  {
                                        c1=F_C0(f1,t1);
                                        t2=THREAD_T0(t1);
                                  }
                                  }
                                  else
                                  {
                                        c1=c;
                                        t2=t;
                                  }
                                  if (C_UDMI(c1,t2,0)<1)
                                  {

      C_UDMI(c,t,6)=C_UDMI(c,t,9);
                                        n2=C_UDMI(c,t,4);
                                        f1=C_FACE(c,t,n2);

      t1=C_FACE_THREAD(c,t,n2);
```

```
                                                C_CENTROID(x,c,t);
                                                c3=c;
                                                while (n2<6)
                                                {
                                                      c1=F_C1(f1,t1);
                                                      t2=THREAD_T1(t1);
                                                      if (c1==c3)
                                                      {
      c1=F_C0(f1,t1);

      t2=THREAD_T0(t1);
                                                      }

      C_CENTROID(x1,c1,t2);

      C_UDMI(c1,t2,2)=x[1]-x1[1];

      n2=C_UDMI(c1,t2,4);
                                                      if (n2<6)
                                                      {

      f1=C_FACE(c1,t2,n2);

      t1=C_FACE_THREAD(c1,t2,n2);
                                                      }
                                                      c3=c1;
                                                }
                                          c_face_loop(c, t, n)
                                          {
                                                f1=C_FACE(c,t,n);

      t1=C_FACE_THREAD(c,t,n);
                                                if
(!BOUNDARY_FACE_THREAD_P(t1))
                                                {

      F_CENTROID(x,f1,t1);
                                                      /*if
(x[0]!=cen)*/
                                                      {

      c1=F_C0(f1,t1);

      t2=THREAD_T0(t1);
                                                            if
((C_UDMI(c1,t2,1)!=.5)&&(c1!=c))
                                                            {

      C_UDMI(c1,t2,1)=2;

      C_UDMI(c1,t2,3)=C_STRAIN_RATE_MAG(c,t);
                                                            }

      c1=F_C1(f1,t1);

      t2=THREAD_T1(t1);
```

```
                                                                    if
((C_UDMI(c1,t2,1)!=.5)&&(c1!=c))
                                                                    {

      C_UDMI(c1,t2,1)=2; /*Cell has been initialized*/

      C_UDMI(c1,t2,3)=C_STRAIN_RATE_MAG(c,t);
                                                                    }
                                                              }
                                                         }
                                                    }
                                                    C_UDMI(c,t,1)=.5;
                                                    cen=1000000;
                                                    }  /*end of if*/
                                               }
                                          }
                                     }
                                }
                           }
      }
      }
}
```

REFERENCES

Aarts, P. A., P. A. Bolhuis, et al. (1983). "Red blood cell size is important for adherence of blood platelets to artery subendothelium." Blood. **62**(1): 214-217.

Aarts, P. A., P. Steendijk, et al. (1986). "Fluid shear as a possible mechanism for platelet diffusivity in flowing blood." Journal of biomechanics. **19**(10): 799-805.

Aarts, P. A., S. A. van den Broek, et al. (1988). "Blood platelets are concentrated near the wall and red blood cells, in the center in flowing blood." Arteriosclerosis : an official journal of the American Heart Association, Inc. **8**(6): 819-824.

Alevriadou, B. R., J. L. Moake, et al. (1993). "Real-time analysis of shear-dependent thrombus formation and its blockade by inhibitors of von Willebrand factor binding to platelets." Blood. **81**(5): 1263-1276.

Artoli, A. M., A. G. Hoekstra, et al. (2006). "Mesoscopic simulations of systolic flow in the human abdominal aorta." Journal of Biomechanics **39**(5): 873-84.

Badimon, L. and J. J. Badimon (1989). "Mechanisms of arterial thrombosis in nonparallel streamlines: platelet thrombi grow on the apex of stenotic severely injured vessel wall. Experimental study in the pig model." The Journal of clinical investigation. **84**(4): 1134-1144.

Badimon, L., J. J. Badimon, et al. (1986). "Influence of arterial damage and wall shear rate on platelet deposition. Ex vivo study in a swine model." Arteriosclerosis (Dallas, Tex.) **6**(3): 312-320.

Barstad, R. M., P. Kierulf, et al. (1996). "Collagen induced thrombus formation at the apex of eccentric stenoses--a time course study with non-anticoagulated human blood." Thrombosis And Haemostasis **75**(4): 685-692.

Barstad, R. M., H. E. Roald, et al. (1994). "A perfusion chamber developed to investigate thrombus formation and shear profiles in flowing native human blood at the apex of well-defined stenoses." Arteriosclerosis And Thrombosis: A Journal Of Vascular Biology / American Heart Association **14**(12): 1984-1991.

Basmadjian, D. (1986). "The hemodynamic and embolizing forces acting on thrombi--II. The effect of pulsatile blood flow." Journal of biomechanics. **19**(10): 837-845.

Basmadjian, D. (1989). "Embolization: critical thrombus height, shear rates, and pulsatility. Patency of blood vessels." Journal of biomedical materials research. **23**(11): 1315-1326.

Basmadjian, D. (1990). "The effect of flow and mass transport in thrombogenesis." Annals of Biomedical Engineering **18**(6): 685-709.

Baumgartner, H. R. (1977). "Platelet interaction with collagen fibrils in flowing blood. I. Reaction of human platelets with alpha chymotrypsin-digested subendothelium." Thrombosis and haemostasis. **37**(1): 1-16.

Baumgartner, H. R., R. Muggli, et al. (1976). "Platelet adhesion, release and aggregation in flowing blood: effects of surface properties and platelet function." Thrombosis And Haemostasis **35**(1): 124-138.

Bennett, J. S. and G. Vilaire (1979). "Exposure of platelet fibrinogen receptors by ADP and epinephrine." The Journal Of Clinical Investigation **64**(5): 1393-1401.

Berger, S. A. and L. D. Jou (2000). "Flows in stenotic vessels." Annual Review of Fluid Mechanics **32**: 347-382.
Berndt, M. C., C. Gregory, et al. (1983). "Additional glycoprotein defects in Bernard-Soulier's syndrome: confirmation of genetic basis by parental analysis." Blood. **62**(4): 800-807.
Bluestein, D., C. Gutierrez, et al. (1999). "Vortex shedding in steady flow through a model of an arterial stenosis and its relevance to mural platelet deposition." Annals of biomedical engineering. **27**(6): 763-773.
Bluestein, D., L. Niu, et al. (1997). "Fluid mechanics of arterial stenosis: relationship to the development of mural thrombus." Annals of biomedical engineering. **25**(2): 344-356.
Bossis, G. and J. F. Brady (1984). "Dynamic simulation of sheared suspensions. I. General method." Journal of Chemical Physics **80**(10): 5141-54.
Boyd, J., J. Buick, et al. (2005). "Application of the lattice Boltzmann model to simulated stenosis growth in a two-dimensional carotid artery." Physics In Medicine And Biology **50**(20): 4783-4796.
Buchanan, J. R., Jr. and C. Kleinstreuer (1998). "Simulation of particle-hemodynamics in a partially occluded artery segment with implications to the initiation of microemboli and secondary stenoses." Journal of Biomechanical Engineering, Transactions of the ASME **120**(4): 446-453.
Caro, C. G., J. M. Fitz-Gerald, et al. (1971). "Atheroma and arterial wall shear. Observation, correlation and proposal of a shear dependent mass transfer mechanism for atherogenesis." Proceedings Of The Royal Society Of London. Series B, Containing Papers Of A Biological Character. Royal Society (Great Britain) **177**(46 (Print)): 109-159.
Cheng, G. C., H. M. Loree, et al. (1993). "Distribution of circumferential stress in ruptured and stable atherosclerotic lesions. A structural analysis with histopathological correlation." Circulation **87**(4): 1179-1187.
Chien, S. (1970). "Shear dependence of effective cell volume as a determinant of blood viscosity." Science **168**(934): 977-979.
Chun, X. and D. Wootton (2002). A model of platelet concentration sampling in arterial flow, Houston, TX, USA, IEEE.
Dalin, T., Y. Chun, et al. (2002). "Simulating cyclic artery compression using a 3D unsteady model with fluid-structure interactions." Computers & Structures **80**(20-21): 1651-65.
Davies, M. J. (1990). "A macro and micro view of coronary vascular insult in ischemic heart disease." Circulation **82**(3 Suppl): II38-46.
Davies, M. J. and A. C. Thomas (1985). "Plaque fissuring--the cause of acute myocardial infarction, sudden ischaemic death, and crescendo angina." British Heart Journal **53**(4): 363-373.
Ding, E. J. and C. K. Aidun (2006). "Cluster size distribution and scaling for spherical particles and red blood cells in pressure-driven flows at small Reynolds number." Physical Review Letters **96**(20): 204502-1.
Donadelli, R., J. N. Orje, et al. (2006). "Size regulation of von Willebrand factor-mediated platelet thrombi by ADAMTS13 in flowing blood." Blood **107**(5): 1943-1950.

Dong, J. F. (2005). "Cleavage of ultra-large von Willebrand factor by ADAMTS-13 under flow conditions." Journal Of Thrombosis And Haemostasis: JTH **3**(8): 1710-1716.
Downing, J. M. and D. N. Ku (1997). "Effects of frictional losses and pulsatile flow on the collapse of stenotic arteries." Journal Of Biomechanical Engineering **119**(3): 317-324.
Eckstein, E. C. and F. Belgacem (1991). "Model of platelet transport in flowing blood with drift and diffusion terms." Biophysical journal. **60**(1): 53-69.
Eckstein, E. C., D. L. Bilsker, et al. (1987). "Transport of platelets in flowing blood." Annals of the New York Academy of Sciences. **516**: 442-452.
Fiechter, J. (1998). Numerical study of platelet transport in flowing blood. Mechanical Engineering. Atlanta, Georgia Institute of Technology. **M.S.:** 76.
Flannery, C. J. (2005). Thrombus formation under high shear in arterial stenotic flow. Mechanical Engineering. Atlanta, Georgia Tech. **M.S.**
Fogelson, A. L. (1984). "A mathematical model and numerical method for studying platelet adhesion and aggregation during blood clotting." Journal of Computational Physics **56**(1): 111-134.
Fogelson, A. L. and R. D. Guy (2004). "Platelet-wall interactions in continuum models of platelet thrombosis: formulation and numerical solution." Mathematical Medicine And Biology: A Journal Of The IMA **21**(4): 293-334.
Fogelson, A. L. and C. S. Peskin (1988). "A fast numerical method for solving the three-dimensional Stokes' equations in the presence of suspended particles." Journal of Computational Physics **79**(1): 50-69.
Folie, B. J. and L. V. McIntire (1989). "Mathematical analysis of mural thrombogenesis. Concentration profiles of platelet-activating agents and effects of viscous shear flow." Biophysical journal. **56**(6): 1121-1141.
Folts, J. D., E. B. Crowell, Jr., et al. (1976). "Platelet aggregation in partially obstructed vessels and its elimination with aspirin." Circulation. **54**(3): 365-370.
Friedman, M. and G. J. Van den Bovenkamp (1966). "The pathogenesis of a coronary thrombus." The American Journal Of Pathology **48**(1): 19-44.
Frojmovic, M. and T. Wong (1991). "Dynamic measurements of the platelet membrane glycoprotein IIb-IIIa receptor for fibrinogen by flow cytometry. II. Platelet size-dependent subpopulations." Biophysical Journal **59**(4): 828-837.
Frojmovic, M., T. Wong, et al. (1991). "Dynamic measurements of the platelet membrane glycoprotein IIb-IIIa receptor for fibrinogen by flow cytometry. I. Methodology, theory and results for two distinct activators." Biophysical Journal **59**(4): 815-827.
Gardiner, C. W. (1985). Handbook of Stochastic Methods for Physics, Chemistry and the Natural Sciences. New York, Springer-Verlag.
Glagov, S., C. Zarins, et al. (1988). "Hemodynamics and atherosclerosis. Insights and perspectives gained from studies of human arteries." Archives of pathology & laboratory medicine. **112**(10): 1018-1031.
Godyna, S., M. Diaz-Ricart, et al. (1996). "Fibulin-1 mediates platelet adhesion via a bridge of fibrinogen." Blood **88**(7): 2569-2577.
Goldsmith, H. L. (1972). "The flow of model particles and blood cells and its relation to thrombogenesis." Progress In Hemostasis And Thrombosis **1**: 97-127.

Goldsmith, H. L. and J. C. Marlow (1979). "Flow behavior of Erythrocytes. II. Particle motions in concentrated suspensions of ghost cells." Journal of Colloid and Interface Science **71**(2): 383-407.

Goldsmith, H. L. and V. T. Turitto (1986). "Rheological aspects of thrombosis and haemostasis: basic principles and applications. ICTH-Report--Subcommittee on Rheology of the International Committee on Thrombosis and Haemostasis." Thrombosis And Haemostasis **55**(3): 415-435.

Goodman, P. D., E. T. Barlow, et al. (2005). "Computational model of device-induced thrombosis and thromboembolism." Annals of biomedical engineering. **33**(6): 780-797.

Hanson, S. R., J. H. Griffin, et al. (1993). "Antithrombotic effects of thrombin-induced activation of endogenous protein C in primates." The Journal Of Clinical Investigation **92**(4): 2003-2012.

Hanson, S. R., H. F. Kotze, et al. (1985). "Platelet interactions with Dacron vascular grafts. A model of acute thrombosis in baboons." Arteriosclerosis (Dallas, Tex.) **5**(6): 595-603.

He, X. (1993). Numerical Simulations of Blood Flow. Mechanical Engineering. Atlanta, Georgia Institute of Technology.

He, X. and D. N. Ku (1996). "Pulsatile flow in the human left coronary artery bifurcation: average conditions." Journal Of Biomechanical Engineering **118**(1): 74-82.

Heinl, E. and M. Bohnet (2005). "Calculation of particle-wall adhesion in horizontal gas-solids flow using CFD." Powder Technology **159**(2): 95-104.

Hellums, J. D. (1994). "1993 Whitaker Lecture: biorheology in thrombosis research." Annals Of Biomedical Engineering **22**(5): 445-455.

Horie, T., M. Sekiguchi, et al. (1978). "Relationship between myocardial infarction and preinfarction angina: a histopathological study of coronary arteries in two sudden death cases employing serial section." American Heart Journal **95**(1): 81-88.

Hubbell, J. A. and L. V. McIntire (1986). "Platelet active concentration profiles near growing thrombi. A mathematical consideration." Biophysical journal. **50**(5): 937-945.

Johnston, G. I., S. Heptinstall, et al. (1984). "The expression of glycoproteins on single blood platelets from healthy individuals and from patients with congenital bleeding disorders." Biochemical and biophysical research communications. **123**(3): 1091-1098.

Joist, J. H., J. E. Bauman, et al. (1998). "Platelet adhesion and aggregation in pulsatile shear flow: effects of red blood cells." Thrombosis Research **92**(6 Suppl 2): S47-52.

Keller, K. H. (1971). "Effect of fluid shear on mass transport in flowing blood." Federation proceedings. **30**(5): 1591-1599.

Kieffer, N. and D. R. Phillips (1990). "Platelet membrane glycoproteins: functions in cellular interactions." Annual review of cell biology. **6**: 329-357.

Kroll, M. H., J. D. Hellums, et al. (1996). "Platelets and shear stress." Blood. **88**(5): 1525-1541.

Ku, D. N. (1997). Blood flow in arteries. **29:** 399.

Ku, D. N., D. P. Giddens, et al. (1985). "Pulsatile flow and atherosclerosis in the human carotid bifurcation. Positive correlation between plaque location and low oscillating shear stress." Arteriosclerosis (Dallas, Tex.) **5**(3): 293-302.

Kunicki, T. J., R. Orchekowski, et al. (1993). "Variability of integrin alpha 2 beta 1 activity on human platelets." Blood. **82**(9): 2693-2703.

Ladd, A. J. C. (1993). "Short-time motion of colloidal particles: numerical simulation via a fluctuating lattice-Boltzmann equation." Physical Review Letters **70**(9): 1339-42.

Lassila, R., J. J. Badimon, et al. (1990). "Dynamic monitoring of platelet deposition on severely damaged vessel wall in flowing blood. Effects of different stenoses on thrombus growth." Arteriosclerosis : an official journal of the American Heart Association, Inc. **10**(2): 306-315.

Li, F., C. Q. Li, et al. (2004). "Shear stress-induced binding of large and unusually large von Willebrand factor to human platelet glycoprotein Ibalpha." Annals Of Biomedical Engineering **32**(7): 961-969.

Li, F., C. Q. Li, et al. (2004). "Shear stress-induced binding of large and unusually large von Willebrand factor to human platelet glycoprotein Ibalpha." Annals Of Biomedical Engineering **32**(7 (Print)): 961-969.

Li, H., H. Fang, et al. (2004). "Lattice Boltzmann simulation on particle suspensions in a two-dimensional symmetric stenotic artery." Physical Review. E, Statistical, Nonlinear, And Soft Matter Physics **69**(3 Pt 1): 031919-031919.

Longest, P. W. and C. Kleinstreuer (2003). "Comparison of blood particle deposition models for non-parallel flow domains." Journal of Biomechanics **36**(3): 421-30.

Longest, P. W., C. Kleinstreuer, et al. (2004). "Efficient computation of micro-particle dynamics including wall effects." Computers & Fluids **33**(4): 577-601.

Ma, P., X. Li, et al. (1994). "Heat and mass transfer in a separated flow region for high Prandtl and Schmidt numbers under pulsatile conditions." International Journal of Heat and Mass Transfer **37**(17): 2723-2736.

Maehara, A., G. S. Mintz, et al. (2002). "Morphologic and angiographic features of coronary plaque rupture detected by intravascular ultrasound." Journal of the American College of Cardiology **40**(5): 904-910.

Markou, C. P., S. R. Hanson, et al. (1993). Role of high wall shear rate on thrombus formation in stenoses, New Orleans, LA, USA, Publ by ASME, New York, NY, USA.

Matas, J. P., J. F. Morris, et al. (2004). "Inertial migration of rigid spherical particles in Poiseuille flow." Journal of Fluid Mechanics **515**: 171-95.

Menter, F. R. (1994). "Two-equation eddy-viscosity turbulence models for engineering applications." AIAA Journal **32**(8): 1598-605.

Minsoo, H., K. Chongyoup, et al. (1999). "Particle migration in tube flow of suspensions." Journal of Rheology **43**(5): 1157-74.

Moroi, M., S. M. Jung, et al. (1989). "A patient with platelets deficient in glycoprotein VI that lack both collagen-induced aggregation and adhesion." The Journal Of Clinical Investigation **84**(5): 1440-1445.

Morsi, S. A. and A. J. Alexander (1972). "An investigation of particle trajectories in two-phase flow systems." Journal of Fluid Mechanics **55**: 193-208.

Novák, L., H. Deckmyn, et al. (2002). "Shear-dependent morphology of von Willebrand factor bound to immobilized collagen." Blood **99**(6): 2070-2076.
Ouared, R. and B. Chopard (2005). "Lattice Boltzmann simulations of blood flow: non-Newtonian rheology and clotting processes." Journal of Statistical Physics **121**(1-2): 209-21.
Peskin, C. S. (2002). "The immersed boundary method." Acta Numerica **11**: 479-517.
Pierschbacher, M. D. and E. Ruoslahti (1984). "Cell attachment activity of fibronectin can be duplicated by small synthetic fragments of the molecule." Nature. **309**(5963): 30-33.
Pierschbacher, M. D. and E. Ruoslahti (1987). "Influence of stereochemistry of the sequence Arg-Gly-Asp-Xaa on binding specificity in cell adhesion." The Journal of biological chemistry. **262**(36): 17294-17298.
Pischel, K. D., H. G. Bluestein, et al. (1988). "Platelet glycoproteins Ia, Ic, and IIa are physicochemically indistinguishable from the very late activation antigens adhesion-related proteins of lymphocytes and other cell types." The Journal of clinical investigation. **81**(2): 505-513.
Raz, S., S. Einav, et al. (2002). Platelet activation in flow through a stenosis model: comparison between CFD and CDPIV results, Houston, TX, USA, IEEE.
Raz, S., S. Einav, et al. (2007). "DPIV Prediction of Flow Induced Platelet Activation-Comparison to Numerical Predictions." Annals Of Biomedical Engineering **35**(4): 493-504.
Richardson, P. D. (2002). "Biomechanics of plaque rupture: progress, problems, and new frontiers." Annals Of Biomedical Engineering **30**(4): 524-536.
Ruggeri, Z. M. (2002). "Platelets in atherothrombosis." Nature medicine. **8**(11): 1227-1234.
Ruggeri, Z. M., R. Lombardi, et al. (1982). "Type IIB von Willebrand's disease: differential clearance of endogenous versus transfused large multimer von willebrand factor." Blood **60**(6): 1453-1456.
Ruggeri, Z. M., J. N. Orje, et al. (2006). "Activation-independent platelet adhesion and aggregation under elevated shear stress." Blood **108**(6): 1903-1910.
Saelman, E. U., H. K. Nieuwenhuis, et al. (1994). "Platelet adhesion to collagen types I through VIII under conditions of stasis and flow is mediated by GPIa/IIa (alpha 2 beta 1-integrin)." Blood. **83**(5): 1244-1250.
Saffman, P. G. (1965). "Lift on small sphere in slow shear flow." Journal of Fluid Mechanics **22**(Part 2): 385-400.
Sakariassen, K. S., R. Joss, et al. (1990). "Collagen type III induced ex vivo thrombogenesis in humans. Role of platelets and leukocytes in deposition of fibrin." Arteriosclerosis (Dallas, Tex.) **10**(2): 276-284.
Savage, B., E. Saldívar, et al. (1996). "Initiation of platelet adhesion by arrest onto fibrinogen or translocation on von Willebrand factor." Cell. **84**(2): 289-297.
Schoephoerster, R. T., F. Oynes, et al. (1993). "Effects of local geometry and fluid dynamics on regional platelet deposition on artificial surfaces." Arteriosclerosis and thrombosis : a journal of vascular biology. **13**(12): 1806-1813.
Siedlecki, C. A., B. J. Lestini, et al. (1996). "Shear-dependent changes in the three-dimensional structure of human von Willebrand factor." Blood **88**(8): 2939-2950.

Siegel Jr., J. M. (1992). Wall Shear Stress Through an Arterial Stenosis and its Implications to Thrombosis. Mechanical Engineering. Atlanta, Georgia Tech. **M.S.**

Sixma, J. J., G. H. van Zanten, et al. (1997). "Platelet adhesion to collagen: an update." Thrombosis and haemostasis. **78**(1): 434-438.

Snabre, P., M. Bitbol, et al. (1987). "Cell disaggregation behavior in shear flow." Biophysical Journal **51**(5): 795-807.

Sorensen, E. N., G. W. Burgreen, et al. (1999). "Computational Simulation of Platelet Deposition and Activation: I. Model Development and Properties." Annals of Biomedical Engineering **27**(4-12): 436-448.

Sporn, L. A., S. I. Chavin, et al. (1985). "Biosynthesis of von Willebrand protein by human megakaryocytes." The Journal Of Clinical Investigation **76**(3): 1102-1106.

Stary, H. C., A. B. Chandler, et al. (1995). "A definition of advanced types of atherosclerotic lesions and a histological classification of atherosclerosis. A report from the Committee on Vascular Lesions of the Council on Arteriosclerosis, American Heart Association." Arteriosclerosis, thrombosis, and vascular biology. **15**(9): 1512-1531.

Strong, A. B., G. D. Stubley, et al. (1987). "Theoretical and experimental analysis of cellular adhesion to polymer surfaces." Journal Of Biomedical Materials Research **21**(8): 1039-1055.

Stubley, G. D., A. B. Strong, et al. (1987). "REVIEW OF MATHEMATICAL MODELS FOR THE PREDICTION OF BLOOD CELL ADHESION." PCH, PhysicoChemical Hydrodynamics **8**(2): 221-235.

Sun, C. and L. L. Munn (2005). "Particulate nature of blood determines macroscopic rheology: a 2-D lattice Boltzmann analysis." Biophysical Journal **88**(3): 1635-1645.

Tamagawa, M. and S. Matsuo (2004). "Predictions of thrombus formation using lattice Boltzmann method (modeling of adhesion force for particles to wall)." JSME International Journal, Series C (Mechanical Systems, Machine Elements and Manufacturing) **47**(4): 1027-34.

Tandon, N. N., C. F. Ockenhouse, et al. (1991). "Adhesive functions of platelets lacking glycoprotein IV (CD36)." Blood **78**(11): 2809-2813.

Tangelder, G. J., D. W. Slaaf, et al. (1982). "Localization within a thin optical section of fluorescent blood platelets flowing in a microvessel." Microvascular research. **23**(2): 214-230.

Tarbell, J. M. (2003). Mass transport in arteries and the localization of atherosclerosis. Annual review of biomedical engineering, Volume 5, 2003, Annual Reviews**:** 79-118.

Taylor, G. I. (1934). "Formation of emulsions in definable fields of flow." Proceedings of the Royal Society of London **146A**: 501-523.

Thubrikar, M. J., M. Labrosse, et al. (2001). "Mechanical properties of abdominal aortic aneurysm wall." Journal of medical engineering & technology. **25**(4): 133-142.

Thurston, G. B. and N. M. Henderson (2006). "Effects of flow geometry on blood viscoelasticity." Biorheology **43**(6): 729-746.

Tilles, A. W. and E. C. Eckstein (1987). "The near-wall excess of platelet-sized particles in blood flow: its dependence on hematocrit and wall shear rate." Microvascular research. **33**(2): 211-223.

Turitto, V. T. and H. R. Baumgartner (1975). "Platelet deposition on subendothelium exposed to flowing blood: mathematical analysis of physical parameters." Transactions - American Society for Artificial Internal Organs. **21**: 593-601.

Turitto, V. T. and H. R. Baumgartner (1975). "Platelet deposition on subendothelium exposed to flowing blood: mathematical analysis of physical parameters." Transactions - American Society For Artificial Internal Organs **21**: 593-601.

Turitto, V. T., H. J. Weiss, et al. (1979). "Rheological factors influencing platelet interaction with vessel surfaces." Journal of Rheology **23**(6): 735-49.

van Breugel, H. H., J. J. Sixma, et al. (1988). "Effects of flow pulsatility on platelet adhesion to subendothelium." Arteriosclerosis : an official journal of the American Heart Association, Inc. **8**(3): 332-335.

Vanhoorelbeke, K., H. Ulrichts, et al. (2003). "Inhibition of platelet adhesion to collagen as a new target for antithrombotic drugs." Current Drug Targets. Cardiovascular & Haematological Disorders **3**(2): 125-140.

Vengrenyuk, Y., S. p. Carlier, et al. (2006). "A hypothesis for vulnerable plaque rupture due to stress-induced debonding around cellular microcalcifications in thin fibrous caps." Proceedings Of The National Academy Of Sciences Of The United States Of America **103**(40): 14678-14683.

Weiss, H. J., V. T. Turitto, et al. (1978). "Effect of shear rate on platelet interaction with subendothelium in citrated and native blood. I. Shear rate--dependent decrease of adhesion in von Willebrand's disease and the Bernard-Soulier syndrome." The Journal of laboratory and clinical medicine. **92**(5): 750-764.

Wing Kam, L., L. Yaling, et al. (2006). "Immersed finite element method and its applications to biological systems." Computer Methods in Applied Mechanics and Engineering **195**(13-16): 1722-49.

Woodside, D. G., S. Liu, et al. (2001). "Integrin activation." Thrombosis and haemostasis. **86**(1): 316-323.

Wootton, D. M. (1998). Mechanistic Modeling of Occlusive Arterial Thrombosis. Mechanical Engineering. Atlanta, Georgia Institute of Technology. **Doctor of Philosophy in Mechanical Engineering:** 421.

Wootton, D. M. and D. N. Ku (1999). "Fluid mechanics of vascular systems, diseases, and thrombosis." Annual review of biomedical engineering. **1**: 299-329.

Wootton, D. M., C. P. Markou, et al. (2001). "A mechanistic model of acute platelet accumulation in thrombogenic stenoses." Annals of biomedical engineering. **29**(4): 321-329.

Young, D. F. (1979). "Fluid mechanics of arterial stenoses." Transactions of the ASME. Journal of Biomechanical Engineering **101**(3): 157-75.

Young, D. F. and F. Y. Tsai (1973). "Flow characteristics in models of arterial stenoses. I. Steady flow." Journal of biomechanics. **6**(4): 395-410.

Zhaoli, G., S. Baochang, et al. (2000). "Lattice BGK model for incompressible Navier-Stokes equation." Journal of Computational Physics **165**(1): 288-306.

Zydney, A. L. and C. K. Colton (1988). "AUGMENTED SOLUTE TRANSPORT IN THE SHEAR FLOW OF A CONCENTRATED SUSPENSION." PCH, PhysicoChemical Hydrodynamics **10**(1): 77-96.